

NIST-GCR-96-702

FIRE PROTECTION FOAM BEHAVIOR IN A RADIATIVE ENVIRONMENT

C.F. Boyd, M. di Marzo

Mechanical Engineering Department
University of Maryland
College Park, MD 20742

September 1996
Issued October 1996



U.S. Department of Commerce
Michael Kantor, *Secretary*
Technology Administration
Mary L. Good, *Under Secretary for Technology*
National Institute of Standards and Technology
Arati Prabhakar, *Director*

Notice

This report was prepared for the Building and Fire Research Laboratory of the National Institute of Standards and Technology under grant number 60NANB5D0136. The statement and conclusions contained in this report are those of the authors and do not necessarily reflect the views of the National Institute of Standards and Technology or the Building and Fire Research Laboratory.

FIRE PROTECTION FOAM BEHAVIOR
IN A RADIATIVE ENVIRONMENT

FINAL REPORT

C.F. Boyd, M. di Marzo

prepared for the
Building and Fire Research Laboratory
National Institute of Standards and Technology
Gaithersburg, MD 20899

Mechanical Engineering Department
University of Maryland
College Park, MD 20742

September 1996

ABSTRACT

A model is developed which predicts the behavior of a fire-protection foam subjected to heat radiation. Foam expansion ratio and radiative heat flux are input to the model. A mass and energy balance yield the foam destruction rate and the temperature distribution within the foam.

The model separates the foam into its liquid, vapor, and air components. Continuity is satisfied for each. Ideal gas relations, a realistic density function, and foam expansion measurements are used in conjunction with continuity to compute the volume fraction and velocity of each component as a function of temperature.

The energy equation is solved in a coordinate system moving with the foam front. Separate air, vapor, and liquid convection terms are computed. Radiation absorption is accounted for with a volumetric generation term. The absorption model is based upon experimental measurements. A volumetric evaporative term accounts for the latent heat of liquid vaporized within the foam. Liquid vaporization rates are determined from the liquid continuity equation. Saturated conditions and thermodynamic equilibrium are assumed throughout. Thermal diffusion is computed using an experimentally determined thermal conductivity.

A steady state solution is computed with a second order Crank-Nicolson technique. Fixed values for the temperature at the evaporative front and in the far field are used as boundary conditions. Dimensionless results indicate the major terms in the energy balance are proportional to applied heat flux. The dimensionless temperature gradient in the near linear range of the profiles collapses to a single value.

Model results indicate the energy balance is dominated by the generation and evaporative terms. The convection terms account for less than ten percent of the energy balance and diffusion is less than three percent.

Experimental data are obtained in tests of foam exposed to radiation from a set of gas-fired panels for heat fluxes up to 18 kW/m². Temperature profiles are measured within the foam. The average temperature gradient in the near linear range is computed for each set of data. The average dimensionless experimental temperature gradient is 17 percent higher than the value predicted by the model. The numerical prediction lies within one standard deviation of the experimental results.

FOREWORD

This report describes the research performed during the period September 1995 - September 1996 under a joint research program between the Mechanical Engineering Department of the University of Maryland at College Park and the Building and Fire Research Laboratory of the National Institute of Standards and Technology. The research was conducted in the laboratories of the BFRL by Dr. Christopher F. Boyd, Graduate Research Assistant of the ME Department at the time, under the joint supervision of Dr. Marino di Marzo (ME Dept. - UMCP) and Dr. David D. Evans (BFRL - NIST). This report also constitutes the doctoral dissertation of Dr. Boyd, which has been completed and was defended in 1996.

TABLE OF CONTENTS

<u>Section</u>	<u>Page</u>
LIST OF TABLES	vi
LIST OF FIGURES	vii
NOMENCLATURE	xiii
 CHAPTER I	
INTRODUCTION	1
OBJECTIVE	1
BACKGROUND	1
LITERATURE REVIEW	5
APPROACH	7
 CHAPTER II	
FIRE-PROTECTION FOAM TESTING	8
EXPERIMENTAL OBJECTIVES	8
EXPERIMENTAL OVERVIEW	8
FOAM	9
RADIATION FIELD	14
FOAM PROTECTION TEST	16
 CHAPTER III	
FOAM PROTECTION MODEL	23
ABLATION PROBLEM	23
FOAM ABLATION PROBLEM	26
ORDER OF MAGNITUDE ANALYSIS	28
FOAM MODEL PRINCIPLES AND ASSUMPTIONS	30
 CHAPTER IV	
SUBMODELS AND ASSOCIATED EXPERIMENTS	34
GENERATION TERM	34
DENSITY	42
SPECIFIC HEAT	50
ABLATION VELOCITY	50
VELOCITY OF COMPONENTS	52
EVAPORATIVE TERM	55
CONVECTIVE TERMS	56
THERMAL CONDUCTIVITY	56

<u>Section</u>	<u>Page</u>
CHAPTER V	
EQUATION SUMMARY AND NUMERICAL SOLUTION	60
EQUATIONS	60
NUMERICAL SOLUTION	60
CHAPTER VI	
RESULTS AND DISCUSSION	65
FOAM TEST RESULTS	65
FOAM MODEL RESULTS	72
DIMENSIONLESS RESULTS	79
CHAPTER VII	
CONCLUSIONS AND RECOMMENDATIONS	84
RECOMMENDATIONS FOR FUTURE WORK	87
APPENDIX A	
FORTRAN CODES	89
FOAM ABLATION MODEL	89
IDEAL DENSITY MODEL	94
RADIATION GENERATION TERM	96
CONSERVATION OF MASS	97
REFERENCES	160

LIST OF TABLES

<u>Number</u>		<u>Page</u>
1.	Oven Uniformity Results	100
2.	Repeatability of Foam Expansion Ratio	100
3.	Average Temperatures and Standard Deviations from Figure 10	101
4.	Summary of Foam Test Conditions	102
5.	Relative Magnitudes of Terms in Foam Ablation Problem	103
6.	Specific Heat Values for Foam Components	103
7.	Foam Thermal Conductivity Estimates	103
8.	Summary of Major Equations	104
9.	Experimental Temperature Gradient	105
10.	Dimensionless Experimental Temperature Gradient	106

LIST OF FIGURES

<u>Number</u>		<u>Page</u>
1.	Schematic of Foam Generator	107
2.	Photograph of Foam Generator	108
3.	Schematic of Coaxial Mixer Design	109
4.	Schematic of Gas-Fired Panel Apparatus	109
5.	Photograph of Gas-Fired Panel Apparatus	110
6.	Photograph of Test Plate	111
7.	Photograph of Foam Covered Test Plate	111
8.	Photograph of Foam Sample During Test	112
9.	Thermocouple Measurements From Foam Test	112
10.	Several Thermocouple Measurements at One Height	113
11.	Steady State Temperature Profile From Foam Test	113
12.	Coordinate System and Boundary Conditions	114
13.	Experimental Radiation Measurement Setup	114
14.	Measured Extinction Coefficient Data	115
15.	Spectral Ranges	115
16.	Measured Scattering Coefficient Data	116
17.	Calculated Absorption Coefficient Data	116
18.	Ideal Foam Density Function	117
19.	Foam Volume Expansion Measurements	117
20.	Foam Volume Expansion due to Temperature Rise	118

<u>Number</u>	<u>Page</u>
21. Realistic Foam Density Function	118
22. Diagram for Steady State Steady Flow Analysis	119
23. Diagram for Liquid Velocity Determination	119
24. Diagram for Gas Velocity Determination	120
25. Thermal Diffusivity Measurement Setup	120
26. Liquid Volume Fraction	121
27. Liquid Velocity Relative to Front	121
28. Vapor Velocity Relative to Front	122
29. Air Velocity Relative to Front	122
30. Convergence of Temperature Profiles	123
31. Generation and Evaporative Terms	123
32. Convective and Diffusion Terms	124
33. Comparison of Numerical and Experimental Temperature Profile	124
34A. Thermocouple Measurements from Foam Test A	125
34B. Experimental and Numerical Temperature Profiles, Case A	125
35A. Thermocouple Measurements from Foam Test B	126
35B. Experimental and Numerical Temperature Profiles, Case B	126
36A. Thermocouple Measurements from Foam Test C	127
36B. Experimental and Numerical Temperature Profiles, Case C	127
37A. Thermocouple Measurements from Foam Test D	128
37B. Experimental and Numerical Temperature Profiles, Case D	128

<u>Number</u>	<u>Page</u>
38A. Thermocouple Measurements from Foam Test E	129
38B. Experimental and Numerical Temperature Profiles, Case E	129
39A. Thermocouple Measurements from Foam Test F	130
39B. Experimental and Numerical Temperature Profiles, Case F	130
40A. Thermocouple Measurements from Foam Test G	131
40B. Experimental and Numerical Temperature Profiles, Case G	131
41A. Thermocouple Measurements from Foam Test H	132
41B. Experimental and Numerical Temperature Profiles, Case H	132
42A. Thermocouple Measurements from Foam Test I	133
42B. Experimental and Numerical Temperature Profiles, Case I	133
43A. Thermocouple Measurements from Foam Test J	134
43B. Experimental and Numerical Temperature Profiles, Case J	134
44A. Thermocouple Measurements from Foam Test K	135
44B. Experimental and Numerical Temperature Profiles, Case K	135
45A. Thermocouple Measurements from Foam Test L	136
45B. Experimental and Numerical Temperature Profiles, Case L	136
46A. Thermocouple Measurements from Foam Test M	137
46B. Experimental and Numerical Temperature Profiles, Case M	137
47A. Thermocouple Measurements from Foam Test N	138
47B. Experimental and Numerical Temperature Profiles, Case N	138
48A. Thermocouple Measurements from Foam Test O	139

<u>Number</u>	<u>Page</u>
48B. Experimental and Numerical Temperature Profiles, Case O	139
49A. Thermocouple Measurements from Foam Test P	140
49B. Experimental and Numerical Temperature Profiles, Case P	140
50A. Thermocouple Measurements from Foam Test Q	141
50B. Experimental and Numerical Temperature Profiles, Case Q	141
51A. Thermocouple Measurements from Foam Test R	142
51B. Experimental and Numerical Temperature Profiles, Case R	142
52A. Thermocouple Measurements from Foam Test S	143
52B. Experimental and Numerical Temperature Profiles, Case S	143
53A. Thermocouple Measurements from Foam Test T	144
53B. Experimental and Numerical Temperature Profiles, Case T	144
54A. Thermocouple Measurements from Foam Test U	145
54B. Experimental and Numerical Temperature Profiles, Case U	145
55A. Thermocouple Measurements from Foam Test V	146
55B. Experimental and Numerical Temperature Profiles, Case V	146
56A. Thermocouple Measurements from Foam Test W	147
56B. Experimental and Numerical Temperature Profiles, Case W	147
57A. Thermocouple Measurements from Foam Test X	148
57B. Experimental and Numerical Temperature Profiles, Case X	148
58A. Thermocouple Measurements from Foam Test Y	149
58B. Experimental and Numerical Temperature Profiles, Case Y	149

<u>Number</u>		<u>Page</u>
59A.	Thermocouple Measurements from Foam Test Z	150
59B.	Experimental and Numerical Temperature Profiles, Case Z	150
60.	Temperature Gradient versus Heat Flux	151
61.	Temperature Gradient versus Expansion Ratio	151
62.	Temperature Profiles for Three Heat Fluxes, $x_p = 18.2$	152
63.	Generation and Evaporative Terms for Three Heat Fluxes	152
64.	Diffusion Term for Three Heat Fluxes, $x_p = 18.2$	153
65.	Liquid Convection Term for Three Heat Fluxes, $x_p = 18.2$	153
66.	Vapor Convection Term for Three Heat Fluxes, $x_p = 18.2$	153
67.	Temperature Profiles for Three Expansion Ratios	154
68.	Generation and Evaporative Terms for Three Expansion Ratios	154
69.	Diffusion Term for Three Expansion Ratios	155
70.	Liquid Convection Term for Three Expansion Ratios	155
71.	Vapor Convection Term for Three Expansion Ratios	155
72.	Dimensionless Temperature Profiles for Three Heat Fluxes	156
73.	Dimensionless Generation and Evaporative Term Profiles	156
74.	Dimensionless Diffusion Term for Three Heat Fluxes	157
75.	Dimensionless Liquid Convection Term for Three Heat Fluxes	157
76.	Dimensionless Vapor Convection Term for Three Heat Fluxes	157
77	Dimensionless Temperature Profiles for Three Expansion Ratios	158

<u>Number</u>		<u>Page</u>
78.	Dimensionless Generation and Evaporative Term Profiles	158
79.	Dimensionless Diffusion Term for Three Expansion Ratios	159
80.	Dimensionless Liquid Convection Term for Three Expansion Ratios	159
81.	Dimensionless Vapor Convection Term for Three Expansion Ratios	159

NOMENCLATURE

a	absorption coefficient [m^{-1}]
A	Area [m^2]
C	constant
conv	convection term [W/m^3]
C_p	specific heat [$\text{J}/\text{kg } ^\circ\text{C}$]
diff	diffusion term [W/m^3]
f	liquid volume fraction
h	specific enthalpy [J/kg]
h_v	latent heat of vaporization [J/kg]
i	radiation intensity [W/m^2]
Ja	Jakob number
k	thermal conductivity [$\text{W}/\text{m } ^\circ\text{C}$]
l	initial foam depth [m]
l_m	mean radiation penetration length [m]
m	mass [kg]
\dot{m}	mass flux [$\text{kg}/\text{m}^2 \text{ s}$]
P	pressure [N/m^2]
Pe	Peclet number
P_s	percent of solid material in struts
q	heat flux [W/m^2]

\dot{q}_g	heat generation term [W/m ³]
\dot{q}_v	evaporative heat sink term [W/m ³]
R	gas constant [J/kg °C]
T	temperature [°C]
t	time [s]
u	velocity [m/s]
u_f	front velocity relative to fixed system [m/s]
V	volume [m ³]
x	distance [m]
xp	foam expansion value

Greek

ρ	density [kg/m ³]
Γ	mass source term from continuity equation [kg/m ³ s]
κ	extinction coefficient [m ⁻¹]
σ	scattering coefficient [m ⁻¹]
ΔT	temperature difference [°C]

Subscripts

a	air component
cv	control volume
f	front
f	foam

i	initial or undisturbed foam condition
l	liquid component
ref	reference value
sat	saturated conditions
v	vapor component
λ	denotes spectral dependence

Superscripts

*	dimensionless variable
---	------------------------

CHAPTER I

INTRODUCTION

This work is part of a larger effort to evaluate the performance of fire-fighting agents used to protect structures from heat and fire damage. A joint research program between the University of Maryland and the Building and Fire Research Laboratory at the National Institute of Standards and Technology supported this effort.

OBJECTIVE

The overall objective of the current research program is to identify the parameters associated with the performance of fire-fighting foams used to protect structures from heat and fire damage. Specifically, the current research focuses on the destruction of a fire-fighting foam subjected to heat radiation. A numerical model which predicts the foam's properties during the destruction process is sought. The model is developed using experimental measurements and observations as a guide. Experimental results and the numerical model are used to identify the role of the various parameters which govern the foam's behavior.

BACKGROUND

The first recorded usage of foam for fire fighting occurred in 1904 [1]. This application was a chemical based foam generated from the reaction of two aqueous solutions. This type of foam generation was standard practice until the mid 1950's

when it was replaced by the currently popular mechanical foam generation [2].

Mechanical foams are formed by mechanical agitation and aeration of a foam solution.

All foams considered in this report are mechanical foams since chemical based foams are not presently in common use.

Mechanical foams are all produced using the same basic principles. A foam concentrate is mixed with water to form a foam solution. The foam solution is mixed with air to form foam. Many varieties of foam generators which follow these basic steps are used. Some generators mix the water and foam concentrate using an in-line proportioner while others operate on batches of a pre-mixed foam solution. Other variations exist in the way the air is introduced into the foam solution. An air aspirated foam generator mixes atmospheric or compressed air with the foam concentrate to produce a foam output. A non-aspirated foam generator outputs foam solution at high velocities and the solution is aspirated in-flight through air entrainment. This method produces a relatively wet foam which can be thrown a large distance.

Another distinction between foams is related to the foam concentrate.

Although scores of foam concentrates are available from foam manufacturers, the concentrates are generally broken down into two main types. The two types are known as protein based and synthetic [3]. A large variety of particular agents in each class are designed to meet a specified type of hazard such as compatibility with other fire-fighting chemicals or resistance to polar solvents common in fuel fires.

For all foams, regardless of type or origin, classification of the foam's

properties is important. Foams are a dynamic material by nature and do not lend themselves to easy classification. As soon as foams are formed, changes begin to occur. The three main instabilities in foams are caused by diffusion of gas, liquid drainage, and coalescence [4]. In order to clarify the foam's properties, foam quality characteristics have been defined for fire-fighting foams. Foam quality measurements are helpful in selecting a given foam for a given application.

Foam quality is typically defined by four characteristics [3]:

1. Quarter life or 25 percent drain time measures the time it takes for 25 percent of the foam solution to drain from a foam sample.
2. Expansion ratio is the ratio of the volume of foam to the volume of foam concentrate used to produce the foam.
3. Fire performance rates the ability of the foam to knock down a given size test fire.
4. Burnback resistance indicates the ability of the foam to withstand heat during a specific test procedure.

Procedures for determination of these and other characteristics are outlined in the Appendix Section of NFPA Standard 11 [5], Underwriters Laboratories Report UL 162 [6], and Military Specification 24385 [7].

The present research looks at fire-fighting foams designed to stop the spread of fire by protecting structures in or near the fire environment. Protein based compressed air foams are typically used for fire protection applications because of their inherent properties [8]. These foams are characterized as sticky and will cling to vertical and

overhanging surfaces. In addition, the internal water does not drain from the foam at any appreciable rate. The appearance and feel of the foams is described as shaving or whipped cream.

Standardized test procedures to determine burnback resistance or fire performance are developed with fire-fighting in mind. No standardized test procedure is available for testing the fire protection capabilities of fire-fighting foams. Requirements for a good fire-fighting foam may render it useless in a fire-protection role. For instance, a good fire-fighting foam should flow freely [3] to cover the fuel surface quickly. In contrast, foam used to protect vertical surfaces must stick in place to maintain a protective barrier. Guidelines for the selection of foams for fire protection need to be developed. For clarity in this report, fire-fighting foams used in the role of fire-protection are referred to as fire-protection foams.

A main reason for using fire-protection foams is structure protection. In the presence of a fire, structures are coated with fire-protection foams which shield the underlying surface from the heat. These foams have good insulation properties and absorb heat which is dissipated through the vaporization of the internal water. Since water evaporates at 100°C, the underlying surface temperature does not exceed this value until the foam is gone. Foams are simply a means of effectively using the available water [9]. Water is the sacrificial material which does the work of absorbing the heat.

One example of the use of fire-protection foams is in the protection of petrol-chemical storage facilities. Fires at petrol-chemical storage facilities can burn for

several hours or even days [2] before extinguishment. During this time, surrounding structures must be protected from the intense heat radiation.

Water sprays or films are applied to structures in this environment and provide effective protection. The water absorbs the incoming heat and runs off. However, this process requires massive amounts of water and the run-off carries chemicals away from the fire. This run-off can pose serious environmental problems.

Foams, on the other hand, stick to vertical surfaces and in effect hold their water to the structure with little or no run-off. Water usage is minimized. In addition, foams typically don't require constant application since they last for several minutes to hours depending upon the heat intensity. This property allows the fire fighter to coat a surface and move on which spreads limited resources over a larger area.

Another common application for fire-protection foam is the protection of dwellings surrounded by combustible vegetation in areas prone to wild fires. In the case of a spreading wildfire, a structure can be coated hours in advance of the fires arrival thereby minimizing the danger to the persons involved. A wildfire typically passes a home in five minutes [10] which is shorter than the expected residence time of a properly applied fire-protection foam. Foams will stick under eaves, in corners, and to window glass which are all suspected areas for fire to enter a home. No structure has been lost in California wild fires when properly coated with foam [10].

LITERATURE REVIEW

Typical literature on foam usage in the fire environment concentrates on the

ability of foam to suppress existing fires of various types [11][12][13]. Data are usually presented in terms of fire knock down times for foam attack versus knock down times for water attack. In certain cases, the tests are not specifically repeatable due to uncontrolled affects such as weather or operator dependent systems.

The use of fire fighting foams in a fire-protection role is an emerging field [8]. Tests specifically tailored to foams used for fire protection are limited. In general, these tests measure the time to ignition of some combustible surface coated by foam. Comparisons are made of time to ignition when foam, no foam, or plain water is used to protect the surface.

Madrzykowski [14] used a compressed air foam system to coat vertical plywood with foam and subjected the specimens to radiant heating from a gas-fired panel. This work shows the foam's ability to delay ignition when compared to the use of an equal mass of water. Ignition times for foamed plywood surfaces are twice those for surfaces coated with water only. Madrzykowski based his water usage on the amount of water the plywood holds in a vertical position. The applied foam thickness is chosen to hold an amount of water equal to the water only tests. It is noted that more foam could potentially be applied to the plywood without sliding off. This fact would magnify the reported ignition delay times obtained for foam protection.

A study with more detailed measurements was carried out in Sweden. Persson [15] tests foams subjected to radiant heat from a cone radiator just above the foam surface. These foams are placed in beakers which are initially dry or initially contain a layer of fuel. Measurements of foam drainage and foam evaporation rates are taken

for various foams. The applied heat ranges from 0 to 35 kW/m². It is noted that evaporation rates are proportional to the incident radiation level. Drainage rates for some of the foams tested increased with the addition of radiant heating. Foam breakdown, accelerated by the radiation, is the suspected cause. The foams used in this study are typical fire-fighting foams with expansion ratios ranging from 6.5 to 11.5. Foams with this range of expansion are considered slightly wet and would not effectively stick to vertical surfaces.

No reports have been found which measure or predict the properties of the foam while it is subjected to the radiant heating. The need for a theoretical modeling approach to the foam protection process is noted by Persson [15].

APPROACH

A simple repeatable test is developed to evaluate the destruction of fire-protection foams subjected to heat radiation. A vertical steel surface is covered with fire-protection foam and subjected to heat radiation from a set of gas-fired panels. Observations and measurements from these experiments are used to identify the parameters needed to numerically model the foam evaporation process. While developing the numerical model, quantitative experimental results are used to formulate the model's assumptions and evaluate its predictive capability. Individual model terms are evaluated with a set of specific experiments. Importance of the governing parameters is quantified with a combination of analysis from the model and the experimental results.

CHAPTER II

FIRE-PROTECTION FOAM TESTING

EXPERIMENTAL OBJECTIVES

The objective of the fire protection foam testing is to determine a fire-protection foam's behavior in the presence of heat radiation. The behavior is determined as a set of quantitative measurements of foam temperature profiles along with qualitative observations of the foam during a specific test procedure. These tests simulate foam used to protect vertical structures in or near a large fire environment.

It is noted that only the affect of heat radiation on the foam is considered. Other affects which influence a foam's fire-protection capability include wind, foam aging, and flying embers. Secondary affects such as these remain for further study.

EXPERIMENTAL OVERVIEW

A simple repeatable test for fire-protection foams subjected to large fire radiation is developed. This test involves foam generation equipment, a fire source for heat generation, repeatable test procedures, and data acquisition techniques. The test simulates a small section of a vertical surface covered with foam and exposed to radiation from a nearby fire.

Experimental results are generated by subjecting a commercially available fire-protection foam to the thermal radiation emanating from two gas-fired panels. The process is designed to establish one-dimensional physics. The gas-fired panels are

oriented to produce a nearly uniform radiation field over the test area. The foam is generated using a custom built laboratory scale foam generator which is designed to produce relatively small amounts of foam consistent with larger commercially available foam generators. A 900 cm² steel plate is instrumented with thermocouples and used as a surface for foam application. A uniform thickness layer of foam is applied to the vertical plate which is positioned just in front of the flame panels. During the 10 to 20 minutes the foam remains on the plate, temperature measurements are made on the plate and within the foam itself in order to determine the foam destruction rate and foam state during the test. All data are recorded using a Hewlett Packard digital voltmeter (HP3456A) connected to a Hewlett Packard data acquisition control unit (HP3497A). Major components of the process are described below.

FOAM

A fire-protection foam must be sticky so it will cling to vertical or overhung surfaces. In addition, the foam must retain its water content and have good heat resistance. In order to achieve these conditions, an appropriate foam concentrate must be selected along with an appropriate foam generation system.

The foam selected for this program is Chubb National Foam's DurraFoam product. This protein based foam is very stable and durable which are beneficial properties for a fire-protection foam. In phone conversations with Chubb National Foam representatives [16], the DurraFoam product is recommended as their best fire-protection foam for the proposed application. Once made, the foam lasts for more

than 24 hours. This property was verified during this test program. Manufacturer claims also state that the foam can withstand 60 mile-per-hour winds [10]. This property is not investigated. The foam product easily sticks to vertical or even inverted surfaces in layers of 10 cm. Absolute limits on foam layer thickness are not determined.

The raw foam concentrate comes in 5 gallon containers and appears dark brown to black in color. The manufacturer recommends a mixture of 3 percent raw concentrate and 97 percent water to produce the foam solution for foam production. The concentrate is water soluble and mixes easily. Three percent solutions are used to generate all foams in this program.

Foam Generator

A custom built compressed air foam generator is used to generate the final foam product. Compressed air foam generators have the capability to produce a wide variety of long lasting foams [8]. A schematic representation of the foam generator is illustrated in Figure 1.

Bottled air is used to pressurize the liquid foam solution and drive it through a small orifice in a coaxial mixer. A second air stream passes through a needle valve and joins the pressurized liquid at the coaxial mixer. Exiting the mixer, the air and solution mixture expand into a packed bed of beads. While passing through the beads, the air and solution mix thoroughly to produce foam which is output through a tube. Control over the foam generation process is obtained by adjusting the needle valve located on the air supply just upstream of the coaxial mixer. Foam expansion ratios

ranging from 12 to 32 are obtainable with this adjustment. The expansion ratio variation is nearly linear with needle valve rotation. Figure 2 displays a photograph of the foam generator. The unit is assembled on a cart for portability.

Air Supply. Air for the foam generator is supplied from a 2000 psi bottle. The air is regulated to a steady pressure between 10 and 25 psig for use by the foam generator. Changing the air pressure in this range changes the foam flow rate but does not significantly affect the foam expansion ratio.

Foam Solution Tank. A large diameter low profile tank is used to hold the concentrate in order to minimize the gravitational head change of the solution during foam production. Earlier foam generator designs evaluated during this program had tall slender tanks and a significant variation in foam expansion ratio was observed as the solution level dropped in the tank. The solution level affects the solution pressure at the coaxial mixer. A change in this pressure changes the ratio of air and solution flow rates at the coaxial mixer and therefore affects the expansion ratio of the foam produced.

Coaxial Mixer. The air and solution streams are brought together at the coaxial mixer. In early foam generators evaluated for these experiments, a standard mixing T is utilized. This arrangement creates an unstable balance between the air and solution streams. A minor change in either streams pressure changed the foam output dramatically. This erratic behavior produced an unsteady foam output which made laboratory operations, such as filling a beaker with foam, difficult to complete.

A coaxial mixer is developed which produces smooth flowing foam output

over a variety of air and liquid stream pressures. The coaxial mixer is illustrated in Figure 3. This design uses a coaxial mixing path which immediately enters a packed bed of mixing beads. The foam solution is forced through a small tube and exits as a liquid jet. Visual inspections of this jet indicate a relatively stable flow rate. The air enters through a needle valve and mixes coaxially with the liquid jet as it exits the coaxial mixer. Stable air flow rates are observed using flow meters to monitor the air flow rates. This coaxial mixing path design exhibits stable air and solution flow rates over a variety of mixing ratios.

Mixing Beads. A packed bed of mixing beads is determined to be very efficient in producing a smooth foam product. Long tubing lengths and static flow rotator designs were tested but yielded inferior results. Both 3 and 6 millimeter glass beads are considered for mixing beads. The 3 millimeter beads are selected because they produce a finer foam in a shorter flow path when compared to the 6 millimeter beads. A compact foam generator is desirable in the confined laboratory space available.

The vertical orientation of the mixing path through the packed beads is found to aid in mixing efficiency. Gravitational affects have a tendency to separate some of the air from the solution when the mixing path is horizontal. The vertical flow path eliminates this problem. A 5 foot section of standard 5/8 inch garden hose is used to deliver the foam product from the mixing beads to the test surface.

Foam Properties

No guidelines have been found to characterize the foam properties for fire-

protection foams. Fire-fighting foams are typically characterized by four foam quality measures as outlined in Chapter 1. With the exception of the expansion ratio, these quality measures are determined from specific test procedures which are not directly applicable to fire-protection. For this program, the foams are characterized solely by expansion ratio.

Foam expansion ratio is not necessarily sufficient to distinguish between two foams. For a given expansion ratio, it is possible to produce a variety of foam textures due to the possible variations in bubble size and free water content. In general, a foam with large air bubbles has more free water than a foam with smaller bubbles. Foam properties such as drainage and resistance to radiation are affected by these differences also. In these experiments, two foams are considered identical if their expansion ratio and average bubble size are the same.

Bubble size is measured in this test program using a microscope fitted with a graduated eyepiece. The average dimension of the bubbles is found to lie between 200 to 300 microns for all the foams tested. With this small variation in bubble size, it is assumed that bubble size is not a significant variable in these experiments and that expansion ratio sufficiently characterizes the foam.

Expansion Ratio. Expansion ratio is the measure of the expansion realized by the foam solution when the air is added to make foam. Expansion ratio is defined as the volume of foam product divided by the volume of foam concentrate used to produce the foam. Expansion ratio for these tests is determined in the manner outlined by Reference 6. In this technique, a known volume container is filled with foam and

the net weight of the foam is determined on a digital scale. The following formula is used to calculate expansion ratio.

$$xp = \frac{\text{Volume of Container (cc)} \times 1(\text{g/cc})}{\text{Weight of Foam within Container (g)}} \quad (1)$$

This equation assumes the density of the foam concentrate is 1 g/cc. Expansion ratios ranging from 12 to 32 are considered in this test program.

RADIATION FIELD

Two vertical gas-fired panels measuring 38 centimeters wide by 83 centimeters high are used to supply the radiant heat for the experiments. Each large panel is comprised of five perforated ceramic panels. The panels burn a regulated mixture of natural gas and air which are both supplied from external sources. Combustion products are vented through a ceiling duct.

Figure 4 illustrates the positions of the major components of the gas-fired panel apparatus as viewed from overhead. The panels are oriented at a 30 degree angle as shown in the figure to produce a uniform radiation field at the foam front. Reflector panels are used as sidewalls to maximize the heating applied to the foam and minimize the heat escape. Water cooling panels surround the back side of the apparatus to minimize the heating of the laboratory. The foam plate is positioned at the center height of the flame panels. Reference heat flux gauges are mounted on each side of the plate at the center height. Figure 5 shows a photograph of the flame panel rig as viewed from the rear of the flame panels.

Measurement of Radiation Field

In order to determine the uniformity of the heat radiation applied to the foam samples, an experimental determination of the heat radiation field at the foam position is completed. Heat flux is measured using commercially available Gardon [17] type heat flux gauges which are calibrated prior to the measurements. Measurements are made over a three dimensional array of points stemming from the center of the test plate. A calibration plate is fabricated for this purpose which allows a heat flux gauge to be mounted at an array of points on a 20 centimeter square grid with 5 centimeter spacings between measurement points. Measurements are made in the plane of the foam plate surface and at parallel planes spaced at distances of 2, 4, 6, 8, and 10 centimeters from the plate surface. All measurements are normalized by the reference gauge readings in order to account for any small variations in the gas-fired panels operation. The position of the reference gauges is not changed throughout the experiment.

Heat flux results for each plane parallel to the plate, normalized by the reference heat flux gauge readings, are presented in Table 1. As shown in the table, the standard deviation of the measurements made in any given plane ranges from 3.2 to 4.1 percent of the average heat flux value. The average value of the normalized average heat fluxes for each plane is 0.923 with a standard deviation of 0.034 between planes. These results are used as a flame panel calibration. The heat flux applied to the foam is assumed to be 92.3 percent of the heat flux measured by the reference gauges. The uncertainty associated with this value is less than 4 percent.

The flame panel radiation can be varied from 0 to 20 kW/m² as measured by the reference gauges. Applying the results noted above, this corresponds to a heating range of 0 to 18.5 kW/m². The heating range is varied by regulating the flow rate of air and gas to the flame panels.

FOAM PROTECTION TEST

Foam samples tested in the flame panel rig are applied to a 30 cm square steel plate which is instrumented with thermocouples. Figure 6 shows a photograph of a test plate instrumented with an array of thermocouples at fixed heights from the plate surface. One thermocouple measures the plate temperature and eight thermocouples measure the foam temperature at distances of 1, 2, 3, 4, 5, 6, 7, and 8 centimeters from the plate. The 8 thermocouples within the foam are arrayed on a 4 centimeter diameter circle at 45 degree increments. The thermocouple on the plate is positioned on the center axis of this circle. Omega brand type K grounded thermocouples are used for the measurements within the foam and an exposed bead type K thermocouple is bonded to the plate for a surface measurement.

The test plates are covered with foam and the outer surface is scraped off to yield a blanket of foam with a uniform thickness for testing. Figure 7 shows a photograph of a test plate covered with a foam layer. Once the foam is applied to the plate and scraped to a uniform thickness, the test plates are immediately placed in front of the gas-fired panels and data acquisition is initiated.

The expansion ratio of the foam on the plate is determined by sampling the

foam from the foam generator just before and just after covering the plate. Expansion ratio typically changes by less than five percent while covering the plate. Expansion ratio is assigned as the average of the before and after measurements.

Steady state operation of the gas-fired panels is verified prior to each foam test by monitoring the reference gauges which are mounted to the sides of the foam sample. Once the reference gauges indicate steady state operation of the panels, the foam is applied to the plate and the test is initiated. Data acquisition begins immediately upon inserting the foamed plate into its test position.

Figure 8 illustrates a photograph of a foam sample in the gas-fired panel rig after about 5 minutes of exposure. The plate is photographed from just below the panels. The relative position of the reference gauges is seen clearly in this figure. At the time the photograph is taken, about 4 centimeters of foam have evaporated leaving 6 centimeters of foam on the plate. Initially, the foam surface is parallel to the front surface of the reference gauges. During the exposure, the foam surface (foam front) moves towards the plate surface.

Quantitative data recorded for each run included foam expansion ratio, reference gauge heat flux, and the thermocouple readings. The compensated thermocouple readings are converted to degrees Celsius using the 10th order polynomial curve fit supplied by Omega [18].

Figure 9 illustrates one example of the measured temperature rise for a plate initially covered with 10 centimeters of foam with an expansion ratio of 18.2. The radiant heat input to the foam for this trial was 17.5 kW/m^2 . Temperature traces are

labeled 0 through 8 with "0" referring to the plate surface thermocouple and "8" referring to the thermocouple positioned 8 centimeters from the plate. For this test example, the foam is nearly gone and the plate temperature is climbing past 65°C at 900 seconds (15 minutes) into the test. Several observations are made from the 15 minutes of data in Figure 9.

Each thermocouple within the foam responded in a similar manner. For some time each trace remains at its initial temperature while the thermocouple is effectively being insulated from the applied heat flux. Next, the thermocouples respond gradually to a temperature of 25 to 30°C. At this point, each trace generally rises at a constant rate to a temperature of approximately 70°C. Once at 70°C the rate of temperature rise slows as the temperature asymptotically approaches 80°C. The measured temperatures near the end of each trace are erratic with fluctuations as high as 5°C. At some point, each trace jumps up to a temperature over 100°C. This behavior of the temperature indicates that the thermocouple is outside of the foam front and is exposed directly to the radiation from the gas-fired panels.

Foam Test Accuracy

The repeatability of the foam temperature measurements is assessed to give an indication of the uncertainty in the measurements. Tests using identical conditions are attempted in rapid succession to compare the results. The measurements are repeatable to some degree. However, differences in the test conditions could not be eliminated from the differences between each measurement set. Due to the limitations of the controls on the foam generator and the gas-fired panels, exact repeatability of

the test conditions from case to case is not achieved.

The foam expansion ratio is the hardest factor to control. Table 2 lists the foam expansion ratios for 3 sets of 5 successive tests. Each set of data are collected in succession with no change in the foam generator control settings. The standard deviation of the foam expansion ratio measurement is approximately 3 percent of the average value.

The gas-fired panels display similar variations. Heat flux tends to change slightly over long periods of time and the control system is too coarse to make minor adjustments. The standard deviations of the measured heat flux values for each of the sets noted in Table 2 ranged from 1.1 to 1.7 percent of the applied heat flux.

To eliminate variations in test conditions and isolate the measurement uncertainty, redundant measurements are made during a single plate test. Several tests are completed in this manner. For each test, 8 thermocouples are placed in a ring 4 centimeters from the plate surface. The plate is covered with foam and exposed to the flame panel radiation. Each set of data consists of 8 thermocouple readings at one distance from the plate. The foam expansion ratio and applied heat flux are the same for all 8 readings since they are obtained from the same foam sample and exposed to the flame panels at the same time. Differences between the readings are considered an indication of the repeatability of the measurements.

Figure 10 illustrates the data for one of the repeatability tests. This particular test begins with 6 centimeters of foam at an initial expansion ratio of 21.6. The applied heat flux is 15 kW/m^2 . Seven thermocouple readings are compared on the

figure. In addition, the average value and standard deviation interval are plotted at 30 second intervals. Table 3 lists the average values and standard deviation intervals which are noted on Figure 10.

Data for times greater than 150 seconds are not considered since the foam front is approaching the thermocouples and the data begin to become erratic. As shown in Figure 10, the standard deviation interval varies from $\pm .1^{\circ}\text{C}$ in the undisturbed foam to $\pm 3.9^{\circ}\text{C}$ during the peak foam heating. Since the accuracy of a thermocouple is approximately $\pm 1^{\circ}\text{C}$ [19], instrument error does not account for the differences in the traces.

It is instructive to view the differences between the temperature profiles as a shift in time rather than a temperature difference. Each of the traces has a similar shape and temperature range but differ from one another by a time shift. This time separation could be caused by two factors. The probes could be at different heights from the plate or the foam thickness above each thermocouple could be different. Since the distances of the probes from the plate are verified prior to each test, a difference in foam thickness is considered to be the leading cause for the time differences between the traces. Table 3 lists the standard deviations on the time values at which the traces reach the given average temperatures. The time variation ranges from near 0 to 18 seconds.

The foam sample is produced with a known uniform thickness as illustrated by Figure 7. Once exposed to the radiation, the exact thickness at any given location is uncertain due to the variations in the surface as one can see by inspecting Figure 8.

This figure illustrates the unevenness of the foam surface during the evaporation process. Generally, the foam is uniformly thick. Locally, however, peaks and valleys exist in the foam. Peak to valley spacings increase with time during the evaporation process. Initially the peak to valley spacings are on the order of the bubble diameters. Near the end of the test, the peak to valley spacings range from 1 to 3 centimeters. Since the thermocouples are spaced laterally over the plate, one thermocouple could be directly under a peak while the adjacent thermocouple might be closer to a valley.

The principal variable which leads to uncertainty in the foam temperature measurements is suspected to be the uncertainty in the foam front position. The data of Figure 10 look good when considering the foam front condition of Figure 8. The peaks and valleys in the foam surface grow with time getting larger as the foam front moves ahead. The longer the elapsed time of the experiment, the greater the expected uncertainty will be for a given temperature trace. The uncertainties listed in Table 3 are smaller than the uncertainties expected in the final data since the thermocouples started out 2 cm from the initial location of the foam front. The thermocouples start out between 4 and 7 centimeters from the foam front in the final test data and the variations in the foam front are more developed.

The development of variations in the foam front results from the foam breakdown induced by the heating of the foam and the vaporization of the liquid. The expanding air and vapor must escape out of the foam matrix. This can happen if the foam bubbles burst and re-coalesce continuously. It is this process that transforms the layer and that generates large variations in its surface appearance.

Test Conditions

After optimizing the foam test procedure and establishing the final test plate configuration, a series of foam tests are completed to generate a data base of foam temperature profiles for various expansion ratios and applied heat flux levels. Table 4 lists the test conditions associated with each of the foam tests completed. A total of 26 foam tests are completed and the foam tests are labeled A through Z.

An attempt is made to span the largest possible range of foam expansion ratio and applied heat flux. Heat flux ranges from 9.7 to 17.8 kW/m². The upper limit on the heat flux is the stable upper limit of the gas-fired panels operation. Foam expansion ratio ranges from 12.8 to 32.8. At expansion ratios below 13, the foam becomes heavy and tends to slide off of the vertical plate. The upper limit on the foam expansion ratio is limited by the capability of the foam generator design.

CHAPTER III

FOAM PROTECTION MODEL

A model describing the behavior of the foam observed during the foam experiments is desired. This model is developed from basic principles and data not directly related to the foam tests outlined above. The foam model developed is an adaptation of the classic ablation problem solved in many heat transfer textbooks [20][21].

ABLATION PROBLEM

In the ablation problem, the energy equation is solved in a reference frame attached to the moving ablation boundary. Incoming heat at the material surface is either absorbed as the heat of ablation (Joule / kg of material) or conducted into the solid material. The ablation velocity is obtained from an energy balance at the surface. The boundary condition at the ablation front sets the temperature to the melting point temperature. The far field boundary condition is set to the initial temperature of the material. The differential equation for a reference frame attached to the solid material front is given below [21].

$$\rho C_p \left(\frac{\partial T}{\partial t} - u_f \frac{\partial T}{\partial x} \right) = \frac{\partial}{\partial x} \left(k \frac{\partial T}{\partial x} \right) \quad (2)$$

The ablation front velocity, u_f , is defined as a positive value in this case. The solution to this equation is a time dependent temperature distribution which moves with the

foam front at the time dependent front velocity.

Steady State Ablation

The steady state ablation problem is governed by Equation 2 without the time dependence and is given by Equation 3.

$$\frac{d}{dx}\left(k\frac{dT}{dx}\right) + \rho C_p u_f \frac{dT}{dx} = 0 \quad (3)$$

The steady state velocity is obtained by equating the heat applied to the material with the rate of change of enthalpy of the material as it is heated up and ablated away. A solution to the steady state ablation problem consists of the ablation velocity and a temperature distribution which moves with the ablation front.

It is observed from the test results of Figure 9 that several of the thermocouples responded in a manner indicative of a steady state temperature profile being moved past the array of thermocouples at a fixed velocity. This assumption is reinforced by plotting the data of Figure 9 in a coordinate system fixed to a moving foam front.

Figure 9 illustrates the temperature rise in the foam associated with the temperature profile which is moving past the fixed probe locations. If the phenomena is described as steady state, each of the temperature traces would be identical. The traces would be separated in time by $0.01/u_f$ seconds where 0.01 is the probe spacing in meters. For the conditions associated with the data of Figure 9, the steady state ablation velocity, determined from an energy balance, is 1.25×10^{-4} m/s. The time space between traces is determined to be 80 seconds.

Manipulation of the data from Figure 9 to remove the affect of the spatial

separation of the thermocouples allows each thermocouple output to be compared for similarity. In addition, the time dependence is scaled to a spatial dependence by assuming a steady state velocity. First, each thermocouple trace from Figure 9 is shifted in time by a multiple of 80 seconds to account for the spatial separation of the probes. Next, the time axis is converted to distance in meters by multiplying it with the steady state ablation velocity. Figure 11 illustrates the result for traces 3, 4, 5, and 6 from Figure 9. Traces 7 and 8 are dropped because they are affected by the initial thermal transient. Traces 0, 1, and 2 are dropped because they are affected by the presence of the support plate. The data of Figure 11 are transformed into a coordinate system attached to the moving foam front.

The traces of Figure 11 are similar enough to encourage a steady state solution. Differences in the traces are mainly attributed to the non-uniformity of the foam front. The differences between the traces are on the order of 0.01 meters which is comparable to the differences observed in the foam front surface.

The majority of the experimental data appear to reach a steady state condition. The notable exceptions are those data where the applied heat flux is low. At the lowest heating rates, the destruction rate of the foam is low and the thermal diffusion plays a major role. Steady state conditions are never reached in these cases. In reality, large fire heating rates are much larger than the heating rates available from the gas-fired panels used in these experiments. Steady state conditions are expected in this case. The steady state ablation model will serve as the basis for the foam model development.

FOAM ABLATION PROBLEM

The destruction of fire-protection foam by heat radiation is similar to the classic solid material ablation problem. The material is heated and slowly evaporates away which creates a moving foam front. Foam, however, is not similar to any continuous material and the assumptions in the ablation model must be modified to account for the foam's unique properties. Modifications made to the ablation model to account for the unique properties of foam are outlined below.

Heat Input

Foam is a structure made mostly of air with thin films of liquid separating the air pockets. Foam does not absorb the incoming radiation in an infinitesimal layer at the foam surface. The radiation penetrates the foam and is absorbed over a finite distance. With this in mind, it cannot be assumed that heat is simply applied at the foam surface. The absorption of the heat takes place over some finite distance within the foam layer. The foam ablation model must incorporate a volumetric generation term to account for the absorbed radiation distribution.

Variable Density and Velocity

A second difference concerns the foam's ability to expand when it is heated. Equation 3 is derived for a constant density material. For that reason, the ablation velocity in the convective term of Equation 3 is constant. In the problem described by Equation 3, all material appears to move towards the front at a single velocity. Foam, on the other hand, expands as it is heated. The expansion is temperature dependent. Consequently, a variable velocity and density field must be accounted for in the foam

ablation problem.

Internal Evaporation

A third difference concerns the evaporation of the water in the foam. In the classic ablation problem, the material is a continuous solid until it reaches the surface of the material. At the surface, the temperature of the material reaches the melting point and the material is melted and removed. In contrast, liquid in the foam can evaporate at any temperature and therefore at any point in the foam. The energy used for the vaporization is equal to the latent heat of vaporization. A volumetric heat sink term is needed in the foam ablation model to account for energy used in the local vaporization of the liquid. This term will vary with distance from the front and will be a function of the rate of change of liquid to vapor.

Governing Equation

The energy equation for the foam ablation problem is obtained by modifying Equation 3 to account for the unique properties of foam described above. The foam ablation model is given by Equation 4

$$\frac{d}{dx}\left(k \frac{dT}{dx}\right) - \rho C_p u(x) \frac{dT}{dx} + \dot{q}_g + \dot{q}_v = 0 \quad (4)$$

where \dot{q}_g and \dot{q}_v are the source and sink terms for radiation absorption and evaporation respectively. The velocity is now written as $u(x)$ to signify its variation within the foam. In addition, the thermal properties are not assumed constant for the foam ablation problem. A solution to Equation 4 requires boundary conditions, property relations, and a mass conservation equation.

The coordinate system for Equation 4 moves with the foam front with its x axis normal to the front and directed into the foam. The velocity term in Equation 4 is defined positive in this coordinate system. Since the foam moves towards the foam front in this coordinate system, the velocity is negative. Figure 12 illustrates the coordinate system and boundary conditions for the foam ablation problem.

ORDER OF MAGNITUDE ANALYSIS

An order of magnitude analysis is used to determine the relative importance of each term in Equation 4. The equation is made dimensionless using the dimensionless variables suggested by White [22] which are given in Equations 5 through 10.

$$x^* = x / l \quad (5)$$

$$\rho^* = \rho / \rho_i \quad (6)$$

$$k^* = k / k_i \quad (7)$$

$$Cp^* = Cp / Cp_i \quad (8)$$

$$T^* = (T - T_i) / (T_f - T_i) \quad (9)$$

$$u^* = u(x) / u_f \quad (10)$$

Subscript i refers to the undisturbed foam conditions far from the foam front. The superscript $*$ denotes the dimensionless variable. The length scale, denoted l , is set to 0.1 meters which is representative of the initial depth of the foam.

In order to complete the dimensional analysis, relations for the source and sink terms are needed. Approximate relations are used at this point to simplify the analysis. The source term is approximated by Equation 11. This term is obtained by assuming the incoming radiative heat flux, q , is distributed evenly over a nominal radiation penetration length denoted by l_m .

$$\dot{q}_g \approx q / l_m \quad (11)$$

The evaporative term is related to the rate of liquid evaporation within the foam. The evaporative rate is obtained from the liquid continuity equation. For the purposes of determining the relative magnitude of the terms in the equation, an approximate equation is used which utilizes the foam density. The foam mass is mainly attributable to the liquid component so this is a reasonable assumption. Equation 12 gives an approximation for the evaporative term.

$$\dot{q}_v \approx h_v \frac{d(\rho u)}{dx} \quad (12)$$

The heat of vaporization is represented by h_v .

Applying the dimensionless variables to Equation 4 and combining terms to produce some relevant parameters results in a non-dimensional foam ablation model which is given by Equation 13.

$$\begin{aligned} \frac{d}{dx^*} \left(k^* \frac{dT^*}{dx^*} \right) - [Pe] \rho^* Cp^* u^* \frac{dT^*}{dx^*} + \\ \left[\frac{q l_m}{k_\infty \Delta T / l} \right] + \left[\frac{Pe}{Ja} \right] \frac{d}{dx^*} (\rho^* u^*) = 0 \end{aligned} \quad (13)$$

The relevant parameters which appear are the Peclet number (Pe) and the Jakob number (Ja). The Peclet number is a measure of the importance of convection relative to diffusion. Jakob number relates the ratio of sensible to latent heat exchange.

To evaluate the magnitude of the parameters in Equation 13, the data from the foam test of Figure 9 are used. It is assumed for the purposes of this analysis that the radiation is absorbed over 10 percent of the overall length scale which makes the ratio of l/l_m equal to 10. Table 5 lists the magnitude of each of the dimensionless terms in Equation 13 assuming the initial conditions of the test illustrated in Figure 9.

Although the terms used to describe the generation and evaporation terms are approximate, this analysis shows that these terms dominate the solution. Convection and diffusion appear to play a minor role in the steady state solution. Convection is approximated to be only 1 percent of the generation and evaporation terms. Diffusion is only 10 percent of the convection terms. Diffusion can obviously be de-emphasized or even ignored in this foam ablation model. It is noted that the evaporation term will have the opposite sign of the generation term. An analysis of these results suggests that the energy from the applied heat flux is absorbed by the foam and used almost entirely to evaporate the liquid in the foam.

FOAM MODEL PRINCIPLES AND ASSUMPTIONS

In order to solve the foam ablation model of Equation 4, assumptions are made to simplify the evaluation of the individual terms. The major assumptions are listed below.

Thermodynamic Equilibrium

Thermodynamic equilibrium is assumed between the liquid and gas components of the foam. In a similar problem of heat and mass transfer in a porous medium [23], it is noted that thermodynamic equilibrium exists between the liquid and gas phases. The thermal response time between the liquid and gas is several orders of magnitude smaller than the times of interest in the problem. This equilibrium assumption is another way of stating that the temperature of the liquid and gaseous phases of the foam are the same at any given location.

Saturated conditions

The gas inside the foam consists of air and vapor. The assumption of saturated conditions is justified in consideration of the very large specific surface area of the foam cell walls and the relatively long time scale of the foam's existence. Sahota and Pagni [24] observe that saturated conditions exist in the similar problem of porous concrete exposed to fire. For the foam model, the vapor pressure within the foam is set equal to the saturated vapor pressure at the given temperature.

Stationary Liquid

The visible foam structure is the liquid component. The stationary liquid assumption states that the liquid making up the foam structure is stationary with respect to the foam structure. The foam structure is free to expand and contract. This assumption implies that the liquid surrounding an air pocket does not drain away from the pocket. The liquid is stationary until it evaporates away.

Essentially this assumption states that the foam drainage is negligible. For the

foams tested in these experiments, little or no foam drainage was observed.

Air and Vapor Escape

It has been observed, and will be quantified in Chapter 4, that the air and vapor have the ability to escape from the foam structure as the foam is heated up. Fresh foam consists of air pockets totally enclosed by liquid with little means of escape. The ability for the air and vapor to escape is increased as the foam structure breaks down due to aging or evaporation. As the air and vapor expand due to the increase in temperature, the foam bubble walls are stretched thinner making it more likely for a rupture and subsequent gas escape.

Separate Convective Terms

Since air and vapor can escape the foam structure, the velocity of the air and vapor are different from the velocity of the liquid making up the structure. This difference affects the evaluation of the convective term. For the purposes of mass and energy balances, the air, liquid, and vapor are considered separately.

Ideal Gases

The air and water vapor are considered ideal gases. This is a valid assumption for these gases in this pressure and temperature range. The ideal gas law is used to relate the density, temperature, and pressure of each gas.

Total gas pressure is assumed constant at 1 atmosphere. The thin cell walls of the foam cannot support any significant pressure difference so the pressure within the foam is considered to be the same as the pressure outside. Surface tension affects on the total pressure are determined to be insignificant.

Steady State

As outlined earlier, a steady state solution approach is used to evaluate the foam ablation problem. As illustrated by Figures 9 and 11, this approach will represent a significant portion of the data available from the foam ablation tests.

Mass Conservation

The basic equations governing the foam ablation model are determined from the fundamental conservation laws. This includes the conservation of mass. For this problem, momentum conservation is insignificant.

A mass conservation equation is written for each of the components in the foam. The continuity equation for each component is listed below.

$$\frac{d((1-f) \rho_a u_a)}{dx} = 0 \quad \text{air} \quad (14)$$

$$\frac{d(f \rho_l u_l)}{dx} = \Gamma_l \quad \text{liquid} \quad (15)$$

$$\frac{d((1-f) \rho_v u_v)}{dx} = \Gamma_v \quad \text{vapor} \quad (16)$$

The term f represents the liquid volume fraction. The liquid and vapor continuity equations contain a sink (or source) term because liquid is evaporating to form vapor. These terms on the right hand side of Equations 15 and 16 account for this loss or gain of mass and have units of $\text{kg/m}^3\text{-s}$. An overall continuity equation indicates that the loss of liquid equals the gain in vapor. Equation 17 specifies this relation.

$$\Gamma_v = - \Gamma_l \quad (17)$$

CHAPTER IV

SUBMODELS AND ASSOCIATED EXPERIMENTS

A description of each of the terms in the energy equation is needed in order to solve the foam ablation problem. Data describing fire-protection foam properties are not generally available. For terms which cannot be described from available data, specific experiments are conducted to uncover their behavior. From available data and the specific experimental results, submodels for the individual terms are developed. A description of the individual models and associated experiments is outlined in this chapter.

GENERATION TERM

The generation term accounts for the input of energy to the foam by absorption of thermal radiation within the foam structure. In order to compute this term it is necessary to know the absorption characteristics of the foam structure. No data are readily available on the absorption characteristics of fire-protection foams due to the complexity of the absorption process. Some simplifying assumptions are made to allow an estimate of the absorption characteristics to be determined.

The geometry of the foam structure complicates the radiation absorption problem. Once the thermal radiation enters the foam it encounters an array of randomly aligned thin liquid surfaces separated by air and steam. The liquid is made up mostly of water which is a strong absorber of radiation in the infrared. Air and

steam at these conditions are weak absorbers compared to the water and do not participate significantly in the absorption process. As radiation encounters each liquid surface, some is reflected away and some penetrates the surface. The radiation penetrating the liquid films is partially absorbed and partially transmitted. Absorbed energy in these thin liquid surfaces is converted to heat and elevates the temperature of the foam. This energy transfer to the foam is the basis for the volumetric generation term in the foam ablation model. The generation term is an important term in the model as illustrated by the order of magnitude analysis summarized in Table 5. This term defines how and where the heat is applied to the foam.

Theoretical Background

For radiation passing through a differential layer of foam, the reduction in radiation intensity is given by the following formula [25].

$$di_{\lambda} = -\kappa_{\lambda}(x) i_{\lambda} dx \quad (18)$$

Equation 18 states that the decrease in intensity is proportional to the incoming intensity multiplied by the distance traveled through the medium. The proportionality constant, κ_{λ} , is called the extinction coefficient. Integrating this relation along a path length leads to Bouguer's Law which gives a relation for the intensity of radiation as a function of penetration distance x . Emission by the foam is neglected. Bouguer's law is given by Equation 19.

$$i_{\lambda}(x) = i_{\lambda}(0) \exp\left[-\int_0^x \kappa_{\lambda}(s) ds\right] \quad (19)$$

The extinction coefficient is made up of an absorption coefficient (a_λ) and a scattering coefficient (σ_λ). Subscript λ indicates the spectral dependence of these properties. The extinction of radiation is the result of absorption and scattering and the extinction coefficient is the summation of these two terms as shown in Equation 20.

$$\kappa_\lambda = a_\lambda + \sigma_\lambda \quad (20)$$

In general, the extinction coefficient increases as the density of the absorbing or scattering medium is increased [25]. Translating this generalization to the foam implies that the extinction coefficient increases as the water content within the foam (or foam density) increases. These coefficients have units of one over length.

Experimental Approach

The complexities of the radiation absorption and scattering process in a composite material like foam make analytic approaches to determining these properties overwhelming. In order to get quantitative information on the extinction coefficient, simplifying assumptions and experimental measurements are made. The properties are assumed to be independent of wavelength. This engineering simplification makes it possible to gain a representative value for the extinction coefficient without the complexities of the spectral dependence.

A common practice has been to approximate extinction coefficients of absorbing and scattering media using Bouguer's Law applied to measured transmission data from relatively thin samples [26]. This method requires a modest

experimental setup and is considered adequate for the purposes of the present investigation. A simple experiment is set up which consists of a uniform slab of foam placed between a radiation source and detector. The detector measures the intensity of radiation reaching it's surface. Figure 13 illustrates the experimental setup. The radiation source is a tungsten filament heat lamp with a filament temperature of approximately 3500K [27]. A photodetector and a heat flux gauge are used separately as radiation detectors. Differences are described below. Output from the detectors is recorded using a calibrated strip chart recorder. Both detectors output voltage proportional to the radiation level.

Two measurements are made for each foam sample tested. First, a value for the transmitted intensity, $i(x)$, is obtained with a foam sample of thickness x placed between the source and detector. Second, the incoming intensity, $i(0)$, is measured at the detector with no foam present. The foam sample is assumed to be uniform so the coefficient does not vary along the path length. Using the prior assumptions along with Bouguer's law, the extinction coefficient is obtained from Equation 21.

$$\kappa = -\frac{1}{x} \ln \frac{i(x)}{i(0)} \quad (21)$$

The extinction coefficient is a measure of how fast the radiation is diminished along the path length through the foam sample. Radiation is diminished through absorption of the radiation by the material and by scattering of the radiation away from the detectors view.

In the one-dimensional foam ablation model, the foam and the radiation source

occupy infinite planes. In this type of problem, the net scattering away from the direction of radiation travel is zero. The net radiation flux travels in the x direction only. The experimental setup is not one-dimensional however. The affect of scattering will increase the measured extinction coefficient.

An absorption only coefficient is desired for the foam ablation model since the net affect of scattering is assumed to be insignificant. An approximate method of separating the absorption and scattering coefficients is proposed. The experimental approach and the results for the extinction and scattering coefficients are outlined below. The absorption coefficient is not measured directly. The absorption coefficient is estimated from Equation 20 using measurements of extinction and scattering coefficients.

Extinction Coefficient

Experiments are conducted on 1.0 cm thick foam samples of various densities. A 250 Watt heat lamp which produces radiation over a broad spectrum is used as the radiation source. A Schmidt-Boelter type heat flux gauge is used as the detector. The heat flux gauge is sensitive to a broad range of radiation in the infrared. Spectral range is discussed below in reference to the scattering coefficient.

Two steps are conducted for each foam sample tested. The heat lamp is turned on for 10 seconds and an initial reading is taken with no foam present. This value is stored as $i(0)$. Next, a foam sample is placed between the light and detector and the light is again turned on. This reading is stored as $i(x)$. Extinction coefficient, κ , is calculated from Equation 21 with x set equal to 0.01 meters.

The results for several different foam samples are illustrated on Figure 14. These data show the value of the extinction coefficient rises with an increase in foam density as predicted by Siegel and Howell [25].

Scattering Coefficient

A modification to the above procedure for determining extinction coefficients is used to obtain an estimate of the scattering coefficient. The technique is based upon minimization of the absorption coefficient so the scattering coefficient can be isolated and measured. The extinction coefficient is equal to the scattering coefficient when the absorption coefficient is zero. Minimization of the absorption coefficient is described below.

Figure 15 illustrates the absorption spectra of water and the spectral response characteristics of the two radiation detectors used for these experiments. The black body distribution for a body at the temperature of the tungsten heat lamp filament is also illustrated for reference.

The water absorption peaks at a wavelength between 2 and 3 microns. The absorption coefficient of water falls several orders of magnitude as the wavelengths drop below 1 micron. Radiation in the spectral range below one micron is not significantly absorbed by water.

The heat flux gauge has a nominal sensor absorptance of 92 percent in the wavelength range from 0.6 to 15.0 microns. This broad range goes from the visible to the infrared. The photodetector sensor is only sensitive to wavelengths smaller than 1 micron. These sub-micron wavelengths are not significantly absorbed by water.

Since the sub-micron radiation is not absorbed by water, it is assumed that the foam does not absorb radiation in this spectral range. When using the photodetector as the sensor for the extinction coefficient measurements, only the wavelengths below one micron are important. The extinction coefficient obtained from these experiments is a good estimate for the scattering coefficient of radiation with a wavelength less than one micron.

In general, scattering coefficients are wavelength dependent and the estimate for the sub-micron scattering coefficient is not directly related to the scattering in the thermal radiation range of interest. In this case, the scale of the bubbles is two orders of magnitude larger than the wavelengths considered. Geometric optics is assumed as a reasonable assumption in these wavelength ranges. The scattering coefficient is assumed to be wavelength independent since it is principally governed by geometric optics [28]. Using this assumption, the measured sub-micron scattering coefficient is assumed to be a good representation of the scattering coefficient in the infrared region of interest.

Experiments are conducted on samples which are systematically sliced down from 2 to 3/8 inches in 1/8 inch increments. Data are collected after each slice is removed. A total of 14 individual measurements are collected for each foam sample. The scattering coefficient results for five different foam samples are illustrated on Figure 16. The average value of each set of 14 measurements is indicated on the plot along with error bars indicating the standard deviation interval for each value. These data show the scattering coefficient is nearly independent of foam density over the

range of densities tested. The average value of the scattering coefficient data is 92.8/m and this value is shown on the figure as a dotted line.

Absorption Coefficient

Once the scattering and extinction coefficients are determined, the absorption coefficient is obtained from Equation 20. Figure 17 illustrates the absorption coefficient of the foam as a function of density. These are the extinction coefficient data from Figure 14 reduced by 92.8/m to account for the affect of scattering in the experimental setup. The data are spread apart but show a definite upward trend of absorption coefficient with foam density.

A proportionality relation is used to fit the data to ensure that zero foam density yields zero absorption. The proportionality constant found for the data of Figure 17 is 3.02 m²/kg. A value of 3 is used in the model. The proportionality relation is shown as the solid line in Figure 17. Equation 22 summarizes the relation for the absorption coefficient.

$$a = C \rho_f \quad C = 3 \left(\frac{m^2}{kg} \right) \quad (22)$$

Model of Generation term

With the preceding simplifications made to obtain the absorption coefficient, the radiation distribution within the foam is calculated. The intensity of radiation as a function of the depth in the foam, $i(x)$, is obtained from Equation 19 using the value of σ for the extinction coefficient. The required generation term is obtained from the spatial derivative of the intensity function. Equation 23 relates the generation term to

the derivative of the intensity function for incoming radiation q .

$$\dot{q}_g(x) = - \frac{d}{dx} [q \exp - (3 \int_0^x \rho_f dx)] \quad (23)$$

This relation states that the volumetric absorption of radiation is equal to the rate of decrease in radiation intensity with distance. Since the absorption coefficient is related to the foam density, the foam density profile must be known in order to compute the generation term. The FORTRAN program used to compute the radiation generation term is listed in Appendix A.

DENSITY

The densities of the various phases (i.e. liquid, steam, and air) are required in the solution of the foam ablation problem. Overall foam density is used in the evaluation of the generation term. Individual component densities are used for their respective continuity equations and the convective terms. Densities of the foam constituents as a function of temperature are known from thermodynamics. The foam density is related to the individual densities through Equation 24 which utilizes the liquid volume fraction.

$$\rho_f = \rho_l(f) + (\rho_v + \rho_a)(1-f) \quad (24)$$

A method is needed to specify the foam density and therefore the liquid volume fraction as a function of temperature.

When the foam is first produced, the initial density and temperature of the foam are recorded. The initial liquid volume fraction is uniquely determined from these data using Equation 24. The initial liquid volume fraction of the foam is also one over the foam expansion ratio. The initial gaseous fraction is equal to one minus the liquid volume fraction.

These initial data are only the starting point for a foam density function. The problem of specifying a density function for the foam lies in the dynamic nature of the foam material. Foam is constantly going through changes. Liquid evaporates from the foam. Individual bubbles burst and coalesce with one another. Air and vapor escapes. All of these processes change the density of the foam and take place at a single uniform temperature.

Consider foam with an initial density of 50 kg/m^3 held at a uniform temperature. After some time the water evaporates away but the foam structure retains most of its initial volume. The density of this dry material approaches the density of air. The density of the foam, therefore, cannot be explicitly determined from temperature alone. Foam density is a transient value dependent at least upon temperature, time, foam breakdown rates, and the surrounding conditions. A model to account for all of the processes which affect the foam density is not practical for the present steady state foam ablation model requirements. A realistic foam density model is proposed.

Ideal Foam Density

First, an ideal model for the foam density as a function of temperature is

proposed. The model is based on an ideal foam which lets no air or vapor escape as the foam expands with temperature. Foam expansion is based on ideal gas relations and the assumption of saturated conditions within each bubble. This is an idealization since a real foam's bubbles tend to break up and let air and vapor escape as they expand. The ideal foam density model serves as an upper bound on the foam's expansion.

The starting point for the ideal foam density function is the initial foam condition. This consists of a measured foam density and temperature. The foam model assumes thermodynamic equilibrium between the liquid and vapor, saturated vapor conditions, and ideal gas relations.

A rise in temperature of the foam causes the air and vapor within the bubbles to expand. As the bubbles expand, more liquid evaporates to maintain saturated conditions within the bubble. It is assumed that each foam bubble remains intact and that the total pressure within the bubbles is one atmosphere. Any pressure difference from inside to outside of the foam is negligible compared to the total pressure.

The vapor pressure is obtained as a function of temperature from thermodynamic tables. A partial pressure analysis is used on the air and vapor. The vapor partial pressure is the saturated vapor pressure at the given temperature. The air partial pressure is the total pressure (one atmosphere) minus the vapor pressure.

Since the mass of the air within each bubble is constant, the volume of the air is calculated from the ideal gas equation given by Equation 25.

$$V_a = \frac{m_a R_a T}{P_a} \quad (25)$$

This relation gives the air volume as a function of the air mass, the gas constant, absolute temperature, and the air partial pressure. The air pressure in the denominator is temperature dependent since it is obtained from the difference between atmospheric pressure and the temperature dependent vapor pressure.

The vapor and air occupy the same space so the vapor volume equals the air volume. Since the vapor pressure is known as a function of temperature, the vapor mass within each bubble is calculated from the ideal gas equation. The increase in mass of vapor due to evaporation is equal to the decrease in the mass of liquid. The remaining liquid mass is directly calculated. Liquid volume is calculated from the known liquid density.

At this point, values for the mass of air, vapor, and liquid are known along with the volume of gas and liquid. Total volume is the simple sum of the gas and liquid volumes. The total mass does not change with temperature since the assumption is made that no air or vapor escapes from the foam structure. The foam density is calculated as the total mass divided by the total volume.

Figure 18 illustrates an ideal density function. As expected, the density of the foam decreases with temperature as the liquid is evaporated. The starting point of the function, labeled "A", is determined from a physical measurement of freshly produced foam. The end point, labeled "C", is essentially the density of the air and vapor mixture at 100°C.

This idealized density function serves as a basis for the determination of a realistic density function. The realistic density function is obtained by manipulating the ideal foam density function so it agrees with the physical measurements and observations made in the lab. The FORTRAN code which computes the ideal foam density model is listed in Appendix A.

Foam Expansion Measurements

To gain some insight on the behavior of the actual foam as it is heated up, foam expansion measurements are made. A beaker containing a volume of foam, V_i , at a uniform initial temperature (usually 20°C) is placed in a convection oven at a fixed temperature T . The volume of the foam, V , is recorded when the foam temperature reaches T . Foam volume peaks as the temperature reaches the desired value and then the foam volume slowly declines as the foam evaporates away. The maximum volume point is recorded as V . Foam expansion is defined as V/V_i .

Figure 19 illustrates the data obtained from these experiments. Nominal expansion ratios of 13, 20, 27, and 32 are tested. The data indicate that the higher expansion ratio, dry foam, is unable to expand as far as the wetter low expansion ratio foam. Bubbles in the high expansion foam tend to rupture at lower temperatures letting air and vapor escape. The wetter foam contains more liquid in the bubble walls which allows it to expand further before bubble rupture. The upper curve on the plot, solid line, represents the volumetric expansion of the ideal foam model described earlier. This ideal expansion curve serves as a theoretical upper limit on the foam's expansion since it assumes that no air or vapor escape.

The measured expansion data generally follow the trend of the ideal curve up to a point. The more liquid the foam contains, the longer it is able to generally follow the upward expansion trend with temperature. By the time 80°C is reached, each of the foam's expansion values seem to level out. It is hypothesized that at 80°C the foam is acting like a porous structure and allows air and vapor to escape freely as they expand with temperature.

These measurements indicate qualitatively how the air and vapor escape from the foam. However, the volume expansion does not indicate how the density will change since the mass is not specified. Mass cannot be specified as a function of temperature because the mass of the foam is constantly decreasing due to evaporation and the associated air and vapor escape. The mass loss is very slow and can be neglected for short periods of time at room conditions. Elevated temperatures, however, accelerate the mass loss process. Mass loss measurements were attempted with little success. The small samples tested had mass differences near the resolution of the available measuring equipment and the data are considered meaningless.

The measured foam expansion data are valuable for use in the foam model. These data set a real upper limit on foam expansion as it is heated. A table of the measured volume expansion data is created by smoothing the data in Figure 19. This table is plotted in Figure 20. These data are interpolated to obtain the volume expansion of a foam at a given temperature with a known initial foam expansion ratio between 13 and 32. This table serves as the basis of the foam volumetric expansion with temperature for the foam ablation model.

Realistic Foam Density Model

A realistic method is proposed to model the foam density as a function of temperature. The density model is a variant of the ideal foam model. The ideal model is modified to account for experimental data and observations.

The first experimental observation is that the foam does not break down very rapidly at low temperatures. Since the foam does not break down rapidly at low temperatures, the realistic density model is expected to follow the ideal density model for the first few degrees of temperature rise. The realistic density model must also begin at the same point as the ideal density model since this is a measured value. The deviation from the ideal density model is expected to increase with temperature.

A second observation comes from the foam protection tests. Figure 9 shows data obtained in a foam protection test. It is noted that the foam temperatures generally level out at approximately 80°C. At some point, the liquid in the foam completely evaporates and the temperature quickly goes over 100°C. Once the liquid is gone the material is no longer considered a fire-protection foam. For the purposes of a density model, 80°C is set as a limiting temperature. The foam density must approach the density of an air and vapor mix at a foam temperature of 80°C.

Figure 21 illustrates a realistic density function which has the appropriate characteristics. This function is a variant of the ideal density function of Figure 18 which is also illustrated on this figure as a reference. The realistic density function endpoints, A and B, are determined from experimental results. The remainder of the function is calculated by linearly scaling the temperature scale from the ideal density

function using the following relation.

$$T_{real} = T_{ideal} - \left(\frac{T_{ideal} - T_i}{T_f - T_i} \right) (T_{sat} - T_f) \quad (26)$$

The ideal and realistic densities are equal at the initial temperature. At the front temperature, 80°C, the realistic density is set to the ideal density associated with 100°C (T_{sat}). A linear scaling of the temperature scale is chosen for its simplicity and is not based on the physics of the foam problem.

The resulting density function has the required characteristics at its endpoints and smoothly translates from one known endpoint to the other. The deviations from the ideal function are small at the low temperatures and grow with temperature. This density function is considered to be a realistic estimate of the foam density as a function of temperature for the purposes of the steady state foam ablation problem.

Liquid Volume Fraction

The proposed foam ablation model separates the foam into its air, vapor, and liquid components. In order to keep track of the amounts of each remaining in the foam structure, the liquid volume fraction is used.

Liquid volume fraction is determined from Equation 24. At a given temperature the foam density is obtained from the foam density function. Component densities are calculated from thermodynamic relations. The liquid volume fraction is the only unknown in Equation 24 and is calculated directly.

Density of foam components

Liquid. The liquid which makes up the foam solution is a mixture of three

percent foam concentrate and 97 percent water. The foam concentrate is water based which makes the foam solution over 97 percent water. For the purposes of the foam model, the density of the liquid is assumed to equal the density of pure water. Changes in density with temperature are neglected. The liquid density is set to the constant value of 1000 kg/m^3 .

Air and Vapor The air and vapor in the foam are treated as ideal gases. The density of each is obtained directly from the ideal gas equation. The pressure used to calculate the density of each component is the components partial pressure. Partial pressure of the vapor is assumed to be the saturation pressure at the given temperature. Total pressure is assumed to be one atmosphere.

SPECIFIC HEAT

The foam model requires the specific heat in the convective terms for each component. Constant specific heats are assumed for this model. Table 6 lists the specific heats used for the individual components. The specific heat of the liquid component is set equal to the specific heat of water since the liquid component is over 97 percent water.

ABLATION VELOCITY

An important step in the foam ablation model is the calculation of the moving foam front velocity. A steady state steady flow [29] control volume analysis is used to compute the ablation velocity. Figure 22 illustrates the control volume used in the

analysis.

The control volume is fixed to the moving foam front at one end and moves at the ablation velocity into fresh unheated foam at the opposite end. With no work done by the control volume, the first law of thermodynamics reduces to

$$q + \sum \dot{m}_i h_i = \sum \dot{m}_f h_f \quad (27)$$

where h is the specific enthalpy, \dot{m} is the mass flux, and q is the rate of heat transfer to the control volume.

The rate of heat transfer to the control volume, q , is equal to the incoming radiative heat flux which is normal to the x direction. The heat flux entering the control volume is completely absorbed by the foam. The total mass within the control volume is constant for steady state conditions so incoming mass flux is equal to the outgoing mass flux. Written in terms of the unheated foam conditions entering the control volume, the mass flux is given by

$$\dot{m}_i = \dot{m}_f = \left(\rho_l \frac{1}{xp} + \rho_v \left(1 - \frac{1}{xp}\right) + \rho_a \left(1 - \frac{1}{xp}\right) \right) u_f \quad (28)$$

where u_f is the velocity of the moving foam front. The mass flux is evaluated at the entrance conditions where the volume fraction and component densities are known from the initial conditions. By definition, the initial liquid volume fraction equals the reciprocal of the foam expansion ratio. The unheated components entering the control volume all move together relative to the foam front at the ablation velocity u_f .

Substituting the mass flux and heat input terms into the first law equation and solving for the ablation velocity results in Equation 29.

$$u_f = \frac{q}{\rho_l \frac{1}{xp} (h_f - h_i)_l + \rho_a (1 - \frac{1}{xp}) (h_f - h_i)_a} \quad (29)$$

Subscripts *l* and *a* denote the liquid and air respectively. The initial vapor mass flux is very small and its contribution is neglected.

Equation 29 gives the ablation velocity as a function of the incoming heat flux, the initial expansion ratio of the foam, initial density of the air and liquid, and the change in enthalpy for each component. The density and enthalpy data are obtained from standard thermodynamic tables for air and saturated water.

VELOCITY OF COMPONENTS

As the foam expands, the air and vapor begin to escape from the foam structure. Each foam component has its own velocity. These velocities are needed in order to represent the convection terms in the foam ablation model. The velocities are determined using mass conservation equations so the continuity equations are satisfied. The velocities are written in terms of the temperature to facilitate the solution. The FORTRAN code which computes the component velocities is contained in the conservation of mass section of Appendix A

Liquid Velocity

The liquid in the foam makes up the visible structure of the foam. It is

assumed that the liquid is stationary with respect to the foam structure. Liquid velocity is therefore the velocity of the foam structure.

Figure 23 is used as an illustration in the determination of the liquid component velocity. This figure illustrates two control volumes in the foam as the foam front moves towards the control volumes. Control volume V1 is within the undisturbed portion of the foam and moves at a velocity $-u_f$ relative to the front. As the front approaches control volume V1 the temperature at this point increases. Control volume V2 represents the size and position of V1 at some later time. Control volume V2 is at an elevated temperature and therefore has expanded relative to V1. Dimensions X1 and X2 represent the physical dimensions of the control volumes.

Given the temperature at the location of control volume V2, the ratio V2/V1 is obtained from the foam volumetric expansion data. Since the problem is one-dimensional, all of the expansion is in the x direction and the ratio V2/V1 equals X2/X1. The velocity of control volume V2 relative to the foam front is u_l . At steady state conditions, the following formula is used to find u_l .

$$u_l = (-u_f) \frac{X_2}{X_1} \quad (30)$$

Since X2/X1 is obtained from the volume expansion data (V/V_i) at a given temperature, the value of the liquid velocity is determined uniquely as a function of temperature. Equation 31 gives the relation for the liquid velocity component.

$$u_l = -u_f \frac{V}{V_i} \quad (31)$$

Vapor Velocity

The vapor is formed from the evaporation of the liquid component. The velocity of the vapor is influenced by two factors. The vapor expands as it is heated up and the mass flux of vapor increases with temperature due to evaporation. Figure 24 is used to outline the determination of the vapor velocity.

Position 1 on Figure 24 defines a position in the unheated foam where the air, vapor, and liquid move at the same velocity. The velocity of all components at this position is $-u_f$ relative to the front and properties at position 1 are denoted by the subscript i. Position 2 defines a position closer to the front where the unknown velocities are computed.

From continuity and the steady state assumption, the combined mass flux of steam and liquid is a constant at any point. The total mass flux for these components is computed at position 1 and given by Equation 32. The total mass flux of vapor and liquid is noted as \dot{m}_{l+v} .

$$\dot{m}_l + \dot{m}_v = \dot{m}_{l+v} = (\rho_l f_i + \rho_{v,i}(1 - f_i))(-u_f) \quad (32)$$

At position 2, the temperature is known so the component densities and volume fraction are uniquely determined. The liquid mass flux is evaluated using the liquid velocity of Equation 31 and is given by Equation 33.

$$\dot{m}_l = \rho_l f u_l \quad (33)$$

In a similar manner, vapor mass flux at position 2 is defined by Equation 34.

$$\dot{m}_v = \rho_v (1 - f) u_v \quad (34)$$

Substituting Equations 33 and 34 into equation 32 and solving for the vapor velocity results in Equation 35.

$$u_v = \frac{\dot{m}_{l+v} - \rho_l f u_l}{\rho_v (1 - f)} \quad (35)$$

For a given temperature, Equation 35 defines the velocity of the vapor component relative to the front. Velocity terms are all negative since the velocity is towards the front. It is noted that the total mass flux, \dot{m}_{l+v} , is defined as a negative value.

Air Velocity

The air velocity is determined in a manner similar to the vapor velocity. Refer again to Figure 24. In this case, the mass flux of air is constant at any point and can be evaluated at position 1. Equating the mass flux at positions 1 and 2 and solving for the velocity at position 2 results in Equation 36.

$$u_a = \frac{\rho_{a,i} (1 - f_i) (-u_f)}{\rho_a (1 - f)} \quad (36)$$

EVAPORATIVE TERM

The evaporative term accounts for the energy absorbed as latent heat by the liquid which vaporizes within the foam. The liquid vaporization rate is determined

from the mass sink term in the liquid continuity equation. The equation for steady state liquid continuity is given by Equation 16. The term Γ_l represents the rate of change of liquid density due to evaporation and has units of kg/m³-s. The evaporative term is obtained by multiplying the rate of change of liquid density by the latent heat of vaporization. Equation 37 defines the evaporative term.

$$\dot{q}_v = h_v \frac{d}{dx} (\rho_l f u_l) \quad (37)$$

The evaporative term has units of Watts/m³.

CONVECTIVE TERMS

Separate convective terms are used since the velocity of the air, liquid, and vapor are not equal. The summation of the convective terms is given by Equation 38.

$$(f \rho_l C_{p_l} u_l + (1 - f) \rho_v C_{p_v} u_v + (1 - f) \rho_a C_{p_a} u_a) \frac{dT}{dx} \quad (38)$$

The temperature derivative is the same for each term since thermodynamic equilibrium is assumed to hold.

THERMAL CONDUCTIVITY

Fire-protection foam is an insulative material with small pockets of air surrounded by a liquid medium which is nearly stationary. No data were found on the thermal conductivity of fire-protection foams. Industrial foams such as building insulations and plastic foams [30] have been studied for some time. An equation

which models the thermal conductivity of closed cell foam insulation is derived by Schuetz and Glicksman.[31] This equation, neglecting radiation, is given below.

$$k_{effective} = k_{gas} + \left(\frac{2}{3} - \frac{P_s}{300} \right) (f) k_{solid} \quad (39)$$

Equation 39 is valid for geometrically isotropic foam. P_s is percentage of the solid material which is contained in the struts of the foam. The solid fraction, f , is equivalent to the liquid volume fraction for the liquid fire-protection foams. In another report, Glicksman and Torpey [32] illustrates the validity of this equation on foam insulations with a nominal cell diameter of 300 μm . It is noted that the average cell diameter of the fire-protection foams used in this study is between 200 and 300 μm .

This equation is applied to the fire-protection foams used in the current experiments. To get an upper bound it is assumed that all of the liquid is contained in the cell walls. This sets the value of P_s to zero. With these assumptions, the formula for the thermal conductivity of the fire-protection foam is

$$k_f = k_{gas} + \frac{2 f k_{liquid}}{3} \quad (40)$$

Values for the thermal conductivity of the foam are easily evaluated using Equation 40. Nominal values for the thermal conductivity of air and water are 0.03 and 0.67 Watt/m-K respectively. Table 7 lists the thermal conductivity of three water and air foams using the above formula.

Experimental Approximation of Thermal Conductivity

Typical methods of determining the thermal conductivity of a material are difficult if not impossible to apply to liquid foams. Guarded hot plate techniques[33], for example, would completely dry the foam without reaching a steady state solution. Due to the transient nature of the foam, a transient technique to estimate the thermal conductivity is needed.

A transient technique outlined by Kennedy [34] is used to determine the thermal diffusivity of the fire-protection foam. Thermal conductivity is then determined from the diffusivity measurement by computing the specific heat and density of the foam. This technique is a simple technique to apply and requires a minimum of instrumentation.

Three thermocouples are placed above a hot plate as illustrated in Figure 25. The plate and thermocouples are covered with a thick layer of foam and heat is applied by the hot plate. Temperature measurements from the three thermocouples are recorded at known time intervals. The set-up is designed to produce a one-dimensional heat flow past the thermocouples.

To determine the thermal diffusivity, the constant property heat equation is solved on the interval between the first and third thermocouples of Figure 25. The boundary conditions for the one-dimensional solution are the measured temperatures at the thermocouple locations. For an input value of the thermal diffusivity, the numerical solution is used to generate the temperature history at the central thermocouple location. The value of the thermal diffusivity is optimized to minimize

the error between the measured and calculated temperature rise at the center point thermocouple. This method functions well at low temperatures before the foam evaporates away.

A nominal value of the thermal diffusivity found from such experiments is $0.5 \times 10^{-6} \text{ m}^2/\text{s}$ with a center point average temperature of 40°C . Assuming an initial foam expansion of 18, the density and specific heat of the foam would be approximately 48 kg/m^3 and 4100 J/kg-K respectively. Using these values, the thermal conductivity is 0.098 W/m-K . This experimental value is consistent with the predicted values of thermal conductivity from Table 7.

For the purposes of the foam ablation model, the thermal conductivity is set to the constant value of 0.1 W/m-K for all foam densities. The order of magnitude analysis summarized in Table 3 indicates the diffusion term plays only a minor role in the energy balance. Further refinement of the thermal conductivity is unwarranted at this point in time.

CHAPTER V

EQUATION SUMMARY AND NUMERICAL SOLUTION

EQUATIONS

Utilizing the submodels and equations outlined in Chapter IV, the full foam ablation model is given by Equation 41.

$$k_f \frac{d^2 T}{dx^2} - (f \rho_l C p_l u_l + (1-f) \rho_v C p_v u_v + (1-f) \rho_a C p_a u_a) \frac{dT}{dx} - \frac{d}{dx} [q \exp - (3 \int_0^x \rho_f dx)] + h_v \frac{d}{dx} (\rho_l f u_l) = 0 \quad (41)$$

Each of the major equations for the submodels are summarized in Table 8 along with the equation number.

NUMERICAL SOLUTION

A numerical procedure is used to solve the foam ablation model. The steady state solution is approached asymptotically using a time dependent approach. A modified second order Crank Nicolson technique is used to advance the solution in time.

Stability problems are encountered when a time dependent generation term is computed for each step. This term is a large contributor to the energy balance and greatly affects the solution. To eliminate unstable oscillations caused by the generation term, this term is fixed during the solution procedure.

Fixing the generation term requires calculation of the term prior to solving equation 41. Calculation of the generation term requires the density profile which is obtained from the temperature profile and density function. Since the temperature distribution is unknown prior to solving Equation 41, an iterative solution procedure must be used.

Iterative Procedure

An iterative solution procedure is used to solve Equation 41. The procedure typically converges within ten iterations. The procedure involves guessing at a temperature profile in order to compute a generation term which in turn is used in the solution of Equation 41 for a new temperature profile. The iterative solution procedure is outlined by the following steps:

- (1) Assume initial temperature profile. A linear temperature profile varying from T_f to T_i over the solution range is used here.
- (2) Compute a density profile from the temperature profile using the foam density model.
- (3) Compute the generation term from Equation 23 using the density profile.
- (4) Compute a new temperature profile utilizing the generation term in Equation 41.
- (5) Repeat steps 2 through 4 until the resulting temperature profiles converge.

Numerical Example

A complete solution is generated to simulate the foam test case illustrated in

Figures 9 and 11. This example uses the test conditions from foam test case K in Table 4. Each step in the solution procedure is described below.

Boundary Conditions. The boundary conditions used to solve Equation 41 are obtained from the foam test conditions. The foam front condition is the maximum foam temperature which is set to 80°C based on the experimental observations. The far field (unheated foam) boundary condition is the initial temperature of the foam. In case K this corresponds to 22°C.

Foam Density Function. The foam density function is obtained using the method outlined in Chapter IV. Figure 21 illustrates the realistic foam density function used for this case. The endpoints of the function, 22°C and 80°C, are the boundary conditions of the foam ablation model.

Liquid Volume Fraction. Once the foam density function is specified, the liquid volume fraction is determined from Equation 24. Note that component densities in Equation 24 are determined from ideal gas relations or thermodynamic tables. Since the gas densities are functions of temperature, the liquid volume fraction is determined as a function of temperature. Figure 26 illustrates the liquid volume fraction determined for this example. Liquid volume fraction starts at 0.055 which is the inverse of the initial foam expansion. The liquid volume fraction goes to zero at 80°C since the water is completely evaporated at this point.

Velocity of Components. The ablation front velocity for this test case is found using Equation 29. The velocity of the front is determined to be 1.25×10^{-4} m/s. Velocities for the individual foam components are calculated using Equations 31, 35,

and 36 respectively. Figures 27, 28, and 29 illustrate the velocity of the liquid, vapor, and air components as a function of temperature.

The velocity of the moving foam front is u_f into the foam. The velocity of the unheated foam components far from the foam front is therefore $-u_f$ relative to the front. Since the components expand, the magnitude of the velocity increases with increasing temperature. The vapor velocity of Figure 28 shows the largest increase with temperature. This is due to the increasing vapor mass flux caused by the evaporating liquid.

Iterative Solution. The iterative procedure is carried out to compute a steady state temperature profile from Equation 41. This procedure is outlined above. The computed temperature profiles for each step of the iteration procedure are illustrated in Figure 30. Profiles are numbered consecutively with “1” representing the initial linear guess at the temperature profile. A total of 12 iterations are completed for this example. The temperature profiles labeled 10 through 12 lie on top of one another indicating convergence of the solution.

Energy Balance. The terms in Equation 41 are computed individually to allow a comparison of the relative importance of each term in the energy balance. Figures 31 and 32 illustrate the terms in the energy balance.

The generation term and the evaporative term are illustrated in Figure 31. These two terms represent the largest contributors to the energy balance. The evaporative term is approximately the mirror image of the generation term.

The diffusion and convective terms are illustrated in Figure 32. The largest

term is the liquid convection term. This term, however, is less than 10 percent of the magnitude of the generation term in Figure 31. Air convection is negligible and is not shown on the figure. The minimal affect of the air convection is not surprising considering the air density. Vapor convection and diffusion play minor rolls in the energy balance.

Generally speaking, the convective and diffusion terms do not significantly affect the energy balance. Elimination of these terms would not greatly influence the results. The results indicate that heat is absorbed by the foam and used almost exclusively to evaporate the liquid in the foam at the point of absorption. These results agree with the approximate order of magnitude analysis summarized in Table 5.

Comparison With Foam Test. The boundary conditions used for this numerical example matched the test conditions for case K in Table 4. This makes a comparison of the numerical and experimental results possible. The steady state temperature as a function of distance is illustrated in Figure 11. These data are plotted with the numerical temperature profile on Figure 33. The numerical solution is positioned on the figure to match the experimental results in the central region of the profile where the experimental results are well defined. This facilitates a visual comparison of the numerical and experimental results. Comparison of the data near the endpoints is difficult since the endpoints of the experimental data are uncertain.

Good agreement is realized between the numerical and experimental result. The numerical solution lies within the band of the experimental data. Detailed results for each case are discussed in the next chapter.

CHAPTER VI

RESULTS AND DISCUSSION

The results consist of experimental data and the output from the foam ablation model. Experimental data are limited to the temperature data because this is the only measured variable. The model computes the temperature profile and is directly comparable to the experimental results. The model results, however, also include the individual terms in the energy balance which work together and give the temperature profile its shape. The terms in the energy balance are used to look at the conditions within the foam which help to form the calculated temperature profile.

FOAM TEST RESULTS

A total of 26 foam tests are completed using the procedures outlined in Chapter II. The test conditions for each of the experiments are listed in Table 4. The 26 test cases reported are all conducted using identical test procedures. The foam generator configuration and foam solution are identical for each case. In addition, each test uses the same test plate and thermocouples. These data are analyzed to look for similarities and trends.

The results of each foam ablation test are illustrated in Figures 34 through 59. Each figure consists of two plots denoted A and B. The temperature measurements versus time are given in Figures 34A through 59A. Each set of data are transformed into a steady state temperature profile and illustrated in Figures 34B through 59B. The

numerical solution obtained from the foam ablation model using the boundary conditions associated with the foam test is plotted along with the experimental temperature profile in Figures 34B through 59B.

Figures 34A through 59A contain the 9 temperature histories. Temperatures are measured on the plate surface and at distances from the plate of 1 to 8 centimeters in 1 centimeter increments. The thermocouple 8 centimeters from the plate is the first to rise since it is closest to the foam front. The traces rise in descending order beginning with the thermocouple 8 centimeters from the plate and ending with the plate temperature. Figure 9 is labeled to identify each trace and illustrates this point.

Figures 34B through 59B contain the temperature data transformed into a steady state temperature profile as described in Chapter III for the development of Figure 11. Only four traces are plotted for each test. For foam tests starting with 10 centimeters of foam on the plate, the outputs of the thermocouples located 3 to 6 centimeters from the plate are used. For tests starting with 11 or 12 centimeters of foam, data from thermocouples located 4 to 7 or 5 to 8 centimeters from the plate are used respectively. This method is used for consistency so the 4 thermocouple readings used to create the temperature profile plot always come from thermocouples located 4, 5, 6, and 7 centimeters from the initial location of the foam front. Table 4 lists the initial foam depth for each case.

The solution to the foam ablation model is illustrated on Figures 34B to 59B. Each solution uses the heat flux and expansion ratio of the specific test case. Alignment of the numerical and experimental results is made away from the foam

front where the experimental data are closer together. A temperature of approximately 40°C is chosen for the alignment point. The numerical solution is aligned to match the experimental data at 40°C. Variations from this point indicate the degree of agreement between the numerical and experimental data for each particular case.

Experimental Problems

Figures 34A through 59A contain the data from all of the attempted foam tests regardless of the test's outcome. All data are presented to give an indication of the type and frequency of problems which occur during testing. Two major factors are identified which make certain sets of data unsuitable for analysis. First, some of the temperature profiles do not approach steady state conditions. Second, pieces of foam shift on the plate under the influence of gravity and in some cases fall from the plate.

The majority of the data appear to attain near steady state conditions with the notable exception of cases E, F, and Q. These cases all lie at the edge of the test envelope. Cases E and F are associated with a heating rate of 9.7kW/m² which proved inadequate to generate steady state temperature profiles on the given foam sample depths. Case Q is associated with an expansion ratio of 12.9 which is a relatively high density and requires a relatively long time to test. During long duration tests, the plate has a tendency to heat up before steady state conditions are achieved. The plate heat up affects the foam temperature profile and steady state conditions are not met. Attaining a steady state temperature profile is an important consideration since the data are being used for the development of a predictive model based on steady state conditions.

The second problem which affects some of the foam test data occurs when the foam shifts on or falls from the plate. Limited shifting of the foam is observed on almost every test. As the peaks and valleys form under the exposure to the radiation, the surface structure becomes unstable. Since the plate is vertical, foam peaks in the surface act as cantilevered sections of foam. The foam material is not rigid and does always support this structure. In some cases, it is noted that valleys (gaps) form over thermocouple locations only later to be covered over by shifting foam. This type of action changes the net foam depth between the thermocouple and the gas-fired panels and in effect changes the rate of temperature rise for the thermocouple.

Consider Figure 57A (case X) as an example. At approximately 350 seconds into the test, a section of foam falls from the plate. Traces 5 and 6 immediately jump up as they are exposed more directly to heat from the gas-fired panels. The affect of this is detected later on the slope of traces 4 and 3. In effect, all data recorded past 350 seconds are suspected of being affected by the falling foam. Cases J, M, N, P, S, T, W, and X are suspected to be affected by falling foam and are eliminated from further consideration at this time. These data are eliminated based on notes taken during the test procedure and visual inspections of the data. Other cases are assumed to have either little or no affect from shifting foam.

Using the above criteria, 11 sets of data are eliminated from further consideration. The remaining 15 sets of data make up 58 percent of the data base. The data eliminated from the present study could be used in future studies which incorporate transient analysis or predictive tools which incorporate terms for foam

loss. Table 9 lists the entire data base and identifies the data which are eliminated.

Analysis of Data

The experimental data are analyzed in the form of the steady state temperature profile. Each temperature profile is generally described by the same shape. The profiles are relatively flat near the foam front which is generally at a temperature of 80°C. From there, the profiles gradually decrease to about 70°C at which point a nearly uniform temperature gradient begins and continues until approximately 35°C is reached. Past this point the temperature gradient decreases and the initial foam temperature is asymptotically approached.

Quantification of the experimental results could include the shape of the profile near its endpoints, the depth of the temperature profile, and the average temperature gradient in the near linear range between 35°C and 70°C. Comparisons between the experimental data are made based on the temperature gradient between 35°C and 70°C because this feature is readily available and is a major factor contributing to the overall depth of the temperature profile. Comparisons based on the end regions of the temperature profile are not attempted due to the irregularities of the experimental data in these regions. These irregularities near the end points also make the exact depth of the temperature profile difficult to determine.

Table 9 lists the gradients for the test cases under consideration. The gradients are reported as an average and standard deviation. The average and standard deviation come from the gradients of the four profiles used to make the temperature profile plots in Figures 34B to 59B. Each gradient is calculated using two data points from the

profile which correspond to temperatures of 35°C and 70°C. In a few cases, these ranges are slightly modified to avoid discontinuities in the data.

Table 9 lists average temperature gradients as a function of foam expansion ratio and applied heat flux. Variations with foam expansion ratio and applied heat flux are considered separately. Figure 60 illustrates the temperature gradient as a function of heat flux for a range of data where the expansion ratio is nearly constant. The standard deviation numbers are also illustrated on this plot as error bars.

Actual trends in the experimental data are difficult to identify when considering the magnitude of the standard deviation intervals. Statistically, the data indicate that the applied heat flux has no effect on the temperature gradient. From the five values on the plot, an average value and standard deviation are computed as 1878 ± 143 (°C/m). The numerical model results are also illustrated on this figure as a reference. The agreement between the numerical model and the measured data is very good. The model result is within 1 standard deviation of each experimental result. It is noted that the model results indicate less than a 2 percent variation in the temperature gradient over a heat flux range of 14.5 to 18. Changes this small are not detectable in the experimental data with the given standard deviations.

Figure 61 illustrates the temperature gradient as a function of foam expansion ratio. Since the data of Figure 60 indicate that the applied heat flux has little or no effect on the temperature gradient, all data are used for Figure 61. The data indicate that the temperature gradient decreases as the expansion ratio increases. The numerical model results are indicated on this figure as a reference. The agreement

between the model and experimental results is generally good. The model lies within one standard deviation of all but 5 data points. These 5 data points each indicate a larger than predicted temperature gradient. A few factors which bias the measured temperature gradients towards larger values are noted below.

A larger than expected experimental temperature gradient could be caused by foam which breaks down faster than expected allowing the temperature to rise faster near the foam front. Small sections of foam falling from the foam front also make the temperature gradient larger than expected. Foam falling from the front typically is the foam which makes up the bulges in the foam surface. The model assumes the foam remains intact until the water is completely evaporated. This is an unrealistic assumption and is an area for future research.

A failure to reach steady state conditions is another cause for a larger than expected temperature gradient. The temperature gradient begins very large and relaxes as steady state conditions are approached. If steady state conditions are not reached, the data indicate a larger than expected temperature gradient.

Another cause for a larger than expected temperature gradient is caused by the radiation profile within the foam. The radiation could have the affect of raising the temperature of the thermocouples to a level above the temperature of the surrounding foam. This effect would be more significant closer to the foam front where the intensity of the radiation is greater. Raising the temperatures near the foam front would make the magnitude of the temperature profile appear larger.

The experimental data indicate several important factors. The temperature

gradient is not strongly affected by the applied heat flux and it decreases with increasing foam expansion ratio. These two trends are both reinforced from the analysis of the numerical foam model results. Also, the foam ablation model appears to predict the behavior of the foam. The numerical temperature profiles have the same characteristics as the experimental results and follow the same trends.

Based on the ability of the numerical model to predict the experimental results, it is assumed that the model accounts for the major mechanisms which govern the foam ablation process. Model results are now studied in detail to quantify the parameters which govern the foam ablation process.

FOAM MODEL RESULTS

The numerical solution procedure for the foam ablation model is summarized in Chapter V. The procedure of Chapter V is used to generate results for a variety of conditions and the results are described below. The convergence of each solution is verified by decreasing the time step and node spacings until a convergence criteria is satisfied. Increasing the number of nodes beyond 50 nodes per centimeter has little affect on the solution. All final data are generated on a grid using 50 nodes per centimeter. Time step variations have little or no affect on the steady state solution.

The foam model solutions are carried out so that each solution depends only on the applied heat flux, the initial foam expansion ratio, and the temperature boundary conditions. The temperature boundary conditions are fixed at 22°C and 80°C for the initial and foam front temperatures respectively. The solutions are therefore dependent

only on applied heat flux and foam expansion ratio. The affect of each of these variables is considered separately.

Variations with Heat Flux

Three model runs are completed for a foam expansion ratio of 18.2 using heating rates of 10, 20, and 30 kW/m². All runs are completed with initial and foam front temperatures of 22°C and 80°C respectively.

Temperature Profile. Figure 62 illustrates the temperature profiles for the three separate model results. The temperature profiles show very little difference. The lowest heating rate case, $q=10$ kW/m², shows the greatest difference. The temperature gradient in the central region of each trace is computed and compared. The gradient changes by approximately 5 percent between the heating rates of 10 and 20 kW/m² and by less than 2 percent between the heating rates of 20 and 30 kW/m².

The differences between the temperature profiles in Figure 62 are attributed to the differences in the importance of thermal diffusion. Thermal diffusion has the tendency to decrease the temperature gradient and further relax the temperature profile. As the heating rate decreases, the role of diffusion increases as illustrated by the order of magnitude analysis summarized in Table 5. The temperature profiles are expected to completely converge for large heating rates where the profiles are entirely dominated by the radiation absorption and evaporative terms.

Table 5 lists the parameters governing the magnitude of the major terms in the energy balance. All terms but the diffusion term are dominated by the Peclet number or the heat flux. The Peclet number is proportional to the applied heat flux since it is

defined proportional to the front velocity which is proportional to the applied heat flux. Since all terms but the diffusion term grow with the magnitude of the applied heat flux, a decrease in the heat flux makes the diffusion term a larger portion of the energy balance. In limiting trials with the foam ablation model, it is observed that artificial increases in the thermal diffusion term had an affect on the temperature profile similar to the affect caused by decreasing the applied heat flux.

Generation and Evaporative Profiles. Figure 63 illustrates the generation and evaporative terms calculated for the three model runs at the same expansion ratio. These terms represent the largest two terms in the energy balance and are almost mirror images of one another. These profiles indicate that energy absorbed by the foam is used almost exclusively to evaporate liquid at the point of absorption.

The generation term profiles increase in magnitude with increasing heat flux as expected. This result is predicted by examining the governing equations. The generation term is calculated from the derivative of the radiation intensity profile as shown in Equation 23. For the same density profiles, Equation 23 shows that the generation term is proportional to the applied heat flux. The density profiles are nearly identical since the temperature profiles are very close.

The evaporative terms show the same trends as the generation terms which suggests they are also proportional to the applied heat flux. The evaporative term is given by the heat of vaporization multiplied by the rate of change of liquid to vapor as illustrated by Equation 37. Equation 37 contains the liquid velocity which is proportional to the applied heat flux as illustrated by Equations 29 and 31. Since the

temperature profiles are nearly the same, the density and volume fraction profiles are approximately equal. Using these equations and the assumption of equal density profiles, the magnitude of the evaporative term is proportional to the applied heat flux for a given expansion ratio.

Each of the generation terms die out at approximately 0.07 meters from the foam front. The model predicts the radiation penetration distance is not a function of the applied heat flux. This relation comes from Equation 19 which shows the radiation profile given by an exponential decay law. Assuming equal temperature profiles, the absorption coefficient variation is the same. The radiation profiles therefore exponentially decay at the same rate and are effectively diminished over the same distance.

The importance of the generation term is evident from Figures 62 and 63. The radiation profile dominates the solution. The foam is undisturbed past the point where the radiation diminishes. Temperatures at locations beyond the reach of the radiation profile are unchanged which highlights the fact that the affects of diffusion are minimal.

Diffusion Profile. Figure 64 illustrates the diffusion term calculated from the three model runs at expansion ratio 18.2. The nomenclature 'diff' is used to indicate the diffusion term. The magnitude of the diffusion profile increases with increasing heat flux but not at a proportional rate. The diffusion term therefore becomes a smaller percentage of the energy balance as the heat flux increases. This point is noted earlier in reference to the order of magnitude analysis from Table 5.

At its largest point, the diffusion term is less than three percent of the peak in the generation term for the 10 kW/m^2 case. For this case, the diffusion peaks at a location between 0.05 and 0.06 meters from the front. This is the location where the temperature profile shows the most deviation from the other cases. This reinforces the idea that the diffusion is the cause of the differences in the temperature profiles.

The diffusion term is the conductivity multiplied by the second derivative of the temperature profile and is the first term in Equation 41. It is noted that the diffusion term had to be smoothed to eliminate oscillations in the data resulting from the numerical estimation of the second derivative.

The diffusion profile is negative for approximately the first 0.045 meters and then goes positive. This profile indicates that heat is being transferred towards the foam front in the region near the front. Past 0.045 meters, heat is carried away from the foam front by diffusion. These profiles are consistent with the generation profiles of Figure 63 and the shape of the temperature profiles in Figure 62. Heat is diffused away, in both directions, from the region of peak radiation absorption.

Liquid Convection Profile. Liquid convection terms for the three heat flux levels are illustrated in Figure 65. The nomenclature 'conv_{*l*}' is used to indicate the liquid convection term.

The first term in Equation 38 describes the liquid convection which is proportional to the volume fraction, liquid velocity, and temperature gradient. Assuming the temperature profiles are the same for a given expansion ratio, the liquid convection term depends only upon the liquid velocity term. Liquid velocity is

proportional to the applied heat flux so the liquid convection term is also proportional to the applied heat flux.

Vapor Convection Profile. Vapor convection terms for the three heat flux levels are illustrated in Figure 66. The second term in Equation 38 describes the vapor convection. The nomenclature ‘conv_v’ refers to the vapor convection term. Assuming the temperature profiles are identical, the vapor convection term is also determined to be proportional to the applied heat flux for a given expansion ratio.

Variations with Expansion Ratio

The results above indicate that all the terms in the energy balance, except diffusion, are proportional to the applied heat flux for a given expansion ratio. Now the variations with foam expansion ratio are examined. Three model runs are completed at foam expansion ratios of 13, 20, and 26.4. All runs are completed with initial and foam front temperatures of 22°C and 80°C respectively. The applied heat flux for each case is 17.5 kW/m².

Temperature Profile. Figure 67 illustrates the temperature profiles for the three different expansion ratios. The temperature profiles penetrate farther into the foam as the expansion ratio increases. This is the result of the absorption coefficient increasing with increasing density. The high expansion ratio foam has a lower average density and therefore a lower average absorption coefficient.

Generation and Evaporative Term Profiles. Figure 68 illustrates the generation and evaporative term profiles. The profiles are substantially different. The wetter low expansion ratio foam absorbs the radiation over a distance of 0.05 meters

which results in a relatively large term. The dry high expansion ratio foam allows the radiation to penetrate farther into the foam and the absorption is distributed over a larger area resulting in a smaller magnitude term. Since the same heat flux is applied in each case, the area under each of the generation term profiles is the same.

The evaporative term mirrors the generation term for each expansion ratio. This reinforces the idea that the radiation energy is absorbed and dissipated almost exclusively by the evaporative process at the point of absorption.

Diffusion Profile. Figure 69 illustrates the diffusion term calculated from the three separate model cases. The magnitude of the diffusion profile decreases with increasing expansion ratio. This is the result of the relaxation of the temperature profile with increasing expansion ratio. The diffusion terms each are negative for a given distance and then become positive. The profiles coincide with the temperature and generation profiles of Figures 67 and 68.

Liquid Convection Profile. The liquid convection terms for the three expansion ratios are illustrated in Figure 70. The liquid convection generally follows the trend of the generation and evaporative terms. The larger temperature gradient of the low expansion ratio case causes the liquid convection term to become larger.

Vapor Convection Profile. Vapor convection terms for the three expansion ratios are illustrated in Figure 71. Once again, these convection terms follow the trend of the generation term in Figure 68. The increase in the convection term with decreasing expansion ratio is partly caused by the increased temperature gradient for the low expansion ratio case.

DIMENSIONLESS RESULTS

The results are generalized by re-plotting Figures 62 through 71 using appropriate dimensionless variables. The selection of appropriate variables is outlined below. Dimensionless variables are needed for the temperature, distance, and power density variables.

The temperature is reported as a temperature rise divided by the temperature difference between the initial and front conditions. The dimensionless temperature is given by Equation 9 and ranges from 1 at the front to 0 in the undisturbed foam.

A length scale is chosen which represents the relative physics of the problem. Diffusion or convection length scales are available but are not relevant in light of the magnitude of these terms compared to the absorption term. The energy balance is governed by the radiation absorption profile. A suitable length scale is the mean radiation penetration length given by Equation 42 [25].

$$l_m = \frac{1}{a} \quad (42)$$

The mean penetration length is the reciprocal of the extinction (absorption) coefficient when the coefficient is constant along the path length. The absorption coefficient is determined from the initial foam conditions so the penetration length is a measure of the distance the radiation will penetrate the unheated foam. The distance from the front is divided by the mean penetration length to make a dimensionless length variable.

Terms in the energy equation have units of power density and are made dimensionless by dividing by q/l_m . The term q/l_m is an average power density based on all radiation being absorbed over the mean penetration length.

Figures 72 through 76 illustrate the dimensionless profiles of the data from Figures 62 through 66 respectively. The temperature profiles remain in the same positions relative to one another in dimensionless form. The generation term, evaporative term, and convection terms all collapse to a single curve. This result is predictable since each term is proportional to the applied heat flux which is used in the dimensionless variable. The length scale has no affect on collapsing the curves in Figures 72 through 76 since these plots all represent a single expansion ratio and use a single mean penetration length scale. The dimensionless diffusion profiles illustrate the point made earlier about the growing importance of diffusion as the applied heat flux decreases. In dimensionless form, the diffusion term for the applied heat flux of 10 kW/m^2 is more than twice the diffusion term for the case of 30 kW/m^2 .

Figures 77 through 81 illustrate the dimensionless profiles of the data from Figures 67 through 71 respectively. In these cases, the length scale plays a major role in shaping the profiles since each different expansion ratio is associated with a separate length scale. The mean penetration length associated with the foam expansion ratio of 26.4 is approximately twice the mean penetration length associated with the foam expansion ratio of 13.

The temperature profiles in Figure 77 take on a more consistent shape in dimensionless form. The profiles differ only in the end regions of each curve. In the

central region of the profiles, the average temperature gradient in dimensionless form collapses to a single value. The average dimensionless temperature gradient has a nominal value of -0.18. This value is a nearly universal result of the model for all expansion ratios and applied heat fluxes. The main exception is the slight decrease in this value caused by the growing importance of diffusion at low heat flux levels.

The generation and evaporative term profiles in Figure 78 are brought close together in dimensionless form. The dimensionless magnitude of the peaks differ by less than 7.5 percent over the range of expansion ratio. In dimensional form, the profiles differed by almost a factor of 2 in the same range of expansion ratio. The separation distance of the peak generation point is also reduced in dimensionless form. The dimensionless peaks in the generation term occurred between 4.5 and 6 radiation penetration depths from the foam front. The range of the dimensionless penetration depths of the radiation, which is roughly defined as the point where the temperature starts to rise, falls between 12 and 13.5 penetration lengths from the foam front. This small range makes it possible to obtain a good estimate of the penetration depth for foams of different expansion ratios.

The dimensionless diffusion terms in Figure 79 suggest that the diffusion plays a more significant role for lower expansion ratio foams. The differences in the traces are attributed to the temperature profiles in Figure 77. The second derivative of the lower expansion ratio profiles is larger.

An important factor is neglected in the diffusion results and is noted here. Since diffusion plays a minor role, a variable conductivity is not used in the foam

ablation model. In fact, a single conductivity value is used for each of the different foams. The conductivity is expected to fall as the expansion ratio rises as predicted by the results in Table 7. This change would magnify the differences in the diffusion of Figure 79. Diffusion makes up only a few percent of the energy balance and its refinement at this point is unwarranted. Refinements first should be focused on the larger terms in the energy balance.

The convection terms in Figures 80 and 81 follow the trend of the generation term in Figure 78. The peaks and peak locations are brought closer together in dimensionless form.

The radiation penetration length does a good job of collapsing the profiles for various expansion ratios. It appears from the data that a slightly different length scale might completely collapse some of the results. The penetration length scale is the reciprocal of the absorption coefficient which is related to the foam expansion ratio. The methods used to determine the absorption coefficient could be refined in future work which would allow a better estimate of the radiation penetration length scale.

Comparison with Experiments

One feature of the dimensionless profiles is the collapse of the temperature gradient in the central region of the temperature profile (35°C to 60°C). Using the dimensionless variables for temperature and distance, the temperature gradient reduces to -0.18 in the central region of the curves. The experimental results are made dimensionless in order to gain a quantitative value for the consistency between the model and the experiments.

Table 10 summarizes the experimental temperature gradients in dimensionless form. The data in Table 10 come from the average values plotted in Figure 61. The average temperature gradients from Figure 61 are made dimensionless using the appropriate length and temperature scales. The average dimensionless temperature gradient obtained from the data in Table 10 is -0.21 ± 0.04 which is 17 percent larger in magnitude than the numerical model result. The numerical prediction of -0.18 lies within 1 standard deviation of the experimental result.

The model result predicts a temperature gradient which is smaller in magnitude than the average experimental value. Reasons which bias the experimental values to larger magnitudes have been outlined earlier. These reasons included failure to reach steady state conditions, foam detachment from the surface, and the effect of radiation on the thermocouples.

Numerical Problems

The numerical code fails to solve the foam ablation problem for certain foam expansion ratios. At certain values of the foam expansion ratio, the code does not converge to a physical solution in a region near the foam front. Over this region, approximately 10 percent of the temperature profile range, energy is not conserved because the model is predicting temperatures outside the range of values covered by the property models. The desired results have been obtained from the foam ablation model and this issue, which only affects certain foam expansion ratios, does not affect the reported results. Further evaluation of this issue is underway.

CHAPTER VII

CONCLUSIONS AND RECOMMENDATIONS

Fire-protection foams can play an important role in the protection of dwellings or structures subjected to heat from encroaching fires. These foams stick to vertical and overhung surfaces holding water in a position where it can absorb the heat. Methods to quantify the ability of fire-protection foams to protect structures are needed. The model which is developed is based upon experimental measurements and observations. This model sheds light on the mechanisms within the foam which absorb the fires energy. Knowledge of the internal mechanisms which play a role in the fire protection process can lead to improvements in the development of future foam products.

The experimental procedure simulates the one-dimensional destruction of fire-protection foam by heat radiation. Results of the experimental procedure indicated that the steady state temperature gradient is nearly uniform over the central region of the temperature profile and is not significantly affected by the applied heat flux. In addition, it is determined that the temperature gradient decreases with increased foam expansion ratio. The experimental procedure is not fool proof and nearly 40 percent of the experimental data are eliminated from consideration. Data are eliminated when large foam pieces fall from the support plate or in a few cases where the temperature profile failed to reach steady state conditions. The major uncertainty in the experimental data is the non-uniformity of the foam front which had peaks and valleys

separated by 1 to 3 centimeters. This variation in the foam surface caused variations in the temperature profiles of adjacent probes.

The foam ablation model is developed using experimental observations and measurements as a guide. The model consists of the steady state energy equation with the addition of a generation and evaporation term. Continuity is satisfied for each foam component in the determination of the velocity fields. A dimensional analysis indicates that the generation and evaporation terms dominate the solution.

The generation term accounts for the absorption of radiation by the liquid in the foam. The magnitude of the generation term is proportional to the applied heat flux. The generation term peaks several centimeters from the foam front where the foam density begins to rise. The model for the generation term is based on an experimentally determined approximation for the absorption coefficient. A value for this coefficient is estimated using a separate set of experimental measurements of radiation intensity and simplifying assumptions in Bouguer's Law.

The foam density is difficult to predict. Foam density is a transient property which depends upon a variety of factors. A realistic model of the foam density as a function of temperature is proposed for the steady state foam ablation model. The proposed model matches measured foam density conditions at its endpoints and smoothly transitions from one known endpoint to the other. The density model is considered to be a realistic approximation for the purposes of the foam ablation model.

The evaporative term accounts for the heat absorbed as latent heat of vaporization as the liquid within the foam is evaporated. The continuity equation for

the liquid in the foam determines the rate of liquid vaporization. The evaporative term is almost the mirror image of the generation term and is also proportional to the applied heat flux. The evaporative term almost entirely balances the generation term which indicates that the radiation energy absorbed by the foam is used almost entirely to evaporate liquid at the point of absorption.

The diffusion and convection terms play only a minor roll in the energy balance. Liquid convected energy is the largest of these terms and represents less than 10 percent of the energy balance. Thermal diffusion and vapor convected energy represent only a few percent of the energy balance. Air convection is negligible.

Temperature profiles from the foam ablation model show the same behavior as the experimental data which suggests that the model accounts for the major mechanisms in the foam evaporation process. The numerical temperature gradient is within 17 percent of the experimentally determined average value which is within 1 standard deviation of the average experimental result. It is noted that only the average temperature gradient in the central portion of the profile is being compared. Comparisons based upon other characteristics may not lead to such a close agreement between the numerical and experimental result. The processes within the model are considered adequate to describe the behavior of the foam.

Results from the model indicate that the radiation is completely absorbed by the foam over a region of approximately 12 mean radiation absorption length scales. The generation term resulting from the absorption process is bell shaped and peaks at approximately 5 mean radiation absorption length scales from the foam front. The dry

foam near the front does not significantly absorb the incoming radiation. The radiation absorption peaks when the radiation encounters the lower temperature higher density foam located behind the foam front.

Using a radiation penetration length as a length scale, the results are made dimensionless. The dimensionless results collapses to a single temperature profile for variations in heat flux. For variations in foam expansion ratio, the dimensionless profiles form a family of curves with the same average temperature gradient over the central regions of the curves. This average dimensionless gradient is -0.18 and is a universal result of this numerical analysis. In dimensionless form, the average temperature gradient for the experimental results is -0.21 ± 0.04 . The numerical model result is 17 percent lower than the average experimental value which is within the standard deviation interval.

The numerical results rely on approximate models for the foam density and radiation absorption terms. These terms are determined using simplifying assumptions and data specific to the foam used for the experiments. It is noted that this model is not a universal model for fire-protection foams. The model serves only as an indication of the importance and behavior of the mechanisms which govern the foam protection process.

RECOMMENDATIONS FOR FUTURE WORK

The current research focused on one typical protein based foam exposed to relatively modest heat flux levels. The affect of the unique properties of the foam are

lumped into the determination of the absorption coefficient. Testing of a variety of foams is needed to see if the results are universal or dependent upon the contents of the foam concentrate. These tests should also be conducted at higher heat flux levels to further validate the model assumptions. In addition, a study of the potential benefits of additives which might change the radiative properties of the foam is warranted.

The energy balance is dominated by the radiation absorption term.

Improvements made in the determination of this term will significantly affect the model results. An improved method to determine the extinction and absorption coefficients is needed to improve the accuracy of the absorption term.

The current research assumes that the radiation absorption is only a function of the foam density (or expansion ratio). Bubble size is determined to be in the 200 to 300 micron range and any affect of bubble size is neglected. It is hypothesized that bubble size will play a role in the radiation absorption process. This in turn will affect the model results. A more detailed determination of the foam's properties could be undertaken which takes into account the variations in bubble size.

Finally, a transient foam ablation model would provide useful results. A transient model could incorporate changes in the applied heat flux levels, foam aging, and affects from the underlying surface. In order to develop a transient model, more detailed studies would be required to determine the foam density and other material properties.

APPENDIX A

FORTTRAN CODES

FOAM ABLATION MODEL

```
      program foamodel

c      This program is used to calculate the SS temperature profile
c      for a foam subjected to radiation.  The radiation input is a
c      fixed function of x.

c      The code obtains the SS solution by allowing a transient C-N
c      code to run for a fixed amount of time sufficient to attain SS.

c      VARIABLES:
c      T      Temperature Array
c      xqtbl  x values for qtbl
c      qtbl   values of generation term wrt x
c      trftbl T values for rftbl
c      rftbl  values of foam density wrt Temperature
c      tbl    T values for velocity and volume fraction table
c      ultbl  liquid velocity wrt Temperature
c      uvtbl  vapor velocity wrt Temperature
c      uatbl  air velocity wrt Temperature
c      ftbl   volume fraction of liquid wrt Temperature
c      kf     thermal conductivity of foam
c      cpf    specific heat of foam
c      cpa    specific heat of air
c      cpv    specific heat of vapor
c      cpl    specific heat of liquid
c      rhf    density of foam
c      rhv    density of vapor
c      rha    density of air
c      rhl    density of liquid
c      ti     initial foam temp
c      tf     front (or final) foam temp
c      xp     initial foam expansion value
c      qin    input radiation value
c      dt     time step for computation
c      dx     node spacing
c      nn     number of nodes
c      d      depth of control volume
c      nt     number of time steps to take
c      ul     liquid velocity
c      uv     vapor velocity
c      ua     air velocity
c

      implicit real*8 (a-h, o-z)
      real*8 t(2501,2),xqtbl(2501),qtbl(2501),trftbl(2501),rftbl(2501),
+      tbl(100),ultbl(100),uvtbl(100),uatbl(100),ftbl(100),
+      xxti(2501),txti(2501),aa(2501),bb(2501),cc(2501),dd(2501)
      real*8 kf

c      function definitions
      pvapor(a)=989.3333d0 - 18.42308d0*a + 4.756563d0*a*a
+      -0.04814188d0*a**3.d0 + 1.02740093d-3*a**4.d0      ! vapor pressure

c      initialize time count
      call gettim(ilhr,ilmin,ilsec,ilhun)

c      open files for I/O
      open(6, file='input.dat')
      open(7, file='rhofoam.dat')
      open(8, file='runttable.dat')
      open(9, file='xq.dat')
```

```

open(12, file='xt.dat')
open(10, file='run.dat')
open(11, file='runchk.dat')

c   define constant values used by code
kf=0.1d0           ! conductivity of foam (W/m-K)
cpf=4100.d0        ! specific heat, foam (J/kg-K)
rhl=1000.d0        ! liquid density (kg/m^3)
cpl=4200.d0        ! specific heat, liquid (J/kg-K)
cpv=1900.d0        ! specific heat, vapor (J/kg-K)
cpa=1008.d0        ! specific heat, air (J/kg-K)
rv=461.5d0         ! vapor gas constant (J/kg-K)
ra=287.d0          ! air gas constant (J/kg-K)
patm=101325.d0     ! total pressure (Pa)
hfg=2350000.d0     ! latent heat, vaporization (J/kg)

c
rhf=50.d0          ! to use a constant density

c   read the input files
read(6,*) ti,tf,xp,qin           ! input.dat
read(6,*) d,nn,dt,nt

read(7,*) nrftbl                 ! rhofoam.dat
do 1, i=1,nrftbl
1   read(7,*) trftbl(i), rftbl(i)

read(8,*) ntbl                   ! runtable.dat
do 2, i=1,ntbl
2   read(8,*) tbl(i), ultbl(i), uvtbl(i), uatbl(i), ftbl(i)

read(9,*) nqtbl                 ! xq.dat
do 3, i=1,nqtbl
3   read(9,*) xqtbl(i), qtbl(i)

read(12,*) nxxti                ! xt.dat
do 5, i=1,nxxti
5   read(12,*) xxxti(i), txtti(i)

c   calculate node spacing
rnn=nn
dx=d/(rnn-1.d0)

c   initialize the temperature profiles
do 4, i=2,nn-1
  x=(i-1)*dx*100.d0             ! need x in cm here
  call locate(xxxti,nxxti,x,jj)
  call polint(xxxti(jj),txtti(jj),3,x,t(i,1),err)
4  t(i,2)=t(i,1)
  t(1,1)=tf
  t(nn,1)=ti

c   set up variables for loop start
l1=1
l2=2
time=0.d0
ttest=0.d0
stest=0.d0

c   time loop start
do 200, j=1,nt
  time=(j-1)*dt                 ! absolute time

c   set up vectors for use in TRIDAG
al=dt/(rhf*cpf)
bl=kf/2.d0

c   loop through the nodes
do 100, i=2,nn-1
  x=dx*(i-1)

```

```

c      generate 2cd derivative at time j
      d2j = ( t(i-1,11) - 2.d0*t(i,11) + t(i+1,11) )/(dx*dx)

c      generate 1st derivative at time j
      dj = (t(i+1,11)-t(i-1,11))/(2.d0*dx)

c      obtain velocity and volume fraction data for time j
      call locate(tbl,ntbl,t(i,11),jj)
      call polint(tbl(jj),ftbl(jj),3,t(i,11),f,err)
      call polint(tbl(jj),ultbl(jj),3,t(i,11),ul,err)
      call polint(tbl(jj),uvtbl(jj),3,t(i,11),uv,err)
      call polint(tbl(jj),uatbl(jj),3,t(i,11),ua,err)

c      generate liquid rho U cp term at time j
      convl = rhl*f*cpl*ul

c      generate vapor rho U cp term
      pv=pvapor(t(i,11))
      rhv=pv/(rv*(t(i,11)+273.15d0))
      convv = rhv*(1.d0-f)*cpv*uv

c      generate air rho U cp term
      pa=patm-pv
      rha=pa/(ra*(t(i,11)+273.15d0))
      conva = rha*(1.d0-f)*cpa*ua

c      obtain sum of rho U cp terms at time j
      cm=convl+convv+conva

c      obtain heat generation term which is constant with j
      call locate(xqtbl,nqtbl,x,jj)
      call polint(xqtbl(jj),qtbl(jj),3,x,qdgen,err)

c      generate evaporative sink term at time j
      call locate(tbl,ntbl,t(i+1,11),jj)
      call polint(tbl(jj),ftbl(jj),3,t(i+1,11),fp,err)
      call polint(tbl(jj),ultbl(jj),3,t(i+1,11),ulp,err)
      call locate(tbl,ntbl,t(i-1,11),jj)
      call polint(tbl(jj),ftbl(jj),3,t(i-1,11),fm,err)
      call polint(tbl(jj),ultbl(jj),3,t(i-1,11),ulm,err)
      qdvap=hfg*(rhl*fp*ulp-rhl*fm*ulm)/(2.d0*dx)

c      compute the D vector component
      dd(i)=t(i,11)+al*bl*d2j-al*cm*dj/2.d0+al*(qdgen+qdvap)

c      geuss at sum of rho U cp terms at time j+1
      cp=cm

c      compute A, B, and C vector components
      aa(i)=-al*cp/(4.d0*dx) - al*bl/(dx*dx)
      bb(i)=1.d0+2.d0*al*bl/(dx*dx)
      cc(i)=al*cp/(4.d0*dx) - al*bl/(dx*dx)
100  continue

c      assign vector endpoints
      aa(1)=0.d0
      bb(1)=1.d0
      cc(1)=0.d0
      dd(1)=tf
      aa(nn)=0.d0
      bb(nn)=1.d0
      cc(nn)=0.d0
      dd(nn)=ti

c      obtain estimate of temperature at time j+1
      call tridag(aa,bb,cc,dd,1,nn)
      do 157, i=1,nn
        t(i,12)=dd(i)
157    if(t(i,12).gt.tf) t(i,12)=tf

c      loop through nodes again and make a better estimate at time j+1
      do 190, i=2,nn-1
        x=dx*(i-1)

```

```

c      generate 2cd derivative at time j
      d2j = ( t(i-1,11) - 2.d0*t(i,11) + t(i+1,11) )/(dx*dx)

c      generate 1st derivative at time j
      dj = (t(i+1,11)-t(i-1,11))/(2.d0*dx)

c      obtain velocity and volume fraction data for time j+1/2
      tjh=(t(i,11)+t(i,12))/2.d0
      call locate(tbl,ntbl,tjh,jj)
      call polint(tbl(jj),ftbl(jj),3,tjh,f,err)
      call polint(tbl(jj),ultbl(jj),3,tjh,ul,err)
      call polint(tbl(jj),uvtbl(jj),3,tjh,uv,err)
      call polint(tbl(jj),uatbl(jj),3,tjh,ua,err)

c      generate liquid rho U cp term at time j+1/2
      convl = rhl*f*cpl*ul

c      generate vapor rho U cp term
      pv=pvapor(t(i,11))
      rhv=pv/(rv*(t(i,11)+273.15d0))
      convv = rhv*(1.d0-f)*cpv*uv

c      generate air rho U cp term
      pa=patm-pv
      rha=pa/(ra*(t(i,11)+273.15d0))
      conva = rha*(1.d0-f)*cpa*ua

c      obtain sum of rho U cp terms at time j+1/2
      cm=convl+convv+conva

c      obtain heat generation term which is constant with j
      call locate(xqtbl,nqtbl,x,jj)
      call polint(xqtbl(jj),qtbl(jj),3,x,qdgen,err)

c      generate evaporative sink term at time j+1/2
      tip1=(t(i+1,11)+t(i+1,12))/2.d0
      tim1=(t(i-1,11)+t(i-1,12))/2.d0
      call locate(tbl,ntbl,tip1,jj)
      call polint(tbl(jj),ftbl(jj),3,tip1,fp,err)
      call polint(tbl(jj),ultbl(jj),3,tip1,ulp,err)
      call locate(tbl,ntbl,tim1,jj)
      call polint(tbl(jj),ftbl(jj),3,tim1,fm,err)
      call polint(tbl(jj),ultbl(jj),3,tim1,ulm,err)
      qdvap=hfg*(rhl*fp*ulp-rhl*fm*ulm)/(2.d0*dx)

c      compute the D vector component
      dd(i)=t(i,11)+al*bl*d2j-al*cm*dj/2.d0+al*(qdgen+qdvap)

c      use average value of rho U cp terms at time j+1
      cp=cm

c      compute A, B, and C vector components
      aa(i)=-al*cp/(4.d0*dx) - al*bl/(dx*dx)
      bb(i)=1.d0+2.d0*al*bl/(dx*dx)
      cc(i)=al*cp/(4.d0*dx) - al*bl/(dx*dx)
190  continue

c      assign vector endpoints
      aa(1)=0.d0
      bb(1)=1.d0
      cc(1)=0.d0
      dd(1)=tf
      aa(nn)=0.d0
      bb(nn)=1.d0
      cc(nn)=0.d0
      dd(nn)=ti

c      obtain estimate of temperature at time j+1
      call tridag(aa,bb,cc,dd,1,nn)
      do 167, i=1,nn
        t(i,12)=dd(i)
167    if(t(i,12).gt.tf) t(i,12)=tf

```

```

c      output points to run.dat at last time
      if(j.eq.nt) then
        write(10,*) nn
        do 158, i=1,nn
          xm=dx*(i-1)
          xcm=100.d0*xm
158      write(10,900) xcm,t(i,12)
        endif

c      output data
      if(time.ge.ttest) then
        print*, ' output data, time =',time
        write(11,250) time, (t(ii,12), ii=1,241,8)
        ttest=ttest+10.d0
      endif

250    format(1x, f8.3, 31f7.1)
900    format(1x, 2f15.10)

c      prepare for next time loop
      lhold=l1
      l1=l2
200    l2=lhold

c      Output time info
      call gettim(i2hr,i2min,i2sec,i2hun)
      time1=((i1hr*60)+i1min)*60+i1sec+i1hun/100.0
      time2=((i2hr*60)+i2min)*60+i2sec+i2hun/100.0
      runtime=(time2-time1)/60.0
      write(*,700) runtime, dt
700    format(1x, ' Execution took ',f7.2,' minutes,  dt = ',f10.6)

      stop
      end

```

IDEAL DENSITY MODEL

```

c      program rhoideal
c      program to compute ideal density model data for air/water
c      foam. Data are tabulated in 1 degree increments

c      Data are required from tinit to 99 C for the model. To aid
c      in interpolation, data points at tinit-1 are added.

c      VARIABLES
c      tinit          initial temp
c      tf             front temp
c      x1             initial foam expansion
c      tc             temperature vector

      implicit real*8 (a-h,o-z)
      dimension tc(200),rf(200)

      open(6, file='input.dat')
      open(7, file='rhoideal.dat')

c      read input file
      read(6,*) tinit, tf, x1, qdum
      t1=tinit + 273.d0          ! initial temperature in Kelvin
      tf=tf + 273.d0            ! final temperature in Kelvin

c      prepare values for counters
      tsat=100.d0
      n1=int(tinit)
      n2=int(tsat)
      ntot=n2-n1+1

c      calculate density values
      do 200, j=n1,n2-1
          t2=t1+j-n1
          call rhofoam(x1,t1,t2,rf(j))
200      tc(j)=t2-273.d0

c      at saturation temp, density of foam will equal vapor density
      tc(n2)=t1+n2-n1-273.0d0
      rf(n2)=0.598d0
c      smooth data at T = 99C
      rf(n2-1)=0.5d0*(rf(n2)+rf(n2-2))

c      output the data to file
      write(7,*) ntot
      do 201, j=n1,n2
201      write(7,300) tc(j),rf(j)
300      format(1x,2f12.7)

      stop
      end

c      SUBROUTINE *****
      subroutine rhofoam(xp,t1,t2,rhof)
c      This Subroutine calculates the density of an air/water foam
c      which was originally made at about 293 K (20 C) and is then heated
c      and expands to some new density. Ideal gas behavior assumed.
c      VARIABLES PASSED
c      xp:          initial expansion value of foam at t1 (typically 10-30)
c      t1:          initial temperature of foam (Kelvin)
c      t2:          temperature value to find rhof and rhol (Kelvin)
c      rhof:        density of foam at t2 (kg/m^3)

      implicit real*8(a-h,o-z)
      real*8 ma1,mv1,mv2,ml1,ml2,mass1

c      curve fits; vapor pressure
      pv(a)=6636168.548630297d0-92155.5577483d0*a+482.3184927621d0*a*a
      +-1.1285233865d0*a**3 + 9.9703797547d-4*a**4

```



```

c    define some parameters
    ra=287.d0          ! gas constant for air
    rv=461.5d0         ! gas constant for steam
    patm=101325.d0     ! assumed pressure inside bubbles
    rho1=1000.0        ! density of liquid

    tt=t2

c    assume foam gas is saturated

c    STATE 1
    weight=1000.0d0/xp          ! weight of foam in 1l beaker (g)
    rhodrya=patm/ra/t1          ! density of dry air in lab (kg/m^3)
    mass1=weight+rhodrya       ! mass of 1l foam sample in grams (g)
    rho1f=mass1                ! density of foam sample (kg/m^3)

    rhoa=(patm-pv(t1))/ra/t1    ! density of air in foam (kg/m^3)
    rhov=pv(t1)/rv/t1          ! density of vapor in foam (kg/m^3)

    f=(rho1f-rhoa-rhov)/(rho1-rhoa-rhov) ! liquid volume fraction

c    assume you start with 1 m^3 of foam
    va1=1.0d0-f                ! initial air volume (m^3)
    ma1=(patm-pv(t1))*va1/(ra*t1) ! initial air mass (kg)
    vl1=f                       ! initial liquid volume (m^3)
    ml1=vl1*rho1               ! initial liquid mass (kg)
    vg=rv*t1/pv(t1)            ! specific volume of vapor (m^3/kg)
    mv1=va1/vg                 ! initial vapor mass

c    STATE 2
    va2=ma1*ra*tt/(patm-pv(tt)) ! air volume at t2
    mv2=va2*pv(tt)/(rv*tt)      ! vapor mass at t2
    ml2=ml1-(mv2-mv1)           ! liquid mass at t2
    vl2=ml2/rho1                ! liquid volume at t2
    v2=va2+vl2                  ! new foam volume at t2

    rho1f=(ma1+ml2+mv2)/v2      ! foam density at t2

c    output a data file containing calculated information
    open(97, file='rhocheck.dat')
    write(97,98) tt-273.,pv(tt),va2,vl2,v2,ma1,ml2,mv2

98  format(1x,8e14.7)
    return
end

```

RADIATION GENERATION TERM

```

      program qdgen
c      program to compute the generation term using a temp profile
c      and a given rhtable

      implicit real*8 (a-h, o-z)
      dimension x(2501),t(2501),r(2501),tr(2501),rx(2501),q(2501),
+          qdot(2501),xfq(2501)

c      open files for input and output
      open (7, file='xt.dat')          ! input containing T profile
      open (8, file='rhofoam.dat')      ! input containing rho(T) table
      open (10, file='input.dat')       ! read run input to get qin

      open (9, file='xq.dat')           ! output file with r(x), i(x)

c      read in the temperature profile data
      read(7,*) nx
      do 1, i=1,nx
        read(7,*) x(i),t(i)
1      x(i)=x(i)/100.d0                !convert x to meters

c      read in the density data
      read(8,*) nt
      do 2, i=1,nt
2      read(8,*) tr(i),r(i)

c      read in the run input file to obtain qin
      read(10,*) tinit,tfrnt,xpand,qin

c      convert T "t" data to rho "rx" data to obtain rho(x) table
      do 3, i=1,nx
        call locate(tr,nt,t(i),j)
3      call polint(tr(j),r(j),3,t(i),rx(i),err)

c      compute I(x) profile q=I (have rx vs. x table, rho(x))
      q(1)=qin
      sum=0.0d0
      do 5, i=2,nx
        sum=sum+((rx(i)*3.d0)+(rx(i-1)*3.d0))/2.d0*(x(i)-x(i-1))
5      q(i)=qin*dexp(-sum)

c      compute qdotgen term versus x (have q vs x table, I(x))
      do 30, i=2,nx
        xfq(i)=(x(i)+x(i-1))/2.d0
30      qdot(i)=(q(i-1)-q(i))/(x(i)-x(i-1))
        qdot(1)=qdot(2)-((qdot(3)-qdot(2))/(xfq(3)-xfq(2)))*xfq(2)
        xfq(1)=0.d0

c      output some data
      write(9,*) nx
      do 6, i=1,nx
c      6      write(9,7) x(i),t(i),rx(i),q(i),xfq(i),qdot(i)
6      write(9,7) x(i), qdot(i)
7      format(1x,2e17.10)

      stop
      end

```

CONSERVATION OF MASS

```

c      program conserve
c
c      This program is used to compute variables as a function
c      of temperature for later use in the solution of the heat
c      equation applied to fire protection foams.
c
c      This program makes use of an estimated model of the foams
c      density as a function of temperature along with measurements
c      of the foams visible expansion as a function of temperature.
c
c      Conservation of mass and energy principals along with
c      tables of thermodynamic data are used in the computation
c      of velocities and density.
c
c      VARIABLES:
c      ti          initial foam temp (C)
c      tf          final (or front) foam temp (C)
c      xp          initial foam expansion
c      qin         radiative heat input (W/m^2)
c      pv(a)       vapor pressure function at temperature "a" (C)
c      ra          gas constant (air) (J/kg-C)
c      rv          gas constant (vapor) (J/kg-C)
c      patm        atmospheric pressure (Pa)
c      uf          front velocity (m/s)
c      ul(i)       liquid velocity (m/s)
c      uv(i)       vapor velocity (m/s)
c      ua(i)       air velocity (m/s)
c      rftbl(i)    foam density table (kg/m^3)
c      trf(i)      temperature for foam density table (C)
c      h           enthalpy (kJ/kg)
c      vrd(i,j)    volume ratio data (temp,xp)
c      xprd(j)     expansion ratio data
c      vxrd(j)     vector containing volume ratio data at fixed T
c      tvr(i)      temperature for volume ratio data
c      vr(i)       volume ratio data
c      ntv         number of temps in vol ratio data
c      nxpr        number of expansion ratios in vol ratio data
c      nrf         number of values in density table rftbl(i)
c      f(i)        volume fraction of liquid content
c      mdota       mass flux, air (kg/m^2/s)
c      mdotv       mass flux, vapor (kg/m^2/s)
c      mdotl       mass flux, liquid (kg/m^2/s)
c      mdotw       mass flux, water (kg/m^2/s) (sum of liquid and vapor)
c
c      implicit real*8 (a-h, o-z)
c      real*8 vrd(25,5),xprd(5),tvr(25),vr(25),vxrd(5),ul(100),uv(100),
c      +      ua(100),rftbl(100),trf(100),f(100)
c      real*8 mdota,mdotv,mdotl,mdotw
c
c      function definitions
c      pv(a)=989.3333d0 - 18.42308d0*a + 4.756563d0*a*a
c      +-0.04814188d0*a**3.d0 + 1.02740093d-3*a**4.d0 ! vapor pressure
c
c      code parameter definitions
c      ra=287.d0 ! (J/kg-C)
c      rv=461.52d0 ! (J/kg-C)
c      patm=101325.d0 ! (Pa)
c      rhol=1000.d0 ! (kg/m^3)
c      cpf=4100.d0 ! specific heat, foam (J/kg-K)
c      cpl=4200.d0 ! specific heat, liquid (J/kg-K)
c      cpv=1900.d0 ! specific heat, vapor (J/kg-K)
c      cpa=1008.d0 ! specific heat, air (J/kg-K)
c
c      open files for I/O
c      open(6, file='input.dat')
c      open(7, file='vratio.dat')

```

```

open(8, file='rhofoam.dat')
open(10, file='runtable.dat')
open(11, file='rhocalc.dat')
open(12, file='coeff.dat')

c   read in data files
read(6,*) ti,tf,xp,qin           !input.dat

read(7,*) ntvr,nxpr             !vratio.dat
read(7,*) dum, (xprd(j), j=1,nxpr)
do 1, i=1,ntvr
1   read(7,*) tvr(i),(vrd(i,j), j=1,nxpr)

read(8,*) nrf                   !rhofoam.dat
do 5, i=1,nrf
5   read(8,*) trf(i),rftbl(i)

c   compute the front velocity
rai=patm/ra/(tf+273.0d0)         ! initial air density (kg/m^3)
rwi=1000.d0                     ! initial water density "
hai=273.02d0+1.0062d0*ti        ! initial air enthalpy (kJ/kg)
haf=273.02d0+1.0062d0*tf        ! final air enthalpy "
hli=0.1863d0+4.1845d0*ti        ! initial water enthalpy "
hvf=2504.08d0+1.744d0*tf        ! final water enthalpy "

uf=(.001d0)*qin/(rai*(1.d0-1.d0/xp)*(haf-hai)+rwi/xp*(hvf-hli))
uf=-uf

c   obtain the volume ratio table for given expansion ratio
do 2, i=1,ntvr
do 3, j=1,nxpr
3   vxrd(j)=vrd(i,j)
call locate(xprd,nxpr,xp,jj)
call polint(xprd(jj),vxrd(jj),3,xp,vr(i),err)
vr(i)=1.d0+vr(i)
2   tvr(i)=ti+tvtr(i)

c   stop volume ratio data at Tf (have tvtr, vr)
tvtrmax=tf
call locate(tvtr,ntvr,tvtrmax,jj)
call polint(tvtr(jj),vr(jj),3,tvtrmax,vrmax,err)
ntvr=jj+1
tvtr(ntvr)=tvtrmax
vr(ntvr)=vrmax

c   obtain the liquid water velocity wrt temperature
do 4, i=1,ntvr
4   ul(i)=uf*vr(i)

c   compute mass flux of components in undisturbed foam (kg/m^2/s)
call locate(trf,nrf,ti,jj)
call polint(trf(jj),rftbl(jj),3,ti,rhof,err) ! rho foam
rhov=pv(ti)/rv/(ti+273.0d0)                 ! rho vapor
rhoa=(patm-pv(ti))/ra/(ti+273.0d0)          ! rho air
ff=(rhof-rhoa-rhov)/(rhol-rhoa-rhov)         ! volume fraction
mdotl=rhol*ff*uf                            ! mass flux of liquid
mdotv=rhov*(1.d0-ff)*uf                     ! mass flux of vapor
mdota=rhoa*(1.d0-ff)*uf                     ! mass flux of air
mdotw=mdotl+mdotv                           ! mass flux of water

c   calculate, volume fraction, and gas velocities, and output density
do 6, i=1,ntvr
call locate(trf,nrf,tvr(i),jj)
call polint(trf(jj),rftbl(jj),3,tvr(i),rhof,err) ! rho foam
rhov=pv(tvr(i))/rv/(tvr(i)+273.0d0)             ! rho vapor
rhoa=(patm-pv(tvr(i)))/ra/(tvr(i)+273.0d0)      ! rho air
f(i)=(rhof-rhoa-rhov)/(rhol-rhoa-rhov)          ! vol frac
if(f(i).le.0.d0) f(i)=0.d0
ua(i)=mdota/rhoa/(1.d0-f(i))                    ! air vel
mdotl=rhol*f(i)*ul(i)                           ! mdot liq
mdotv=mdotw-mdotl                               ! mdot vap

```

```

        uv(i)=mdotv/rhov/(1.d0-f(i))                ! vap vel

c      output coefficients for energy equation
      c1=rhol*ul(i)*cpl*f(i) +
+      (rhov*cpv*uv(i)+rhoa*cpa*ua(i))*(1.d0-f(i))
      c2=rhol*f(i)*ul(i)
      write(12,101) tvr(i),c1, c2

6      write(11,100) tvr(i), rhof, rhov, rhoa, vr(i)    ! rhos out

c      output the run data
      write(10,*) ntvr
      do 7, i=1,ntvr
7        write(10,100) tvr(i), ul(i), uv(i), ua(i), f(i)
100      format(1x,5e15.8)
101      format(1x,3e15.8)

      stop
      end

```

Distance from Plate (cm)	Average Heat Flux ($q / q_{ref.}$)	Standard Deviation ($s / q_{ref.}$)
0	0.95	0.032
2	0.95	0.035
4	0.95	0.030
6	0.92	0.031
8	0.89	0.036
10	0.87	0.036
average	0.923 ± 0.034	-

TABLE 1. Oven Uniformity Results

sample	xp, set 1	xp, set 2	xp, set 3
1	24.1	23.4	23.2
2	24.6	23.8	23.4
3	25.1	24.7	22.2
4	23.6	23.4	24.0
5	24.9	24.2	22.2
average +/- std. deviation	$24.5 \pm .5$	$23.9 \pm .5$	$23.0 \pm .7$

TABLE 2. Repeatability of Foam Expansion Ratio

time	average temperature	Standard Deviation	Standard Deviation
(s)	(C)	(C)	(s)
0	19.1	± 0.1	-
30	19.3	± 0.2	-
60	29.3	± 2.7	4.1
90	54.0	± 3.9	6.2
120	68.9	± 3.3	12.2
150	75.5	± 2.3	18.0

TABLE 3. Average Temperatures and Standard Deviations from Figure 10

test	expansion ratio	heat flux (kW/m ²)	foam depth (m)
A	21.0	16.7	.10
B	21.4	16.8	.10
C	23.2	16.9	.10
D	12.8	16.8	.10
E	17.8	9.7	.10
F	17.7	9.7	.10
G	20.0	15.7	.11
H	17.7	14.4	.10
I	18.4	14.6	.10
J	18.0	17.2	.10
K	18.2	17.5	.10
L	18.0	17.5	.10
M	23.4	17.8	.12
N	23.1	16.6	.12
O	17.8	17.8	.12
P	17.4	16.6	.12
Q	12.9	17.6	.12
R	15.0	17.5	.12
S	18.6	17.5	.12
T	20.0	17.5	.12
U	19.9	17.5	.12
V	30.7	17.6	.11
W	25.8	17.7	.11
X	20.3	17.6	.11
Y	32.8	15.3	.11
Z	26.5	15.3	.11

TABLE 4. Summary of Foam Test Conditions

Term	Parameter	Magnitude
diffusion	1	10^0
convection	Pe	10^1
generation	$(q \, l / l_m) / (k \, \Delta T / l)$	10^3
evaporation	Pe / Ja	10^3

TABLE 5. Relative Magnitudes of Terms in Foam Ablation Problem

component	liquid	air	vapor
Cp (J/kg-K)	4200	1008	1900

TABLE 6. Specific Heat Values for Foam Components

foam expansion ratio (expansion ratio)	k_f (W/m-K)
10	0.075
20	0.052
30	0.045

TABLE 7. Foam Thermal Conductivity Estimates

description	equation
(41) foam ablation model	$k_f \frac{d^2 T}{dx^2} - (f \rho_l C_{p_l} u_l + (1-f) \rho_v C_{p_v} u_v + (1-f) \rho_a C_{p_a} u_a) \frac{dT}{dx} -$ $\frac{d}{dx} [q \exp(-(3 \int_0^x \rho_f dx))] + h_v \frac{d}{dx} (\rho_l f u_l) = 0$
(29) front velocity	$u_f = \frac{q}{\rho_l \frac{1}{xp} (h_f - h_i)_l + \rho_a (1 - \frac{1}{xp}) (h_f - h_i)_a}$
(31) liquid velocity	$u_l = -u_f \frac{V}{V_l}$
(35) vapor velocity	$u_v = \frac{\dot{m}_{l \rightarrow v} - \rho_l f u_l}{\rho_v (1-f)}$
(36) air velocity	$u_a = \frac{\rho_{a,i} (1-f_i) (-u_f)}{\rho_a (1-f)}$
(23) generation term	$\dot{q}_g(x) = - \frac{d}{dx} [q \exp(-(3 \int_0^x \rho_f dx))]$
(37) evaporative sink	$\dot{q}_v = h_v \frac{d}{dx} (\rho_l f u_l)$
(24) density relations	$\rho_f = \rho_l (f) + (\rho_v + \rho_a) (1-f)$
(14) air continuity	$\frac{d((1-f) \rho_a u_a)}{dx} = 0$
(15) liquid continuity	$\frac{d(f \rho_l u_l)}{dx} = \Gamma_l$
(16) vapor continuity	$\frac{d((1-f) \rho_v u_v)}{dx} = \Gamma_v$
(1) expansion ratio	$xp = \frac{\text{Volume of Container (cc)} \cdot 1(\text{g/cc})}{\text{Weight of Foam within Container (g)}}$

TABLE 8. Summary of Major Equations

test	expansion ratio	heat flux (kW/m ²)	average dT/dx T=35 to 60 (C/m)	standard deviation (C/m)
A	21.0	16.7	-2162	684
B	21.4	16.8	-2320	545
C	23.2	16.9	-1986	267
D	12.8	16.8	-2681	592
E	17.8	9.7	failed to reach steady state	
F	17.7	9.7	failed to reach steady state	
G	20.0	15.7	-1544	143
H	17.7	14.4	-1451	406
I	18.4	14.6	-1813	543
J	18.0	17.2	partial foam loss from plate	
K	18.2	17.5	-1626	430
L	18.0	17.5	-1759	422
M	23.4	17.8	partial foam loss from plate	
N	23.1	16.6	partial foam loss from plate	
O	17.8	17.8	-1739	207
P	17.4	16.6	partial foam loss from plate	
Q	12.9	17.6	failed to reach steady state	
R	15.0	17.5	-1904	752
S	18.6	17.5	partial foam loss from plate	
T	20.0	17.5	partial foam loss from plate	
U	19.9	17.5	-2184	311
V	30.7	17.6	- 1563	384
W	20.3	17.7	partial foam loss from plate	
X	20.3	17.6	partial foam loss from plate	
Y	32.8	15.3	-1279	302
Z	26.5	15.3	-1240	185

TABLE 9. Experimental Temperature Gradient

Experimental Case	Dimensionless Temperature Gradient
A	-0.2545
B	-0.2782
C	-0.2576
D	-0.1942
G	-0.1733
H	-0.1445
I	-0.1876
K	-0.1665
L	-0.1781
O	-0.1742
R	-0.1612
U	-0.2440
V	-0.2660
Y	-0.2320
Z	-0.1830
average \pm standard deviation	-0.21 \pm .04
model result	-0.18

TABLE 10. Dimensionless Experimental Temperature Gradient

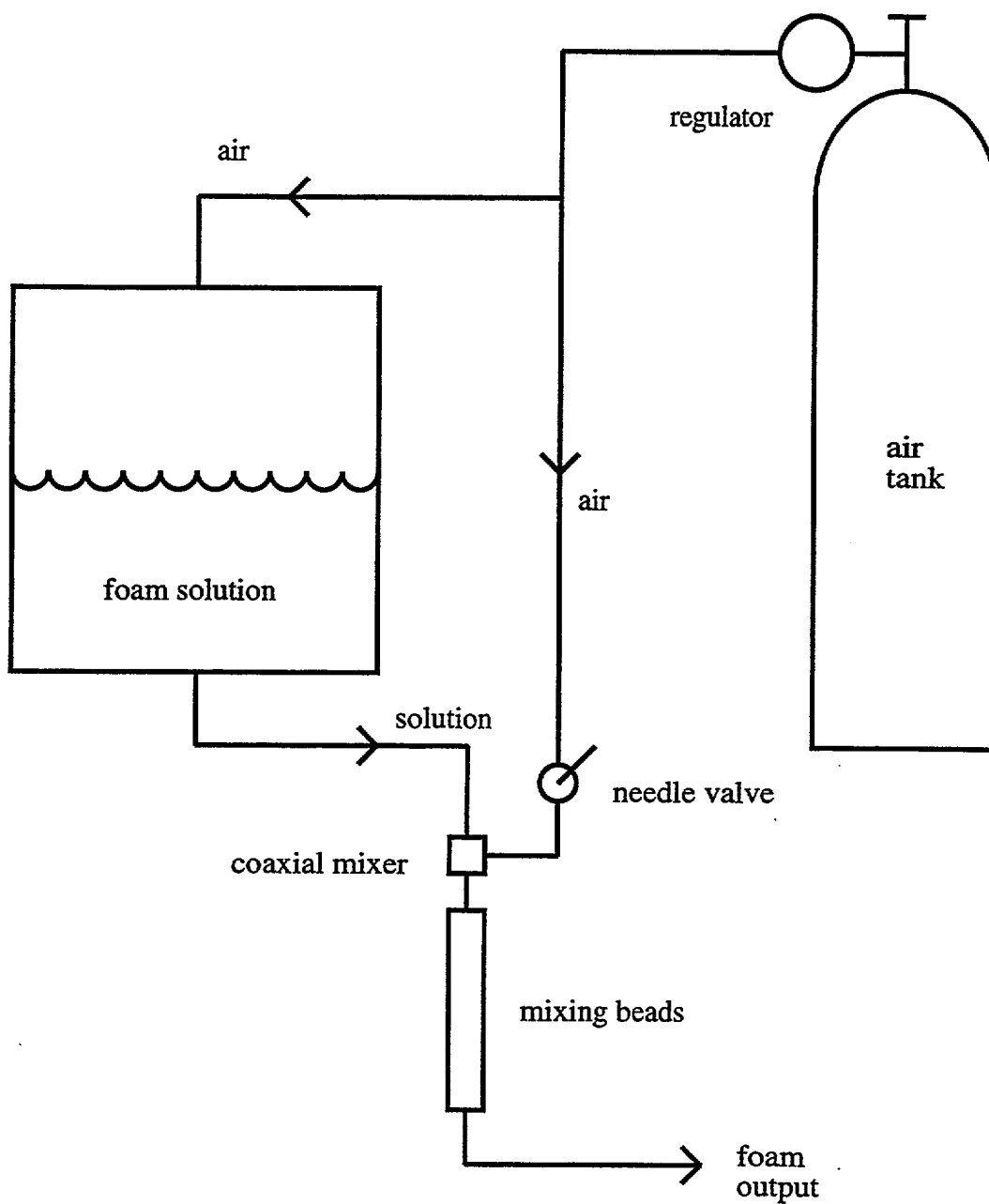


FIGURE 1. Schematic of Foam Generator

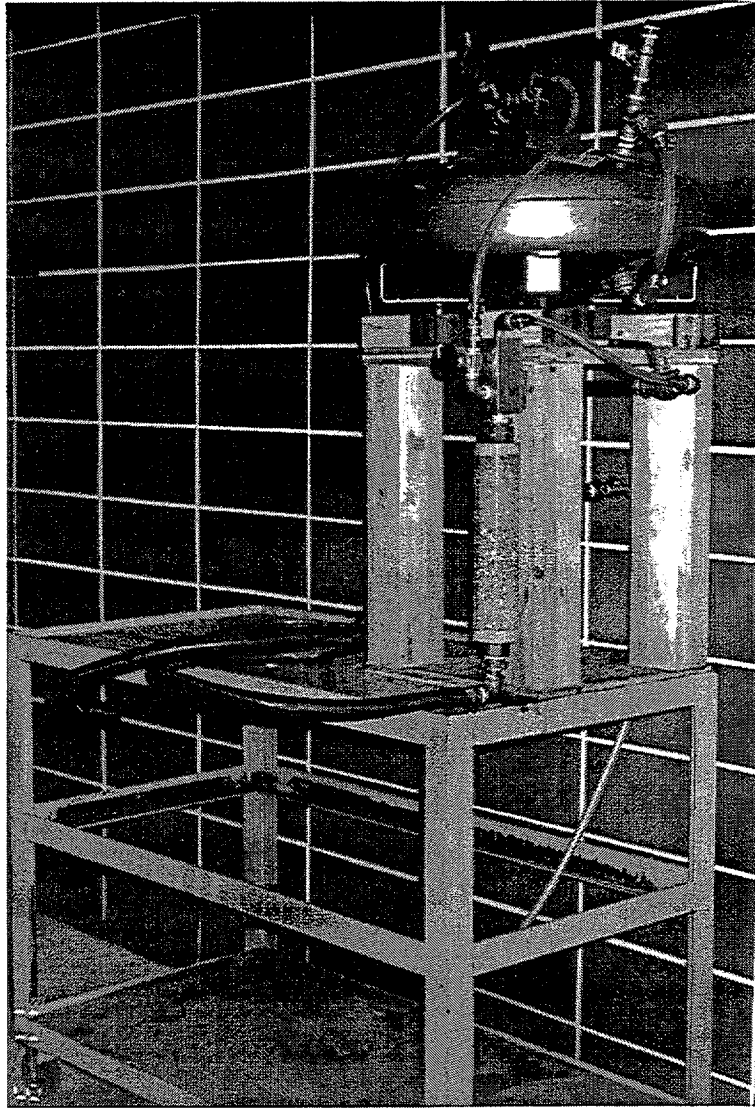


FIGURE 2. Photograph of Foam Generator

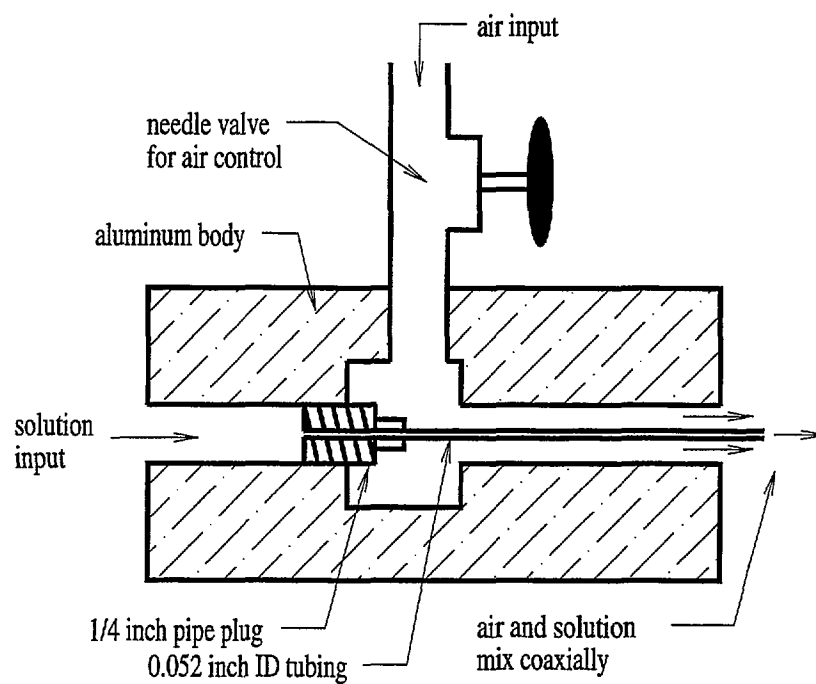


FIGURE 3. Schematic of Coaxial Mixer Design

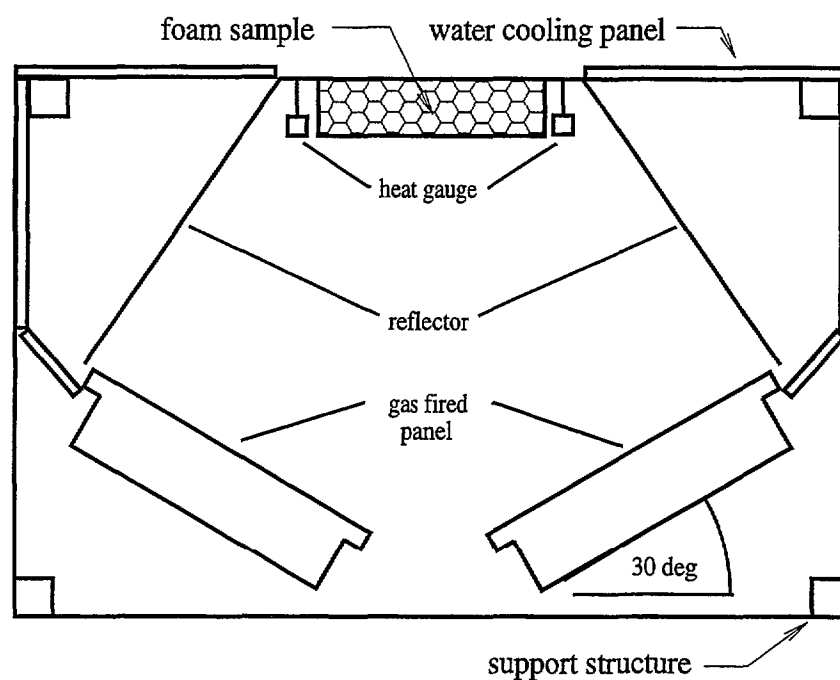


FIGURE 4. Schematic of Gas-Fired Panel Apparatus

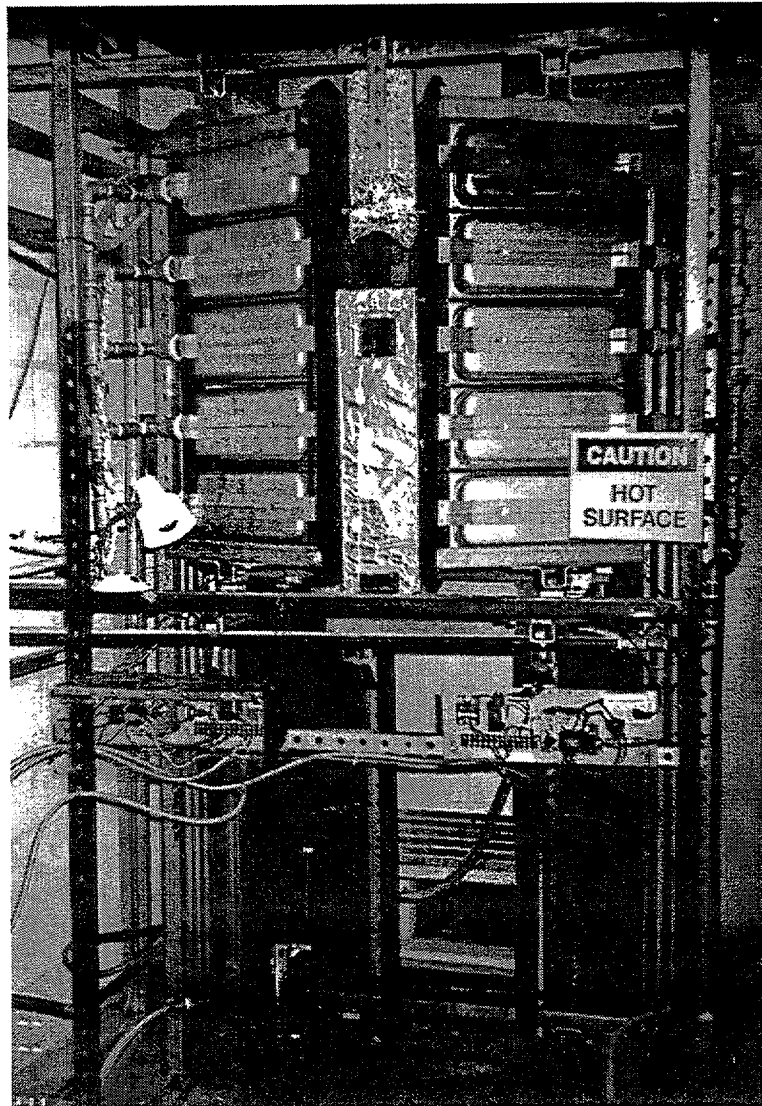


FIGURE 5. Photograph of Gas-Fired Panel Apparatus

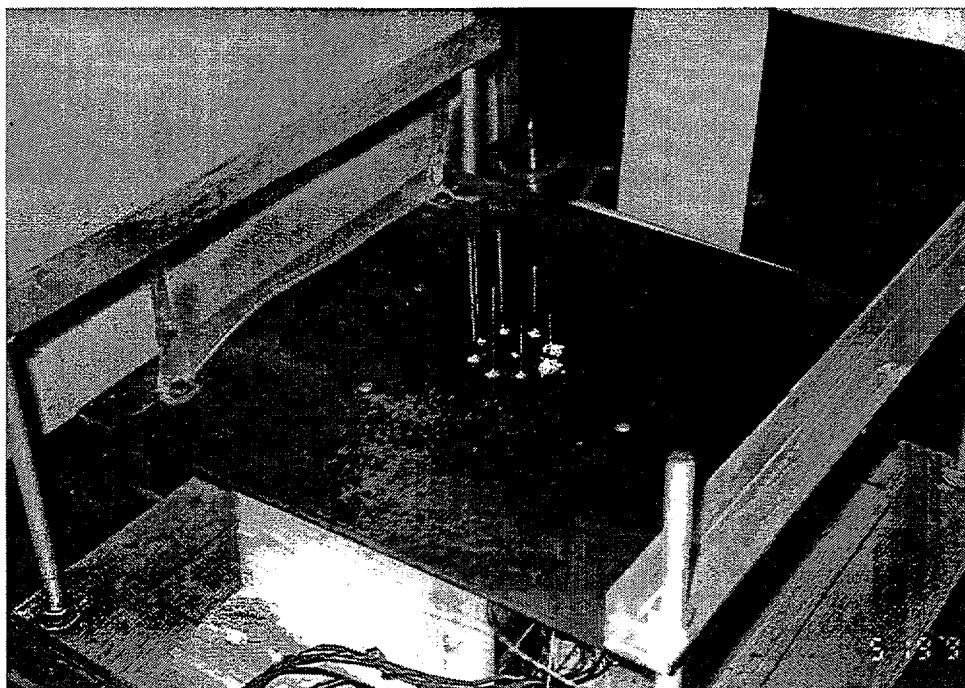


FIGURE 6. Photograph of Test Plate

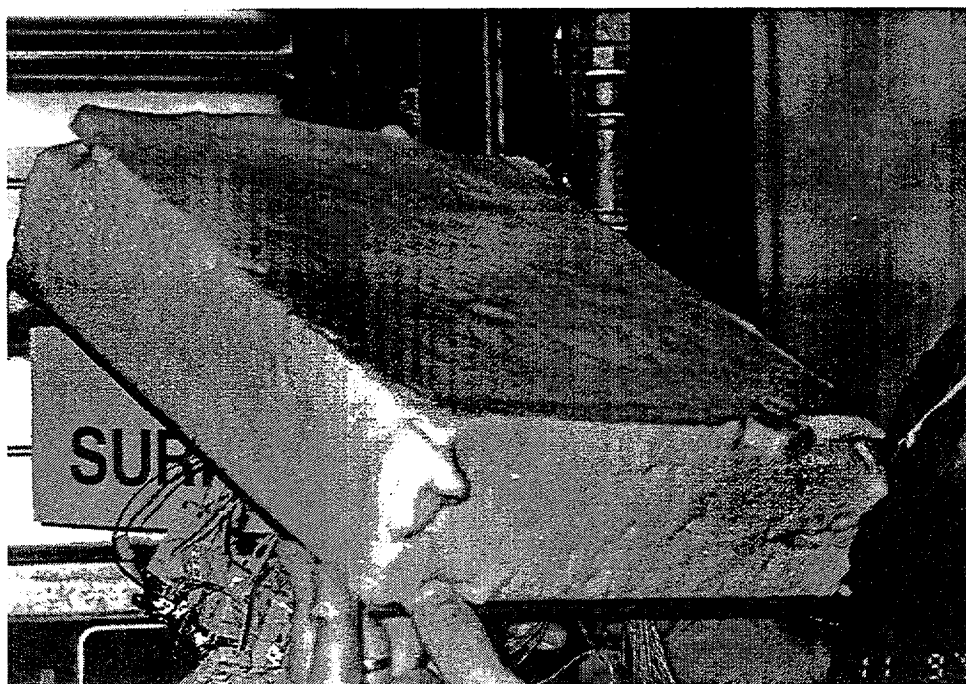


FIGURE 7. Photograph of Foam Covered Test Plate

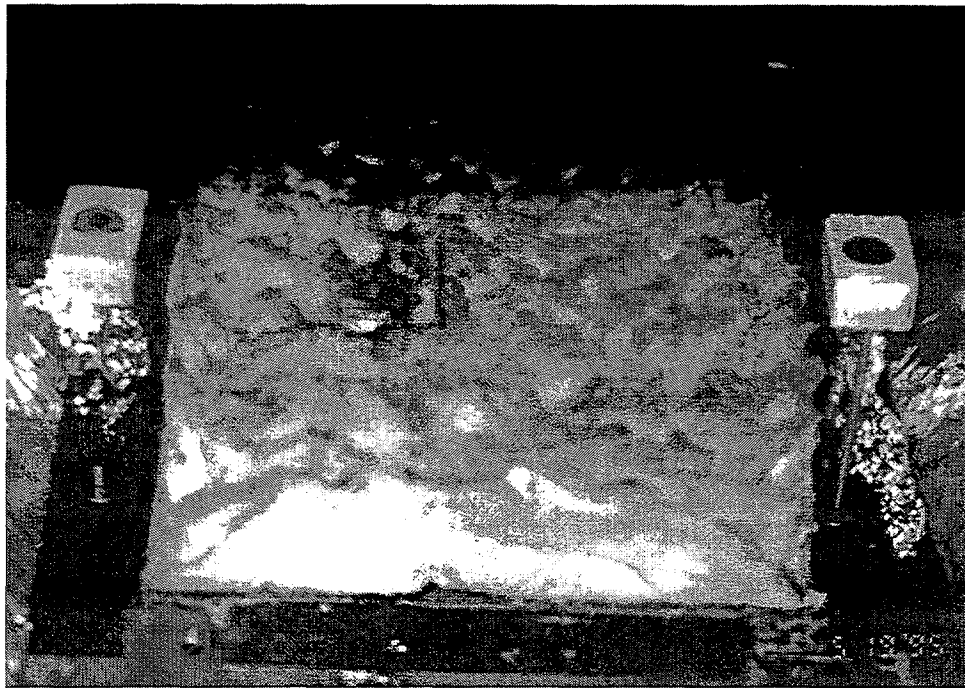


FIGURE 8. Photograph of Foam Sample During Test

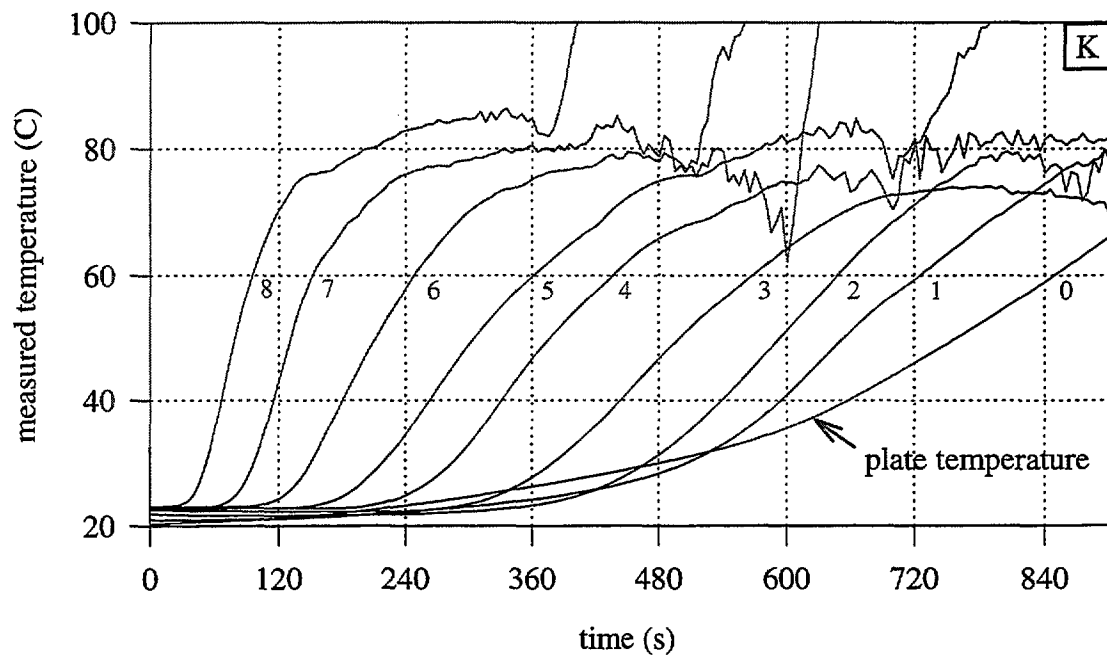


FIGURE 9. Thermocouple Measurements From Foam Test

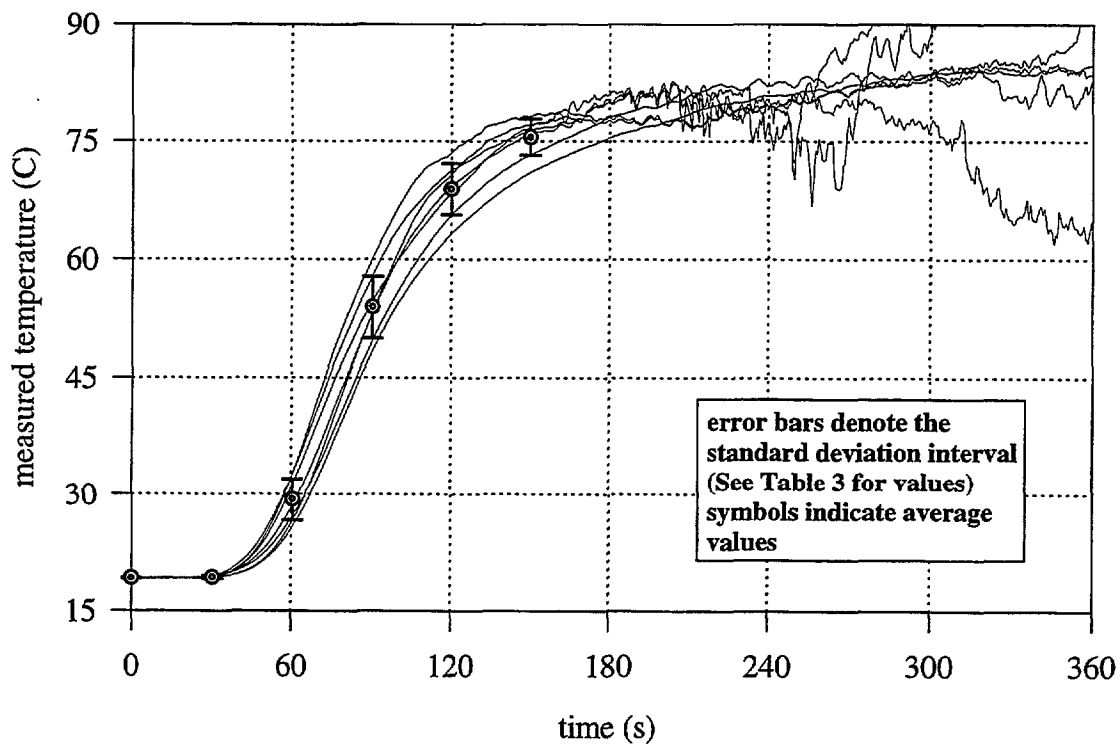


FIGURE 10. Several Thermocouple Measurements at One Height

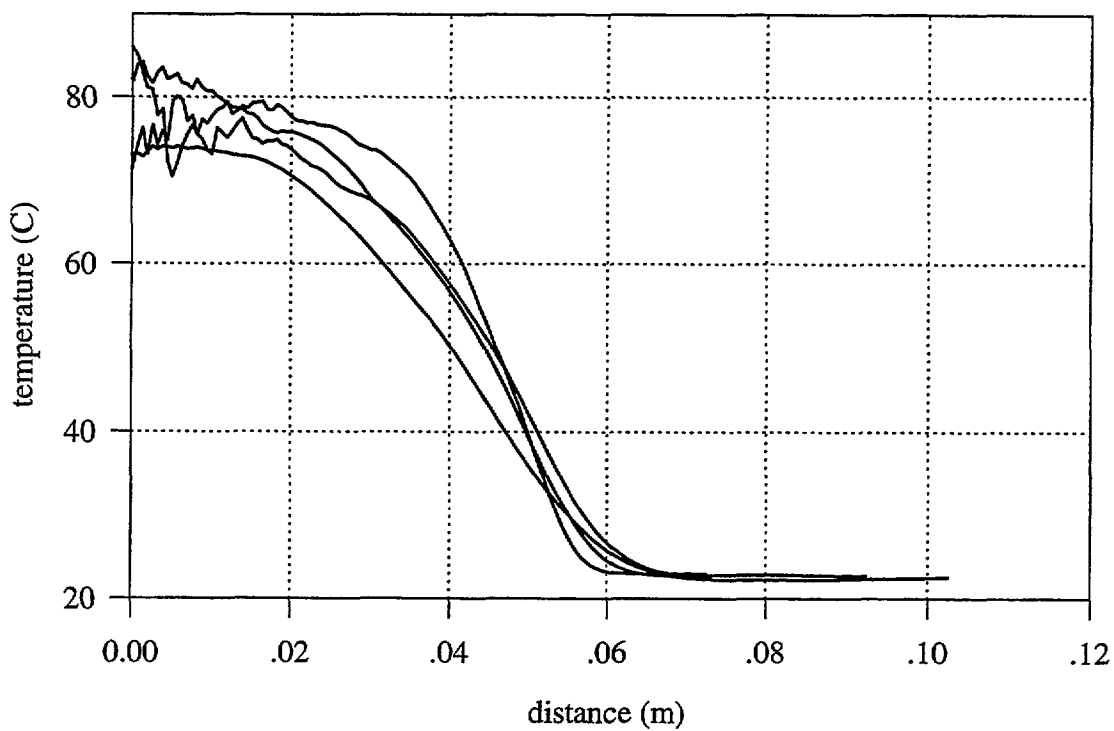


FIGURE 11. Steady State Temperature Profile From Foam Test

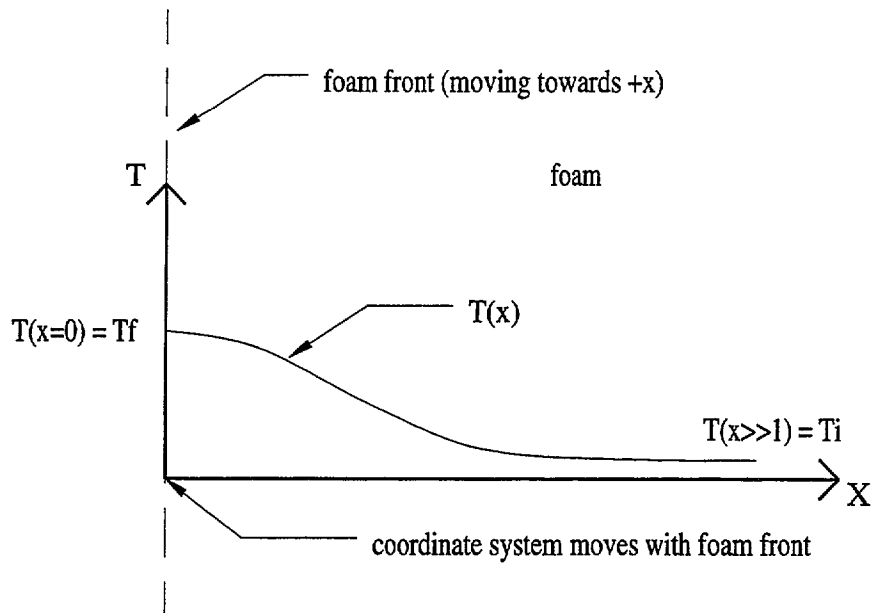


FIGURE 12. Coordinate System and Boundary Conditions

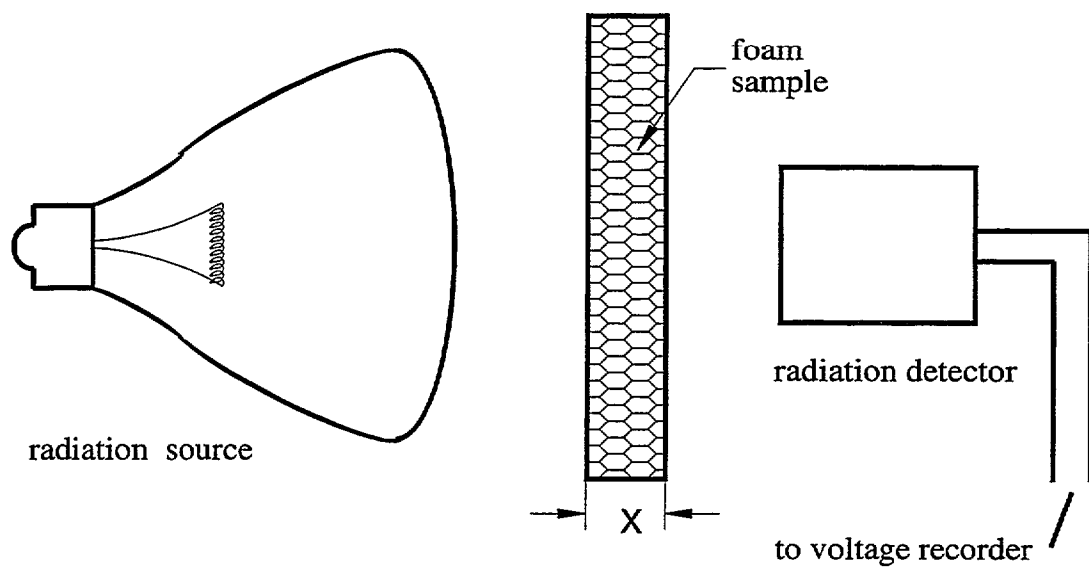


FIGURE 13. Experimental Radiation Measurement Setup

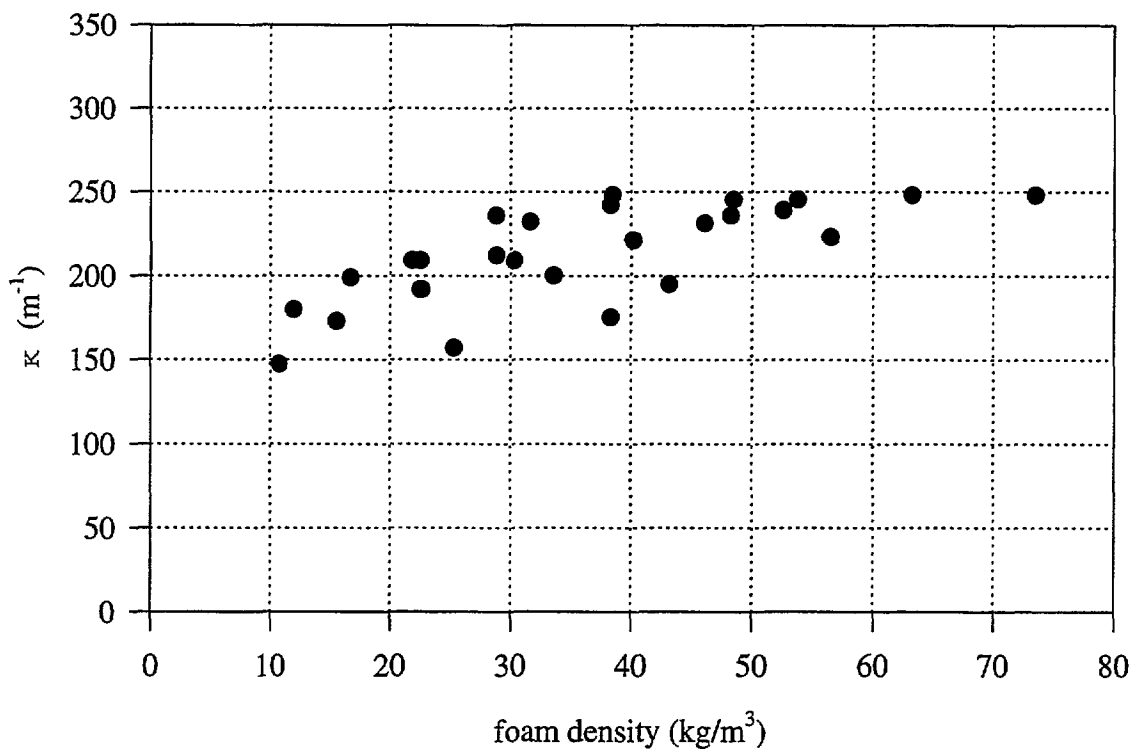


FIGURE 14. Measured Extinction Coefficient Data

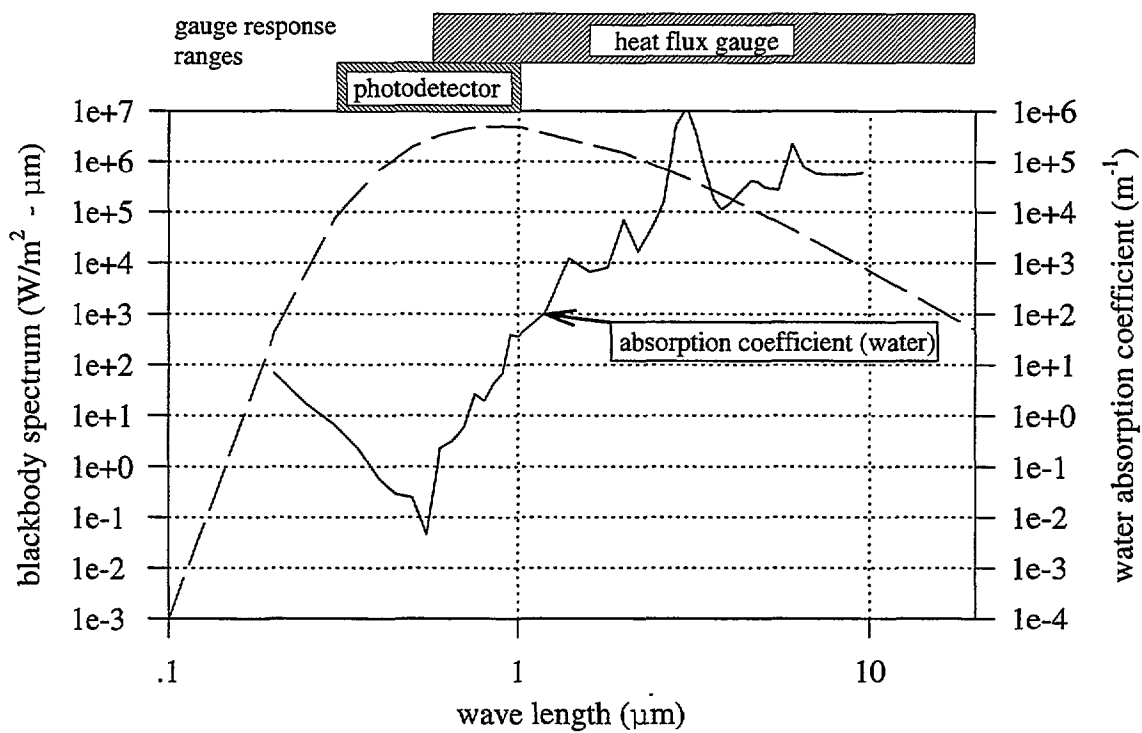


FIGURE 15. Spectral Ranges

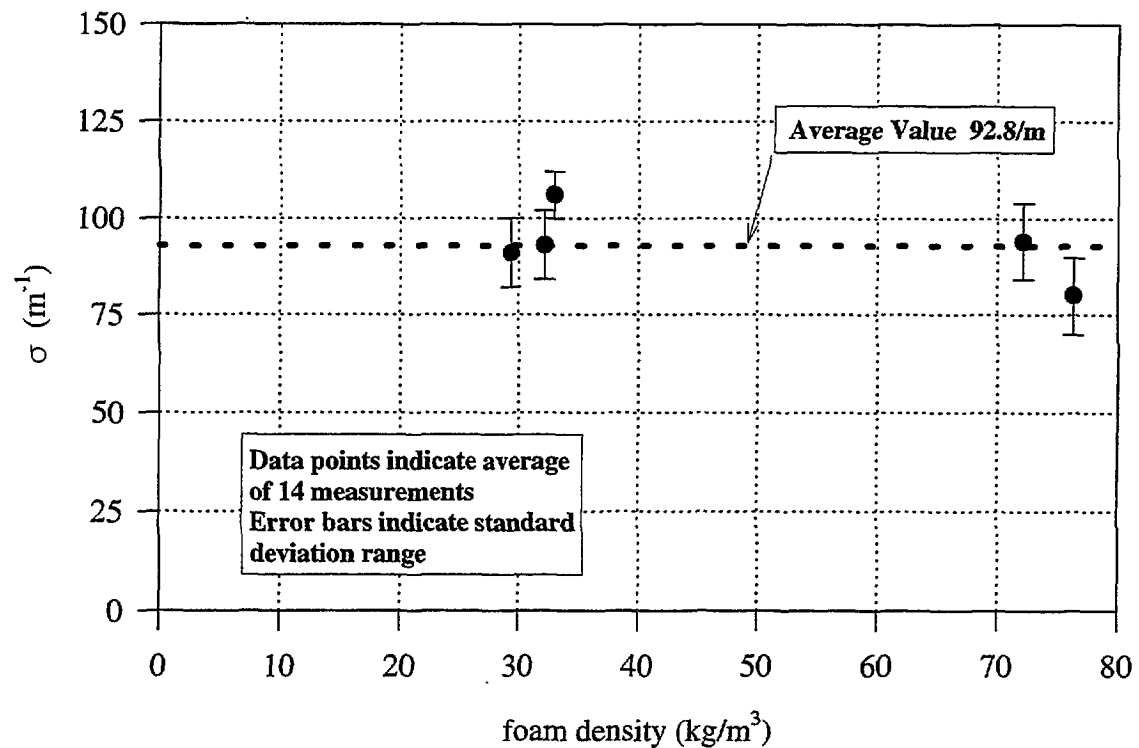


FIGURE 16. Measured Scattering Coefficient Data

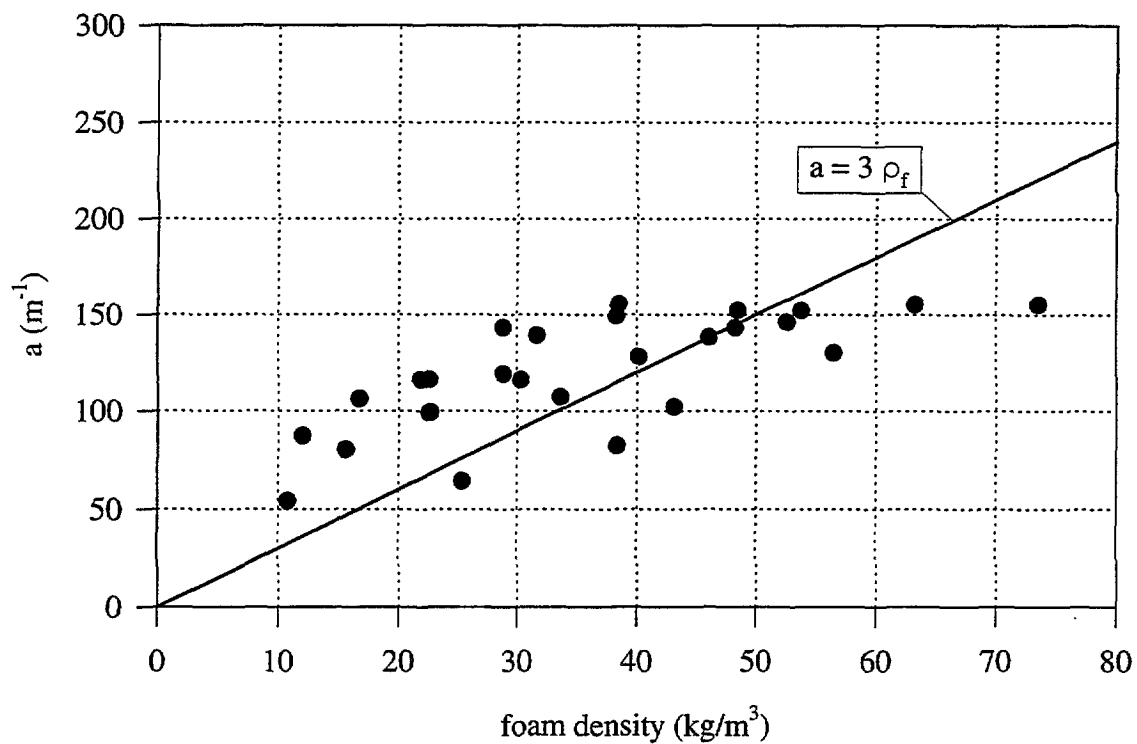


FIGURE 17. Calculated Absorption Coefficient Data

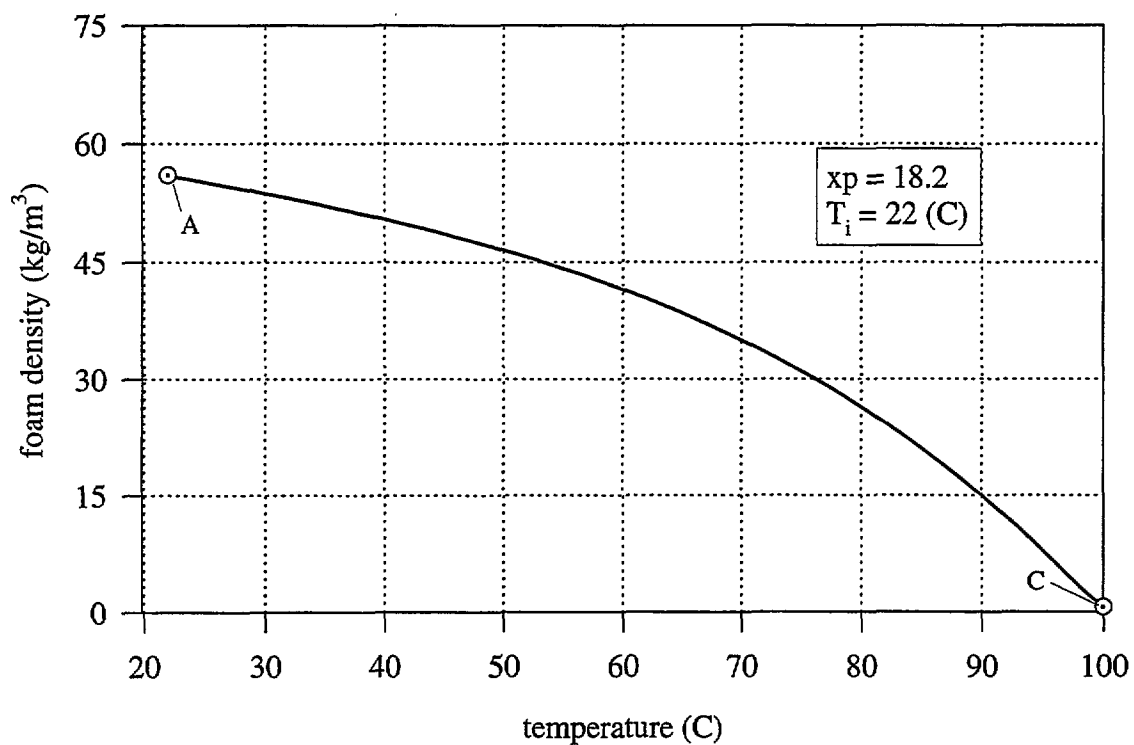


FIGURE 18. Ideal Foam Density Function

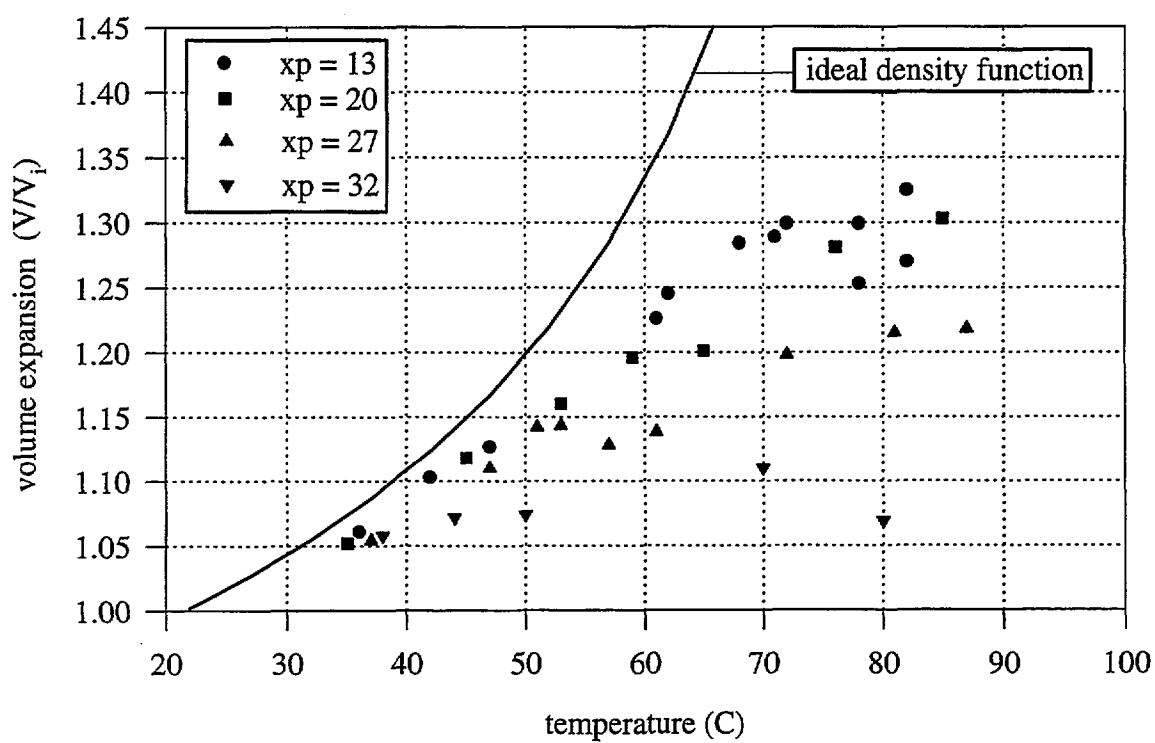


FIGURE 19. Foam Volume Expansion Measurements

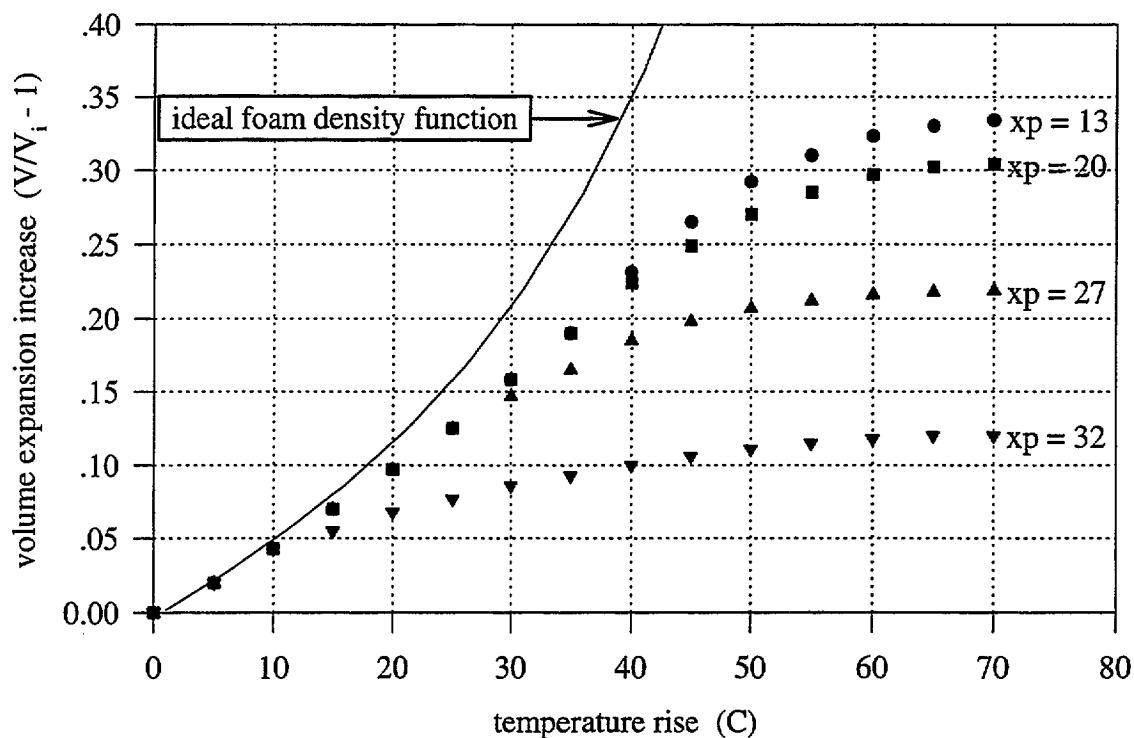


FIGURE 20. Foam Volume Expansion due to Temperature Rise

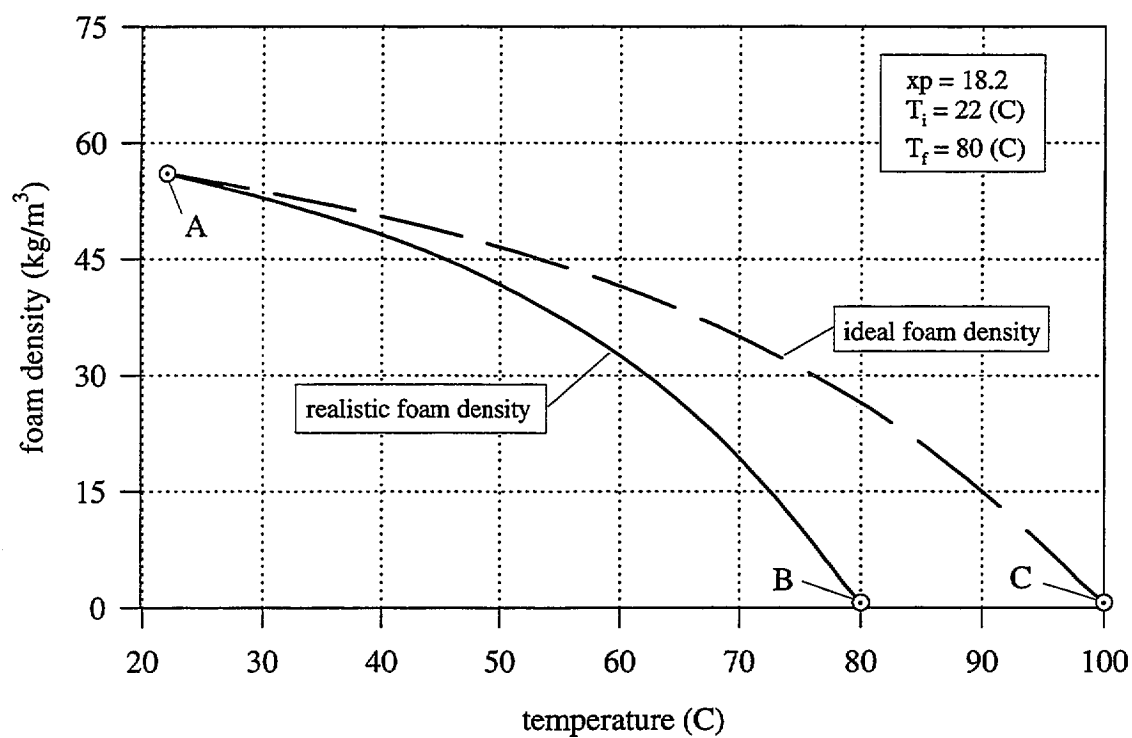


FIGURE 21. Realistic Foam Density Function

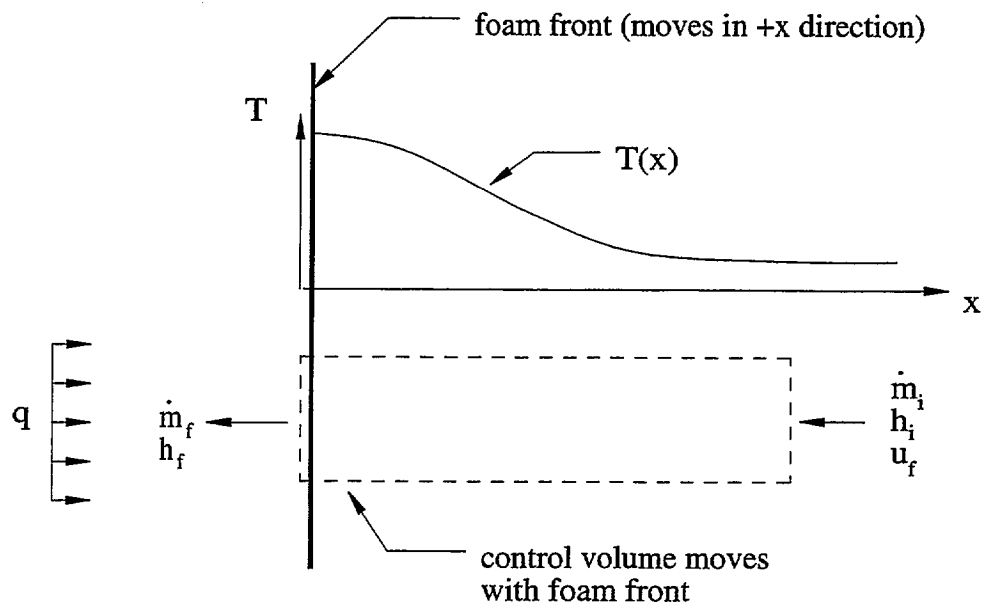


FIGURE 22. Diagram for Steady State Steady Flow Analysis

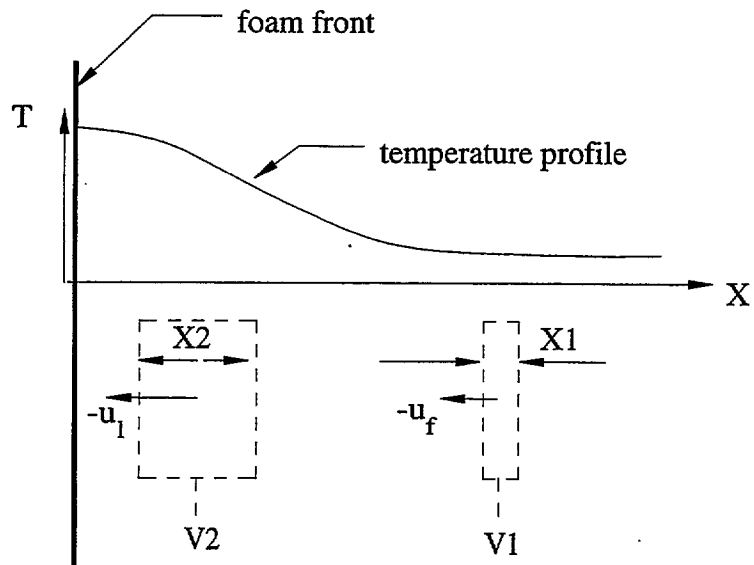


FIGURE 23. Diagram for Liquid Velocity Determination

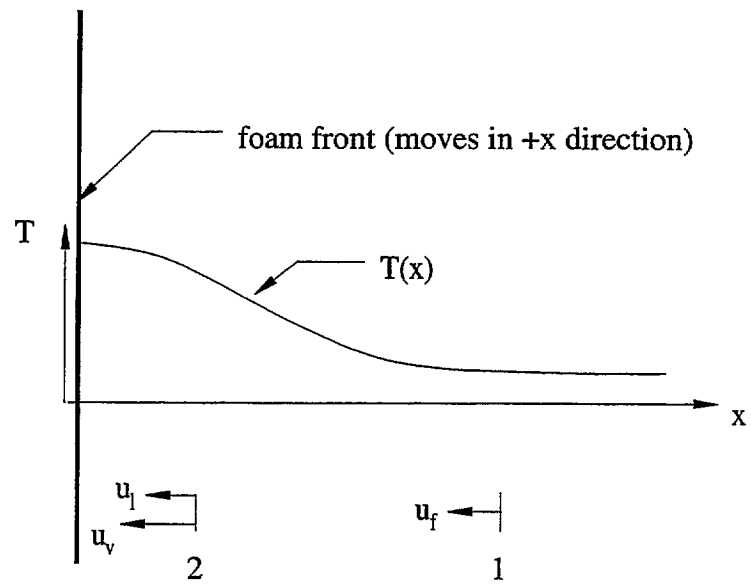


FIGURE 24. Diagram for Gas Velocity Determination

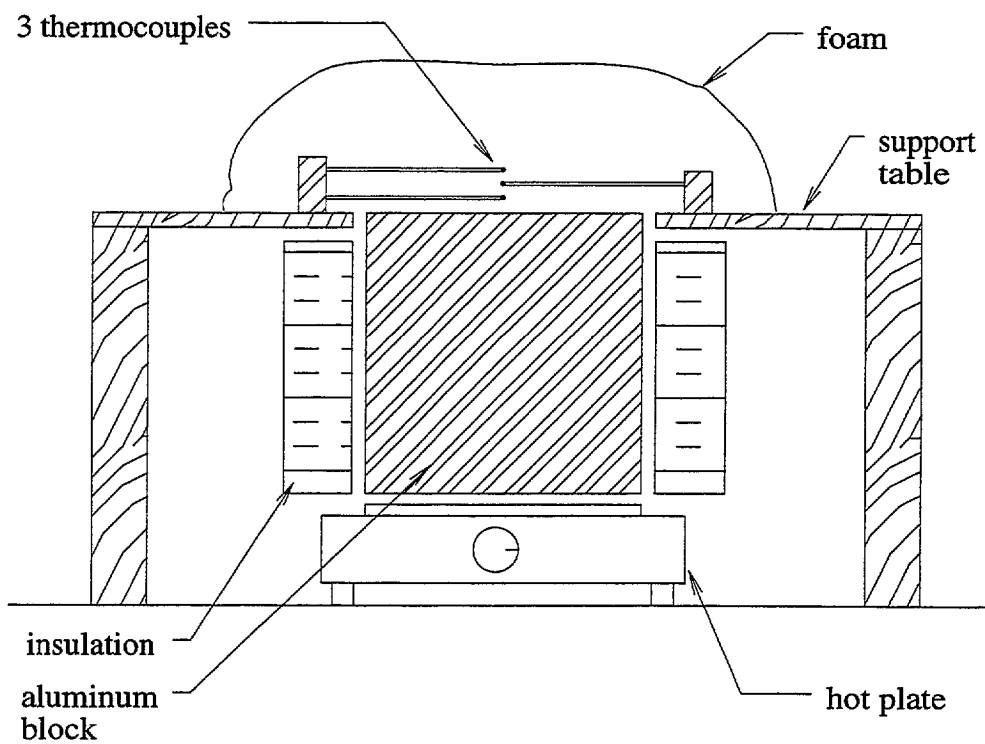


FIGURE 25. Thermal Diffusivity Measurement Setup

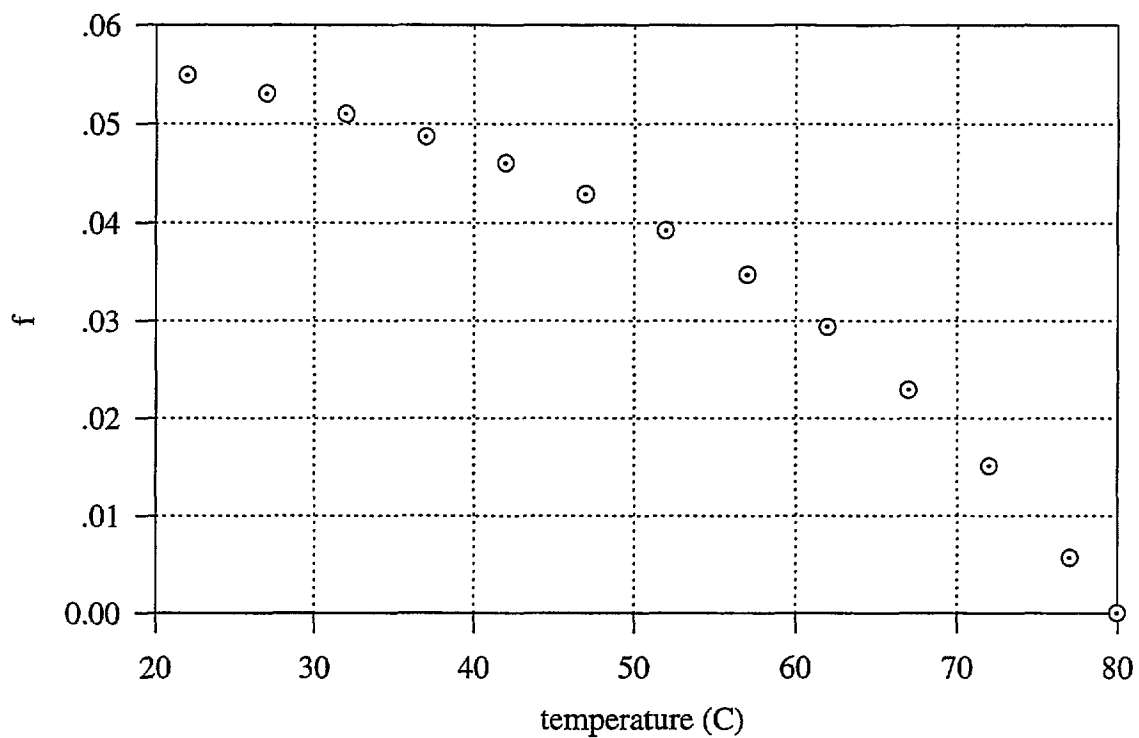


FIGURE 26. Liquid Volume Fraction

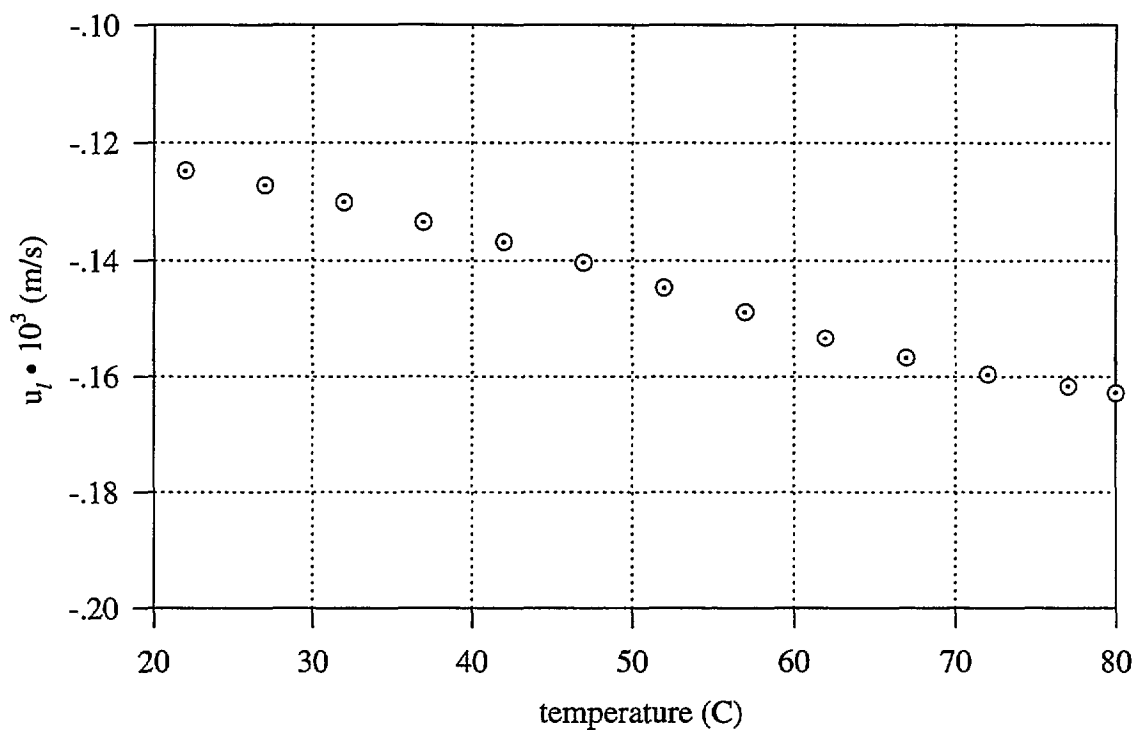


FIGURE 27. Liquid Velocity Relative to Front

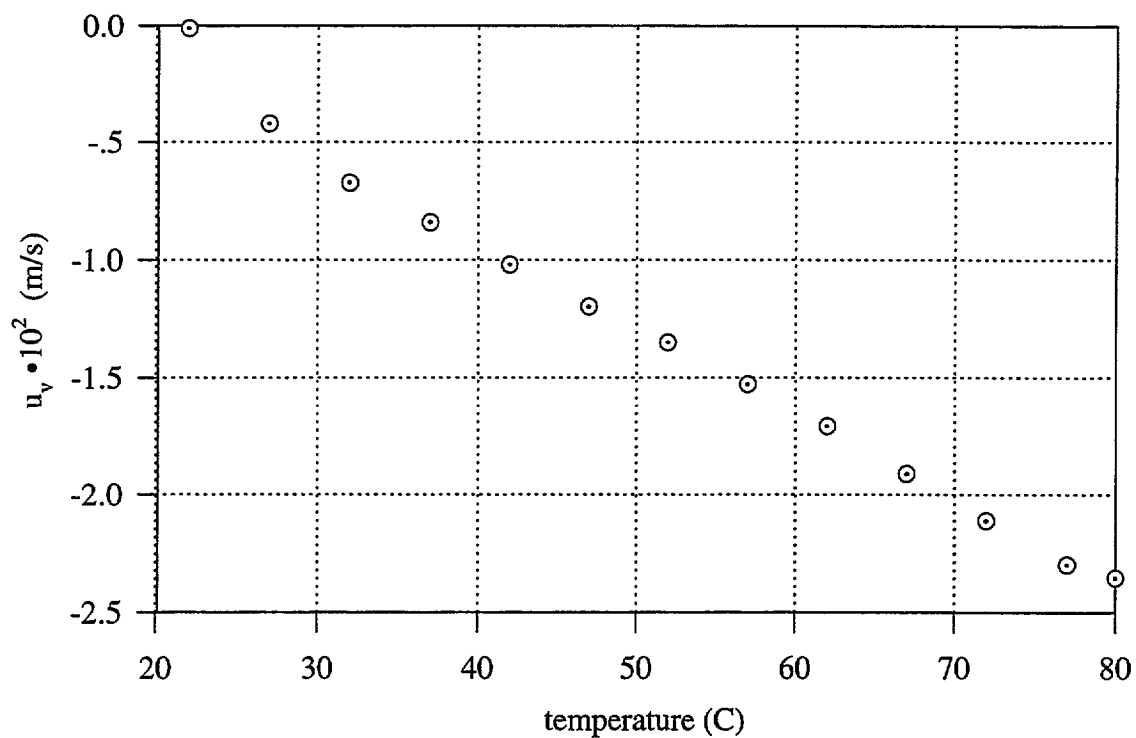


FIGURE 28. Vapor Velocity Relative to Front

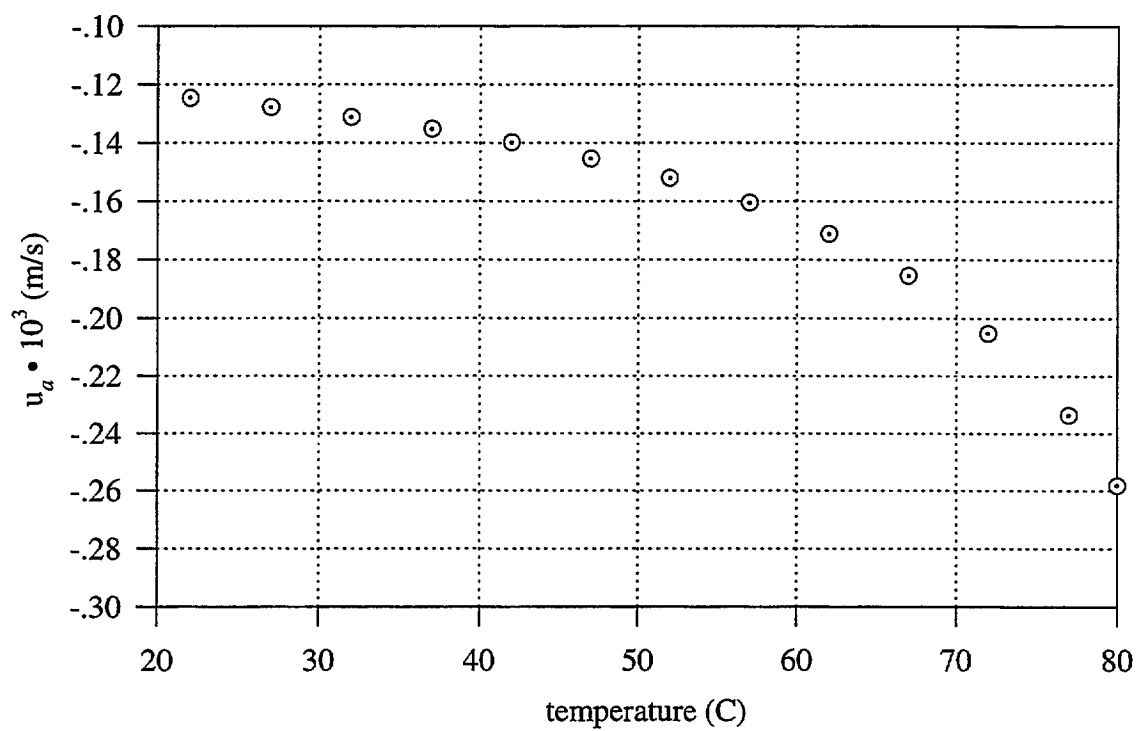


FIGURE 29. Air Velocity Relative to Front

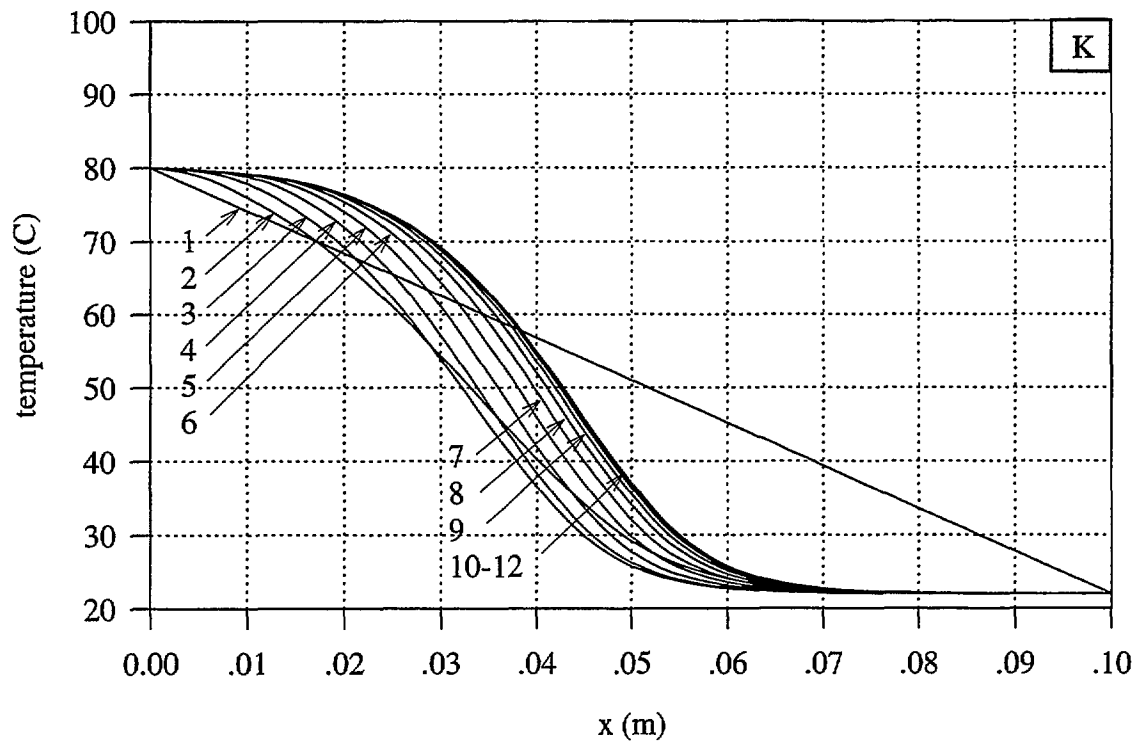


FIGURE 30. Convergence of Temperture Profiles

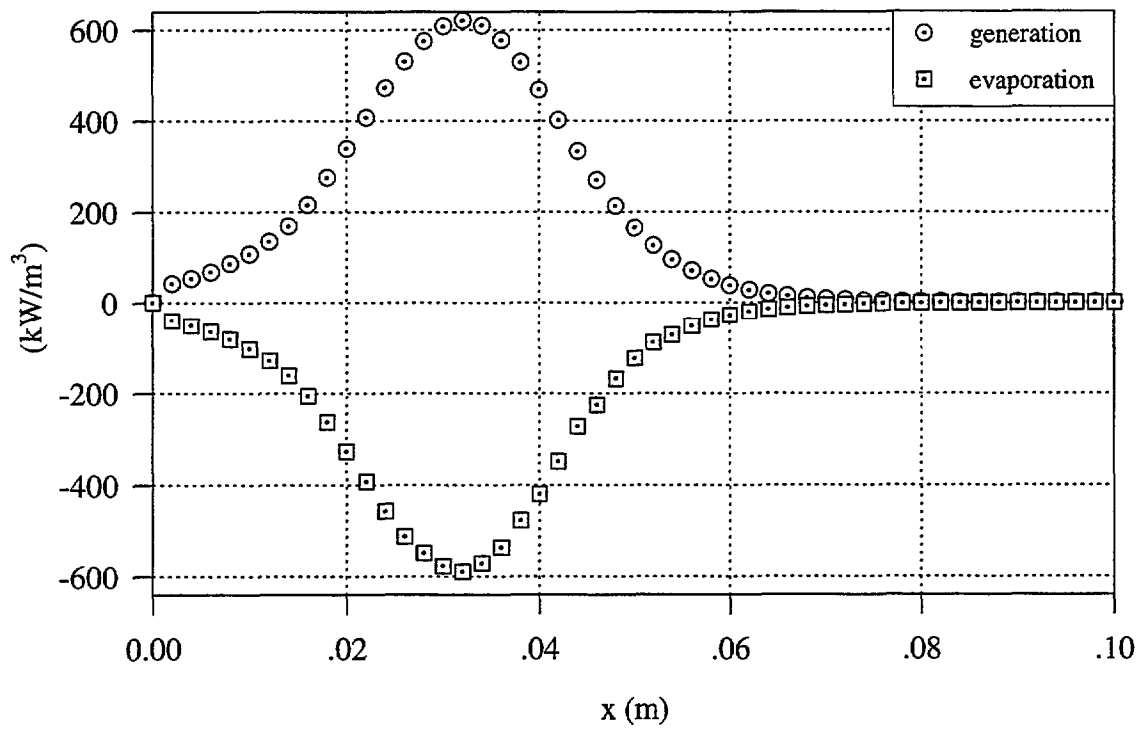


FIGURE 31. Generation and Evaporative Sink Terms

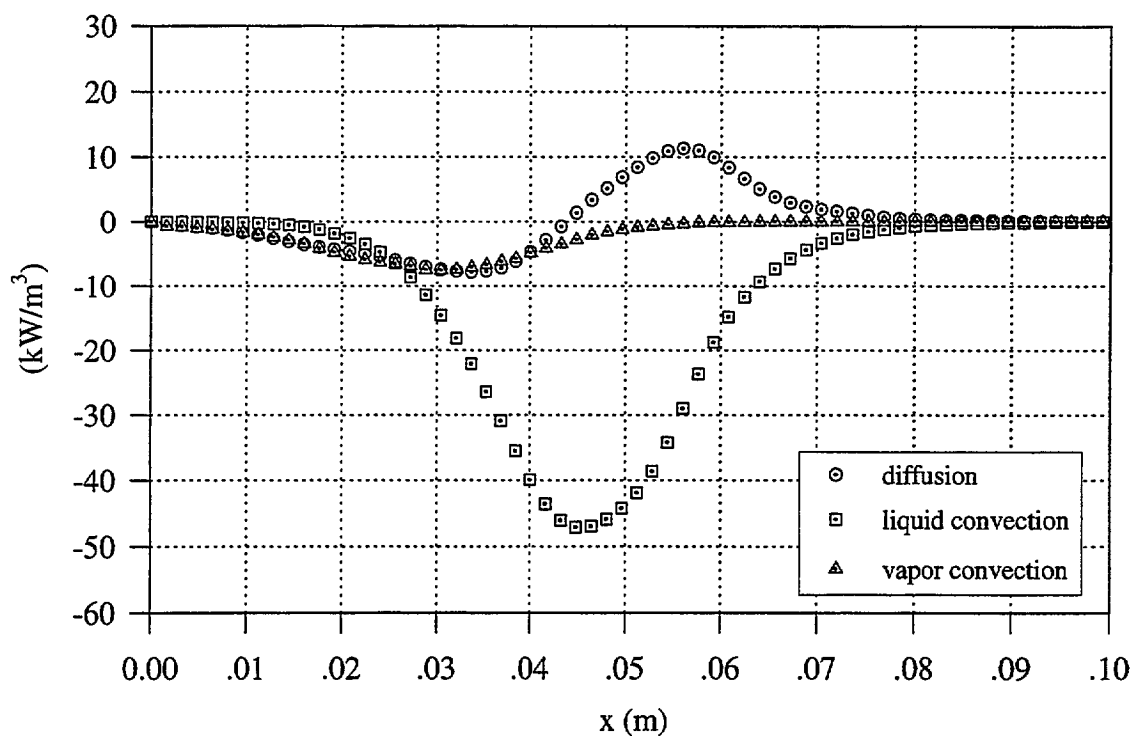


FIGURE 32. Convective and Diffusion Terms

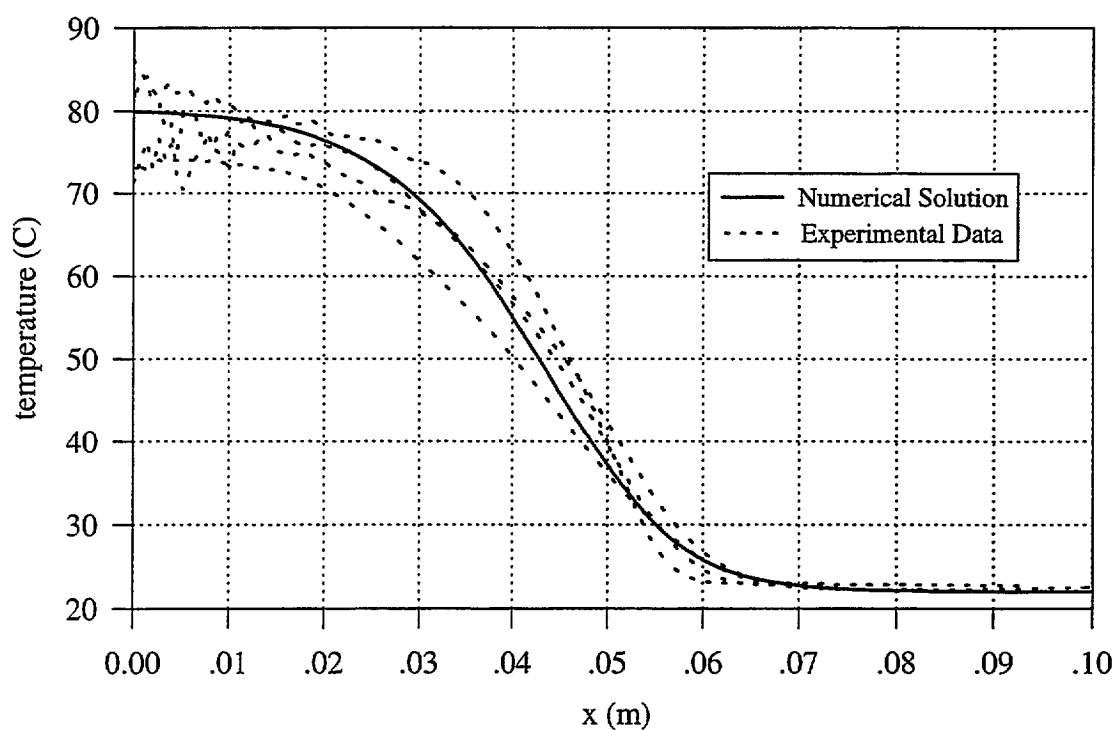


FIGURE 33. Comparison of Numerical and Experimental Temperature Profile

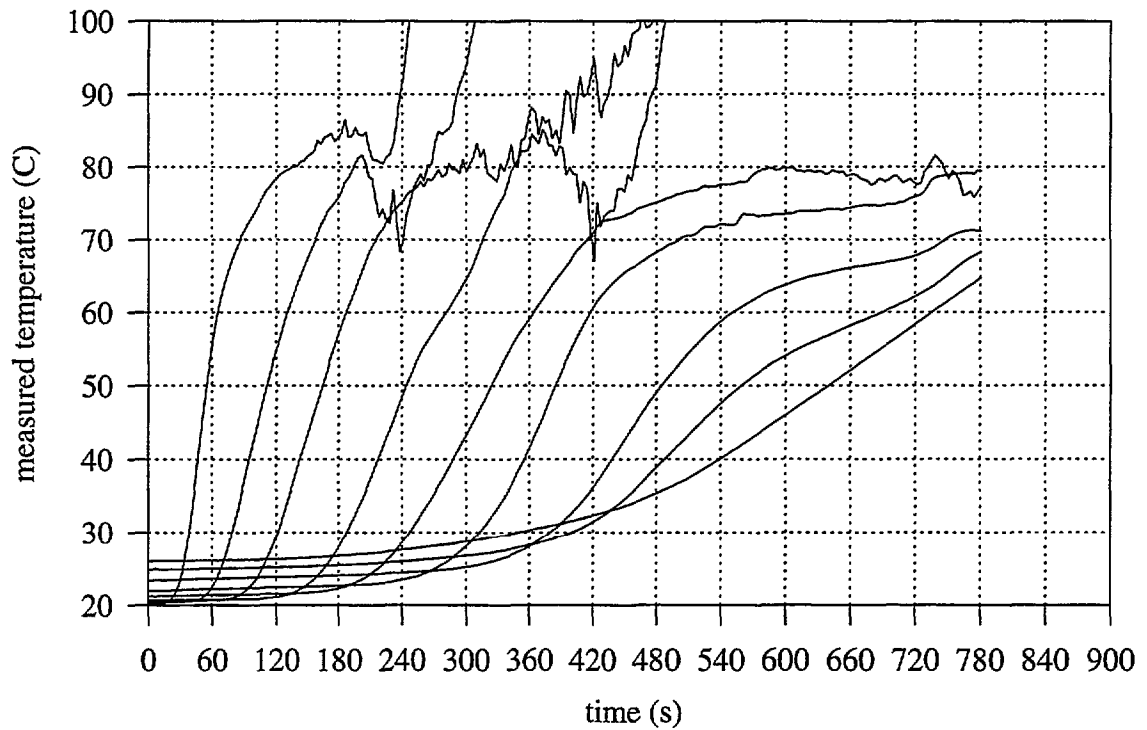


FIGURE 34A. Thermocouple Measurements From Foam Test A

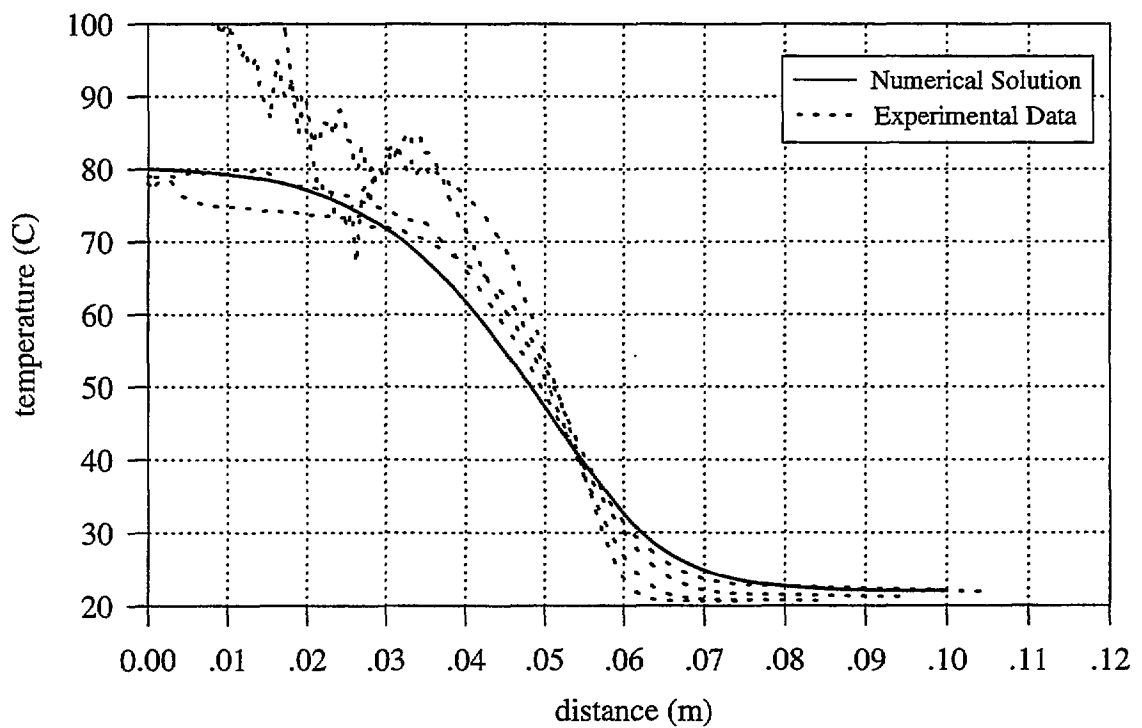


FIGURE 34B. Experimental and Numerical Temperature Profiles, Case A

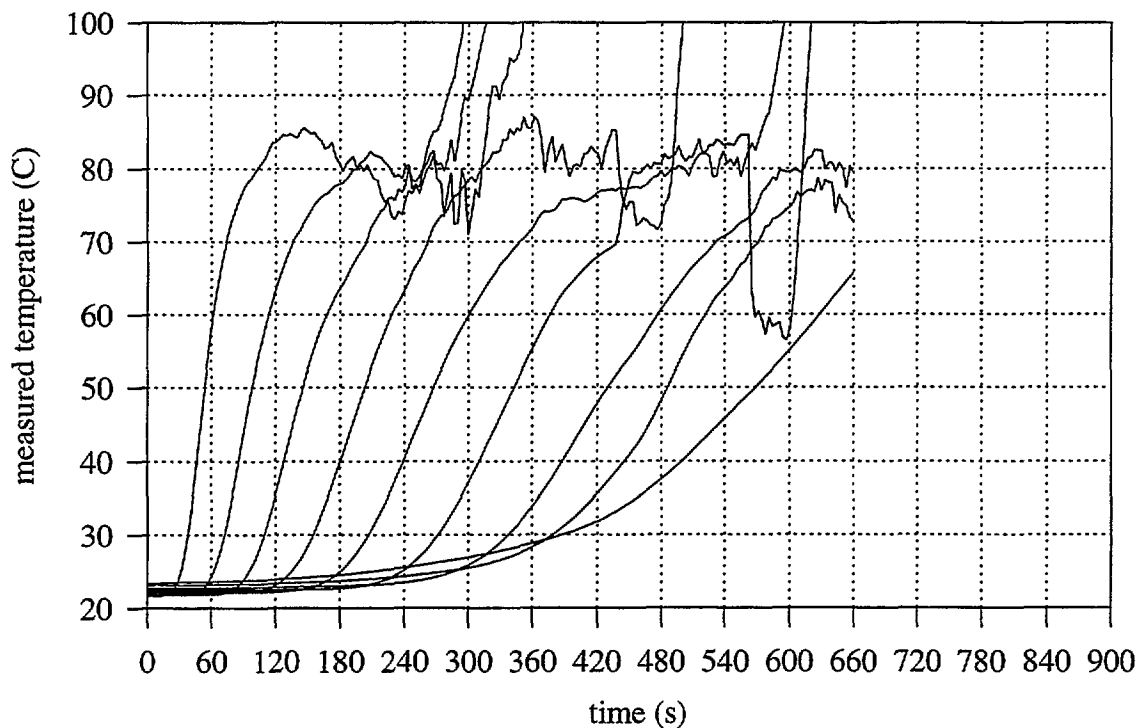


FIGURE 35A. Thermocouple Measurements From Foam Test B

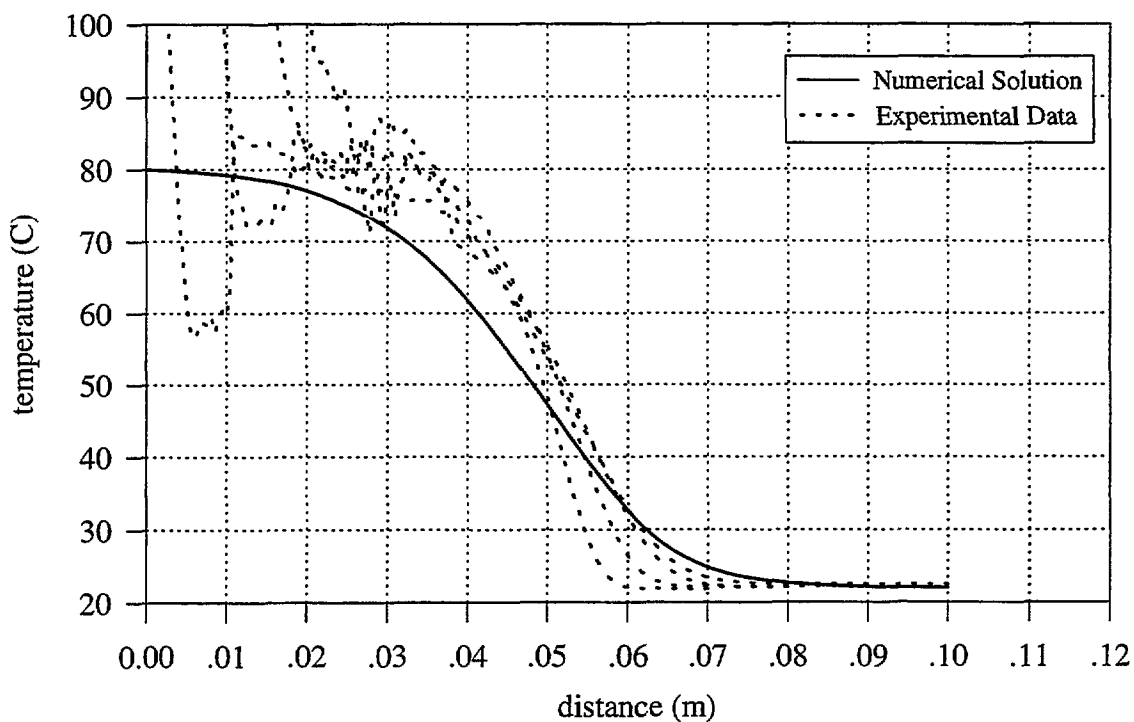


FIGURE 35B. Experimental and Numerical Temperature Profiles, Case B

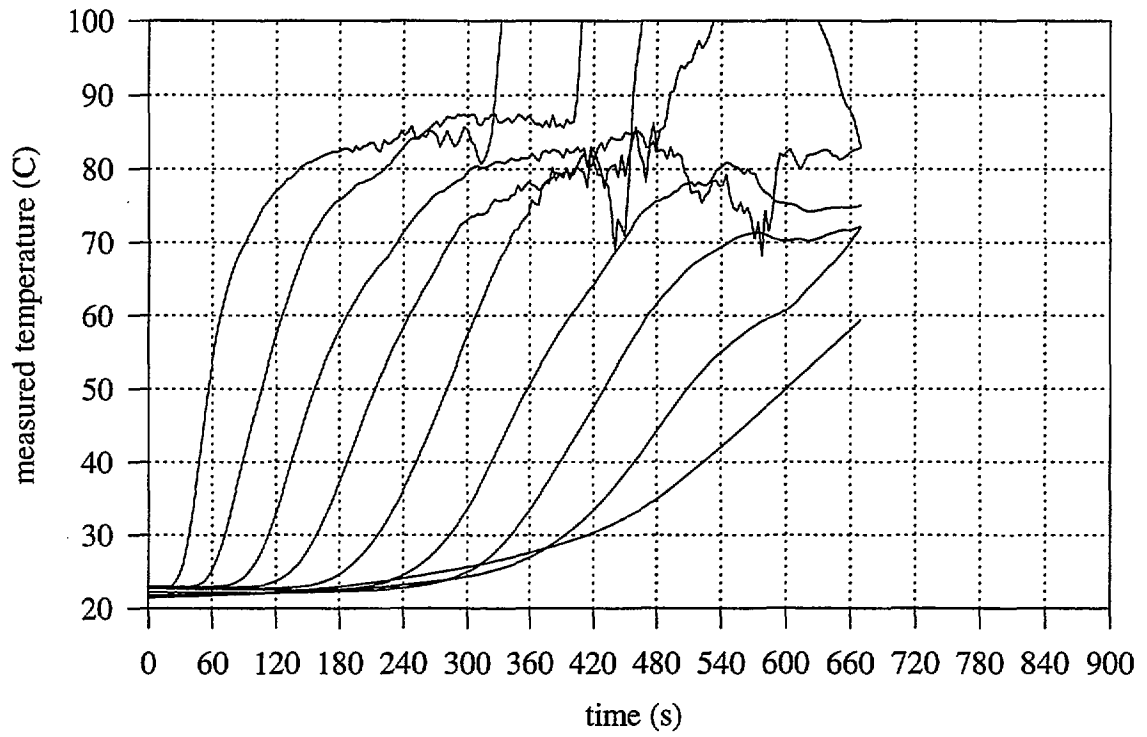


FIGURE 36A. Thermocouple Measurements From Foam Test C

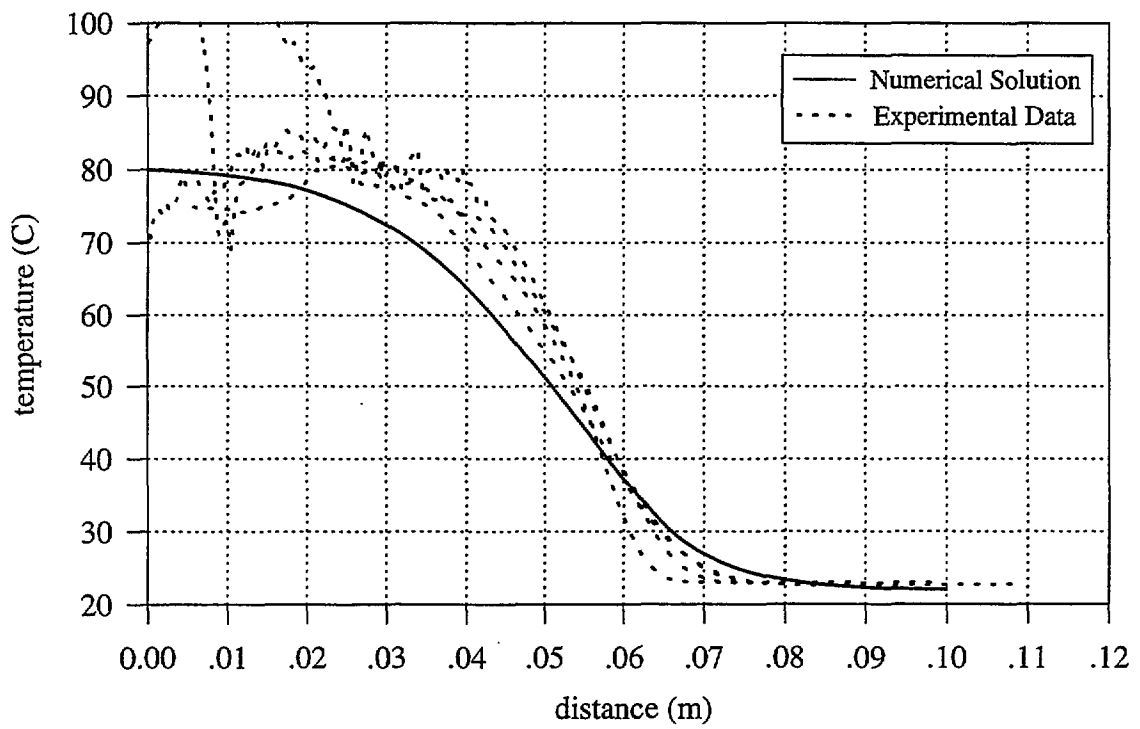


FIGURE 36B. Experimental and Numerical Temperature Profiles, Case C

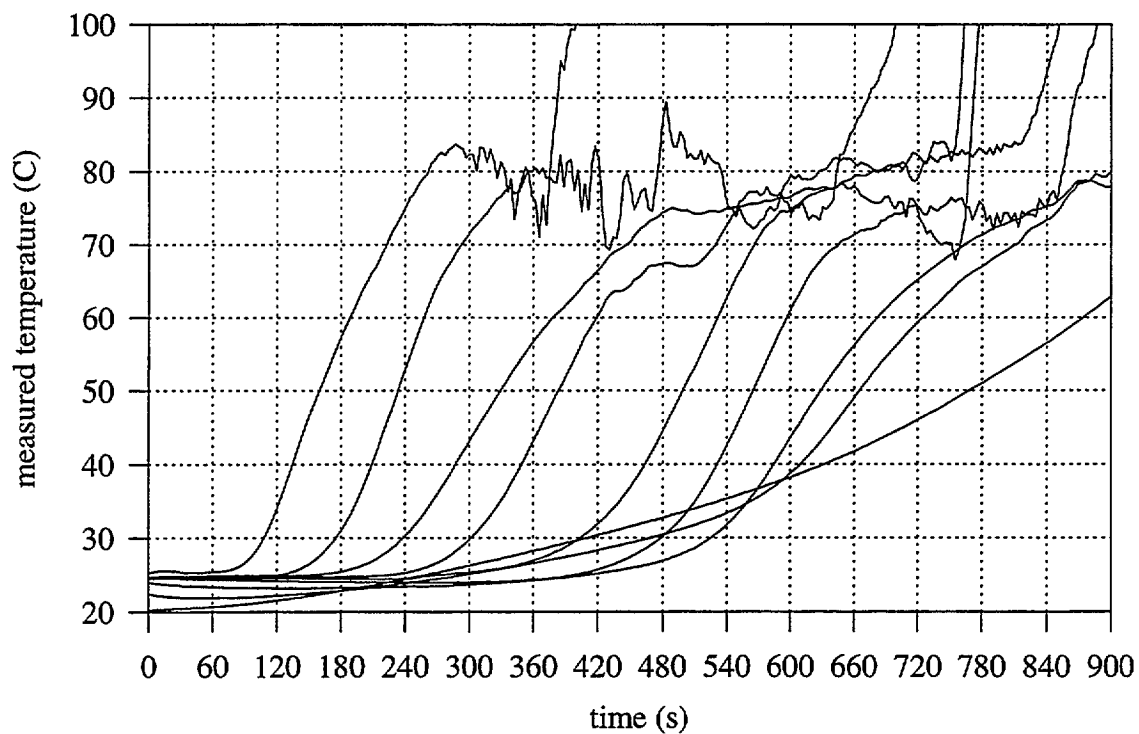


FIGURE 37A. Thermocouple Measurements From Foam Test D

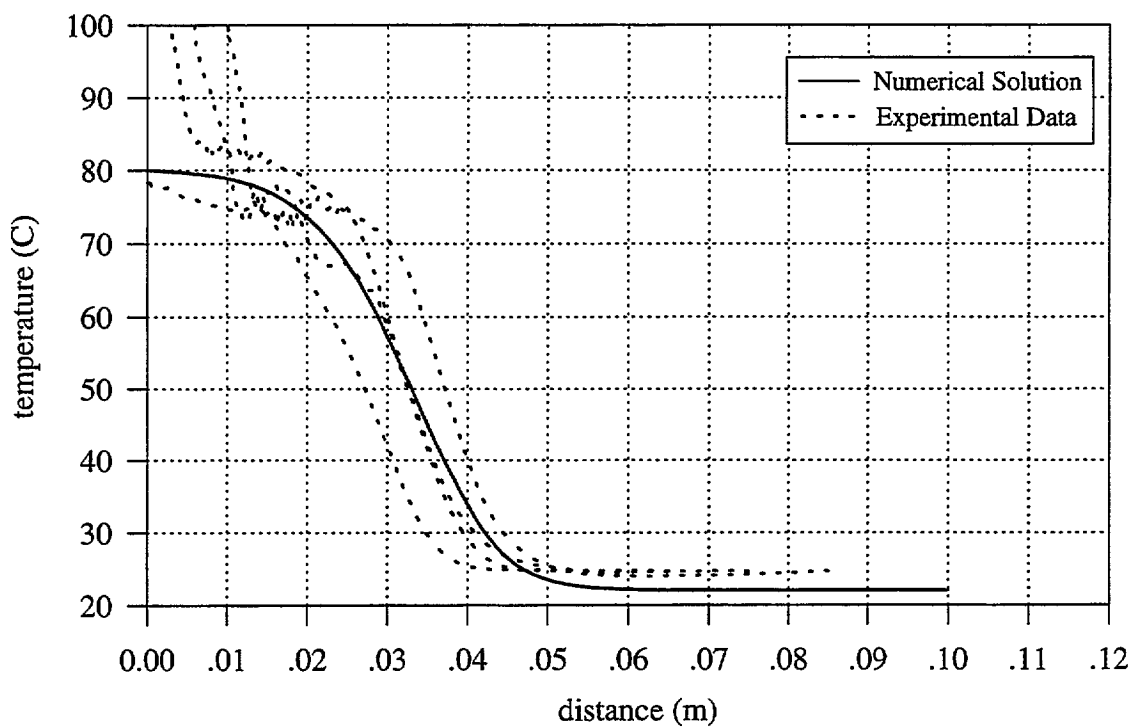


FIGURE 37B. Experimental and Numerical Temperature Profiles, Case D

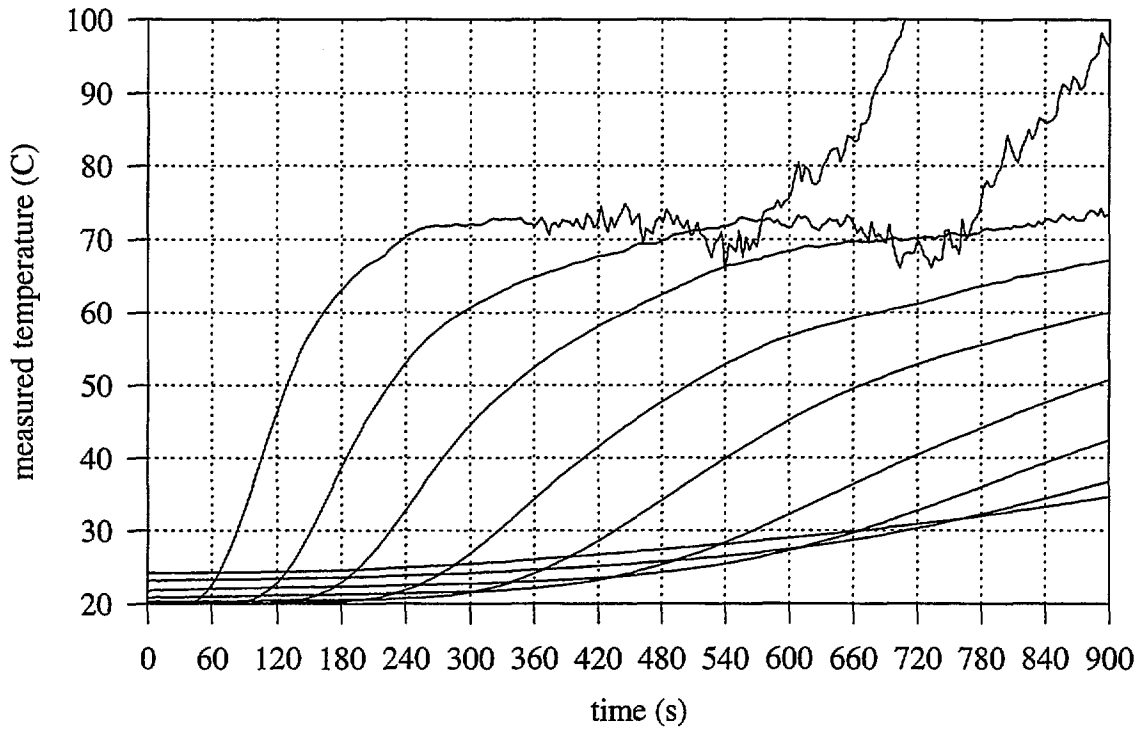


FIGURE 38A. Thermocouple Measurements From Foam Test E

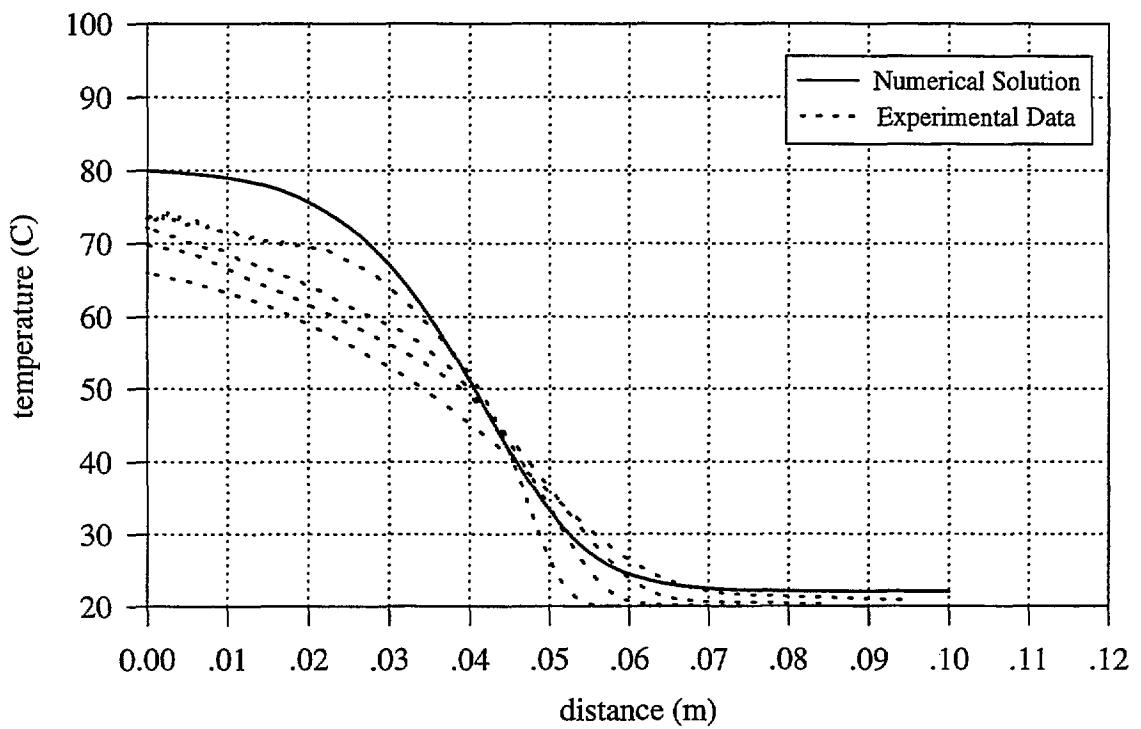


FIGURE 38B. Experimental and Numerical Temperature Profiles, Case E

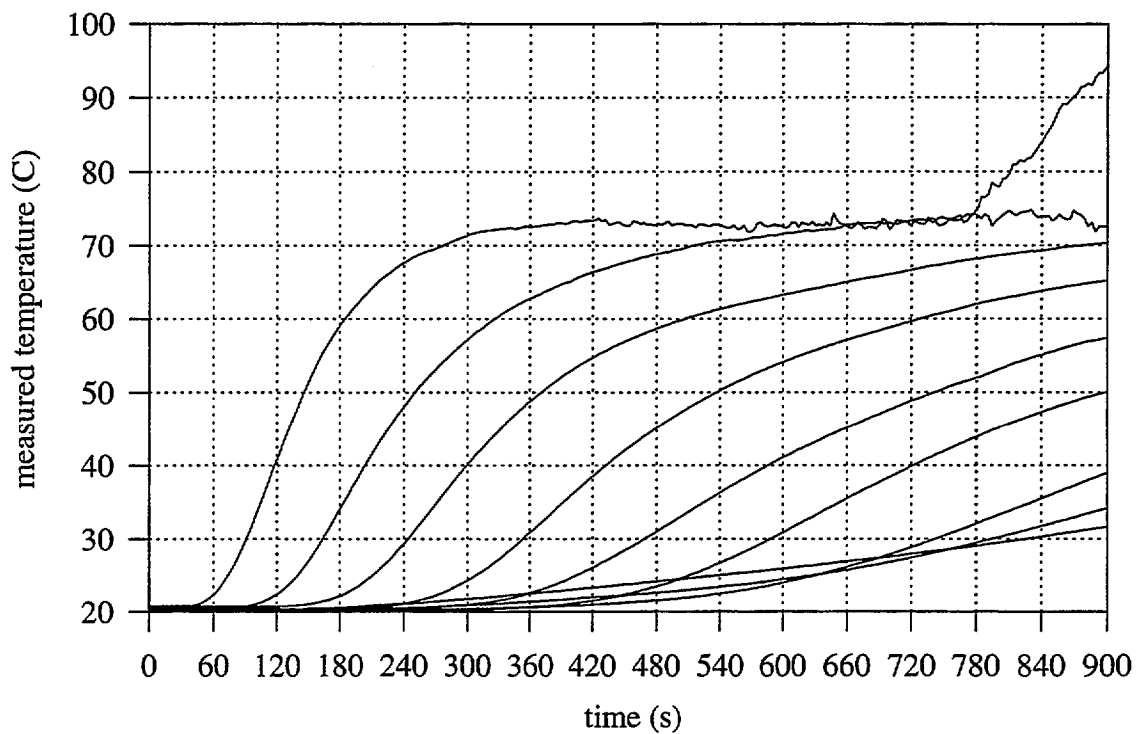


FIGURE 39A. Thermocouple Measurements From Foam Test F

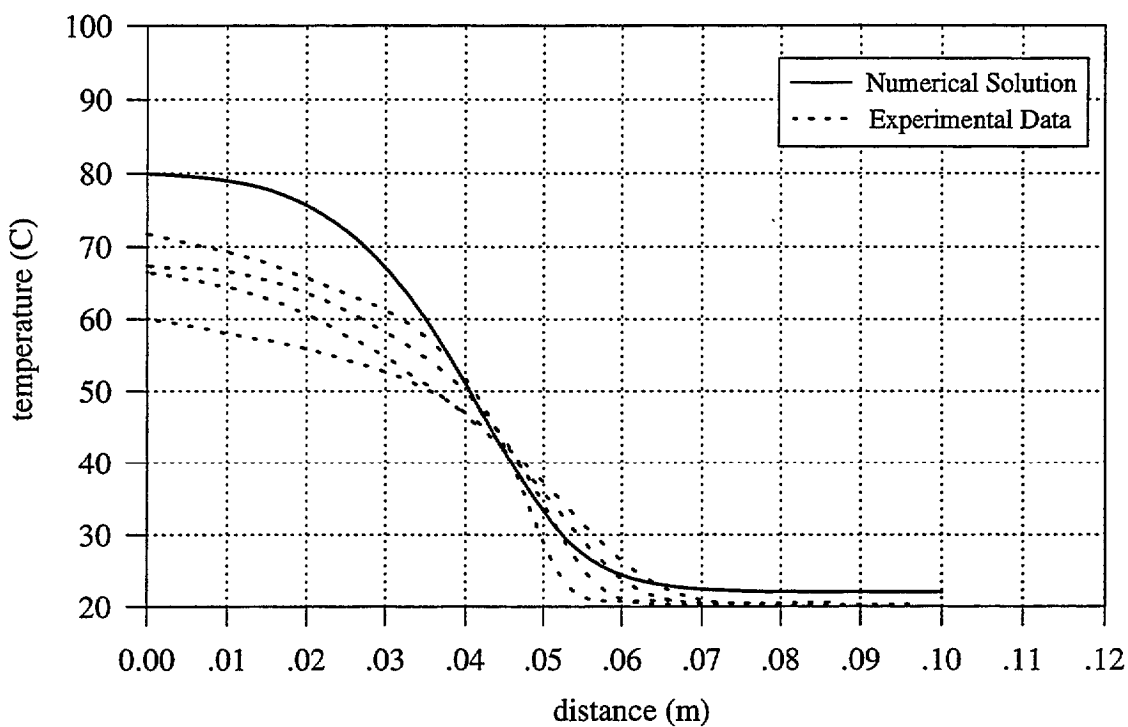


FIGURE 39B. Experimental and Numerical Temperature Profiles, Case F

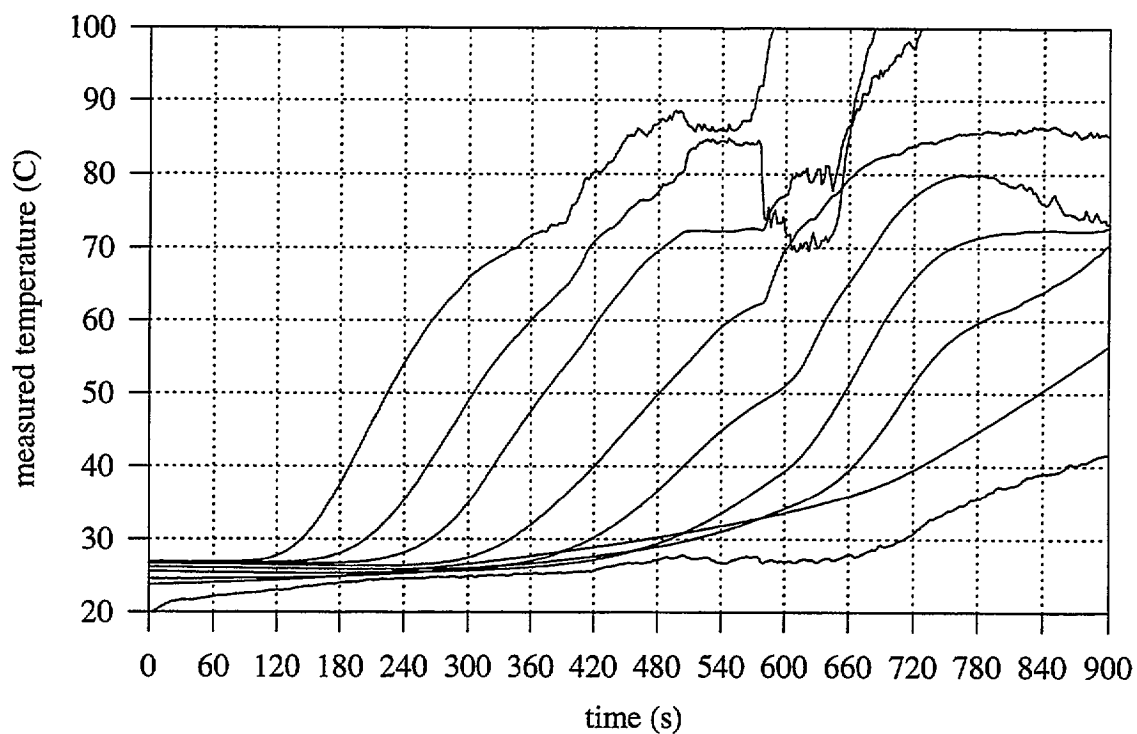


FIGURE 40A. Thermocouple Measurements From Foam Test G

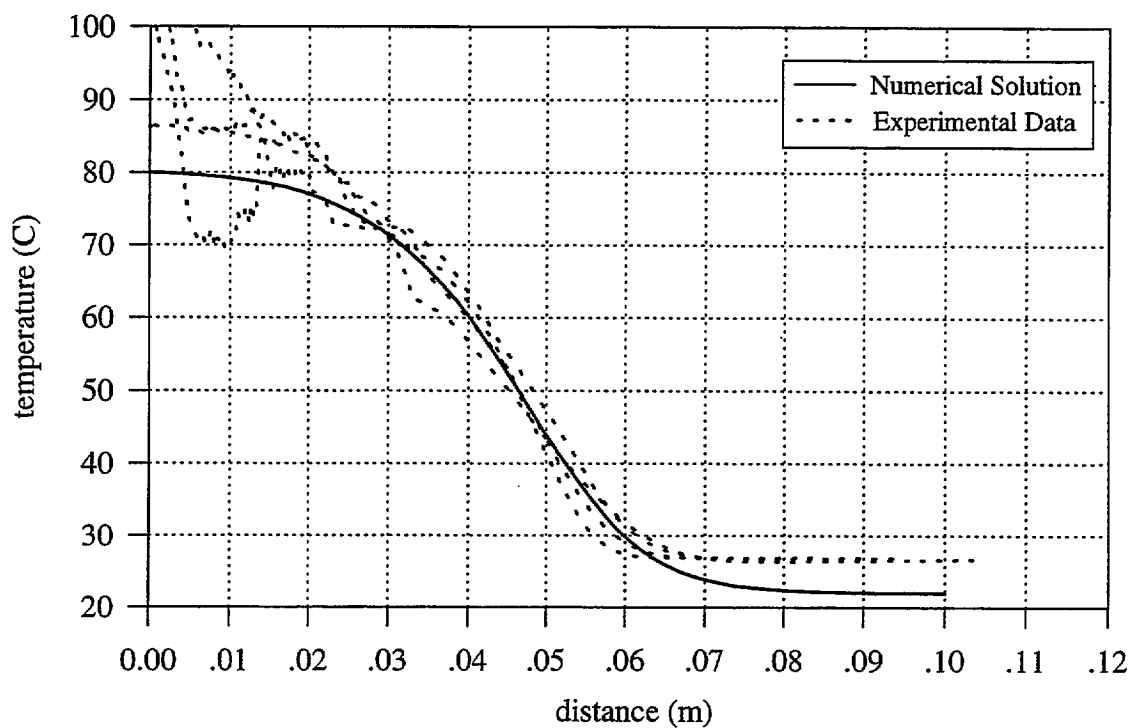


FIGURE 40B. Experimental and Numerical Temperature Profiles, Case G

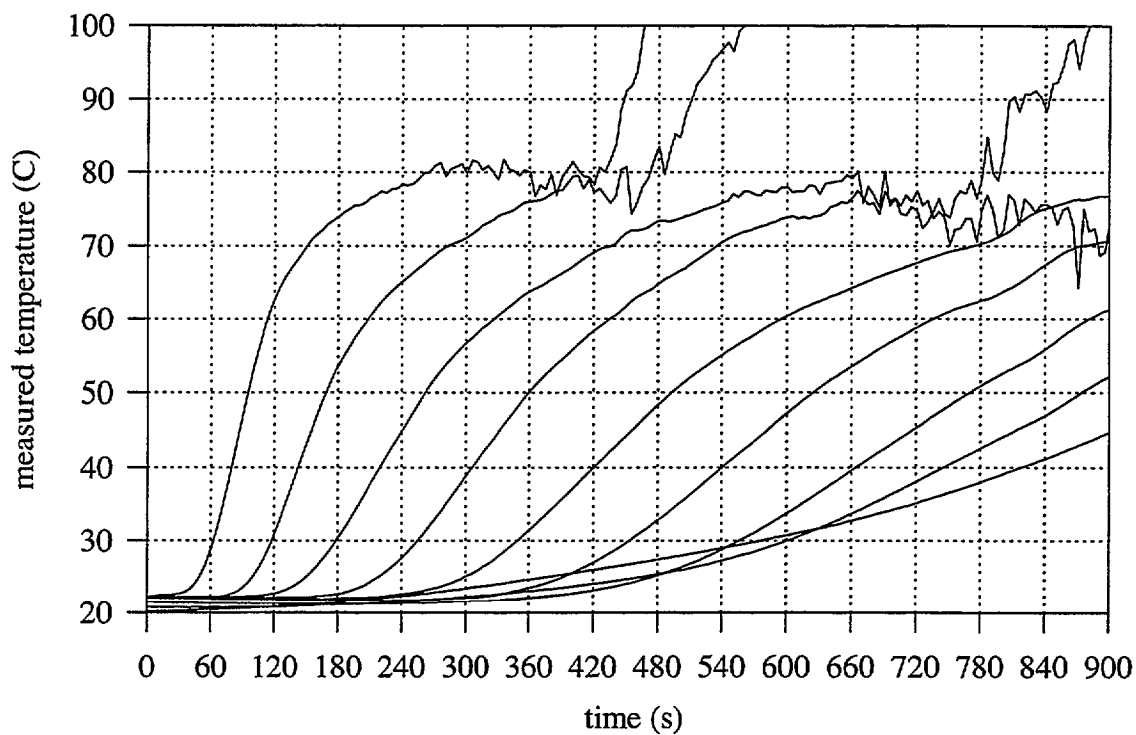


FIGURE 41A. Thermocouple Measurements From Foam Test H

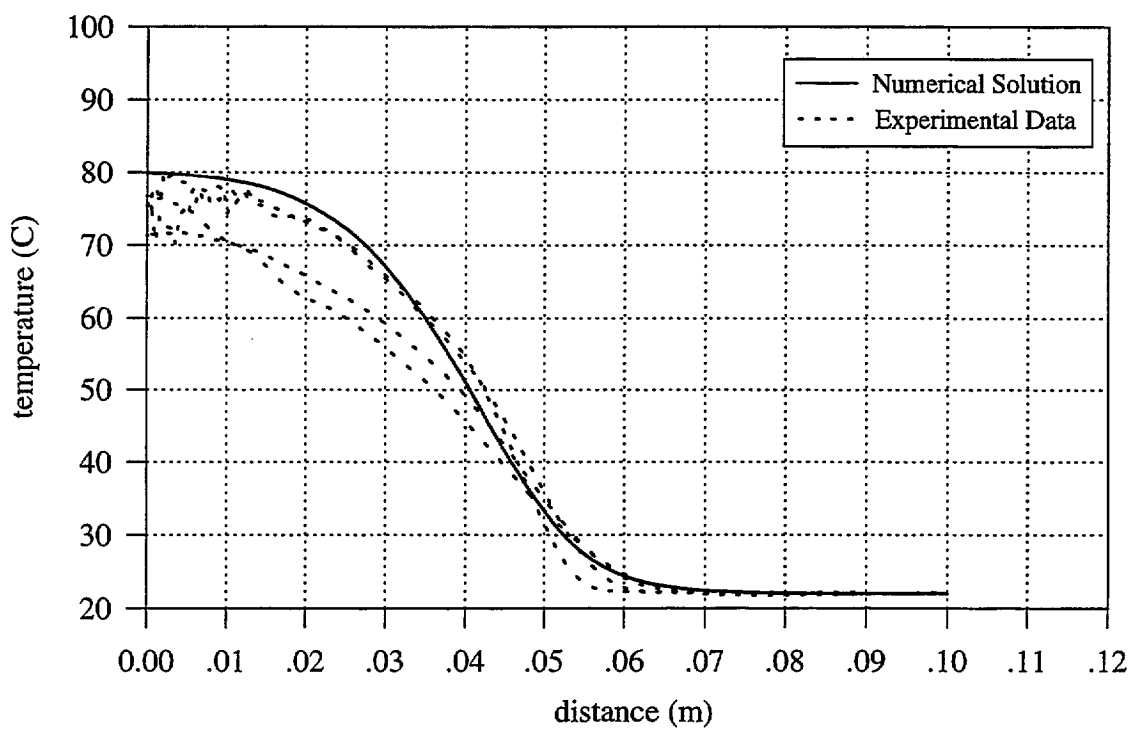


FIGURE 41B. Experimental and Numerical Temperature Profiles, Case H

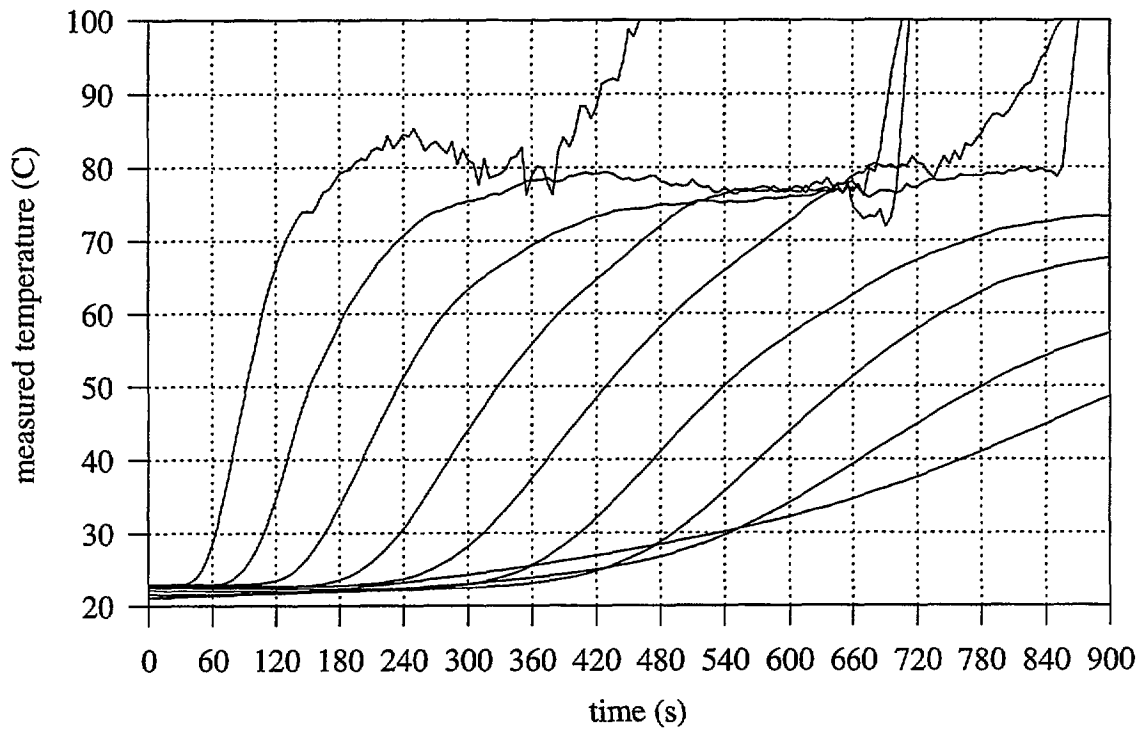


FIGURE 42A. Thermocouple Measurements From Foam Test I

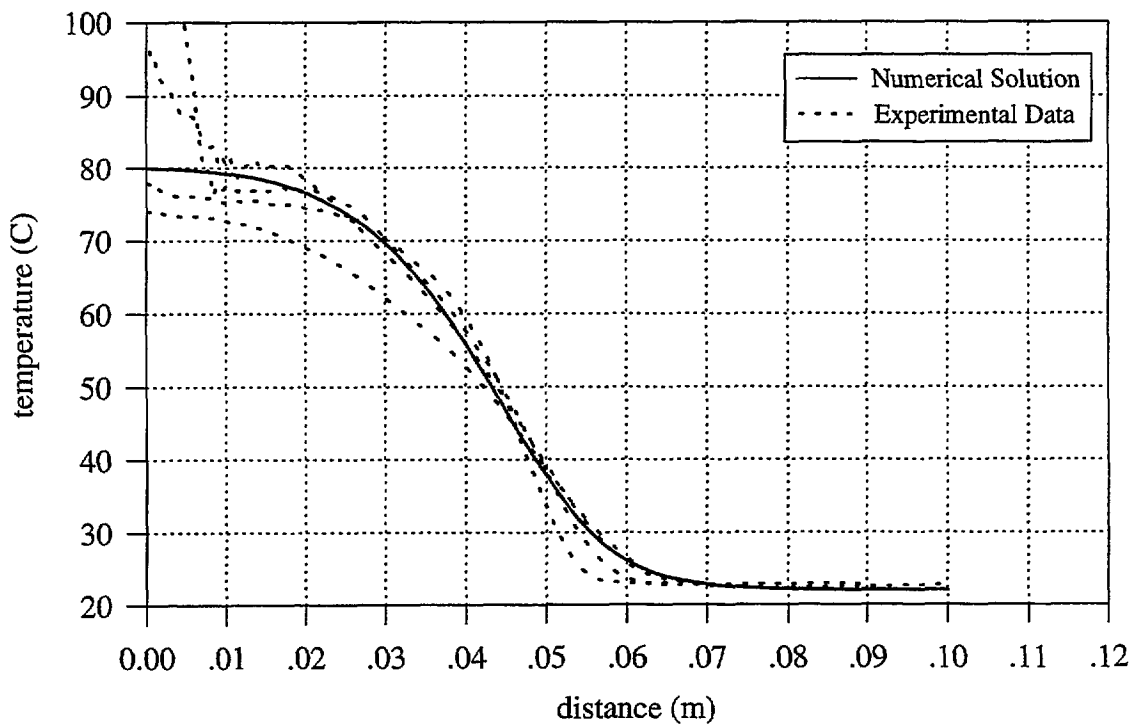


FIGURE 42B. Experimental and Numerical Temperature Profiles, Case I

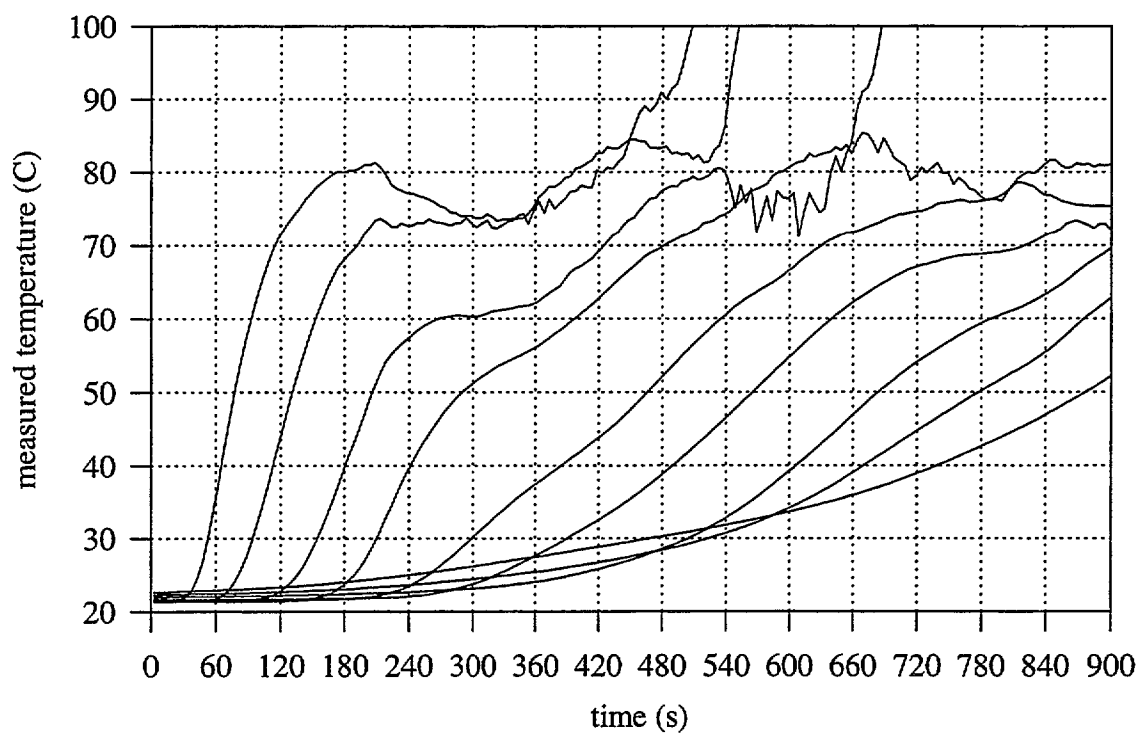


FIGURE 43A. Thermocouple Measurements From Foam Test J

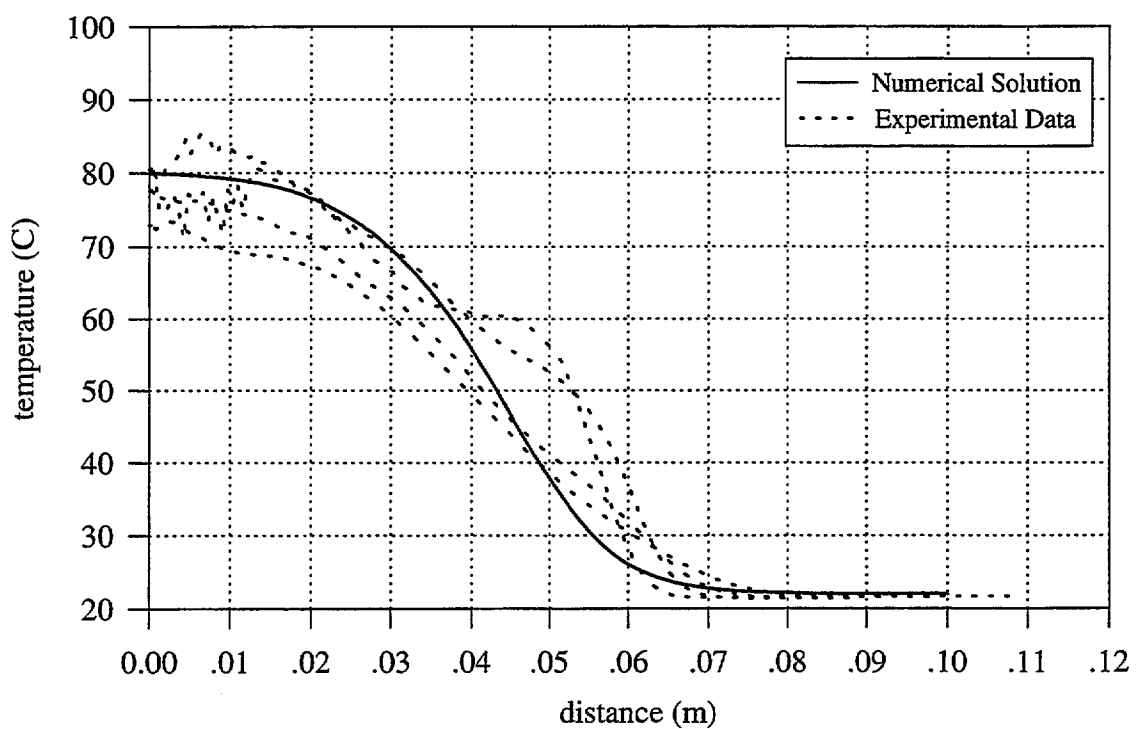


FIGURE 43B. Experimental and Numerical Temperature Profiles, Case J

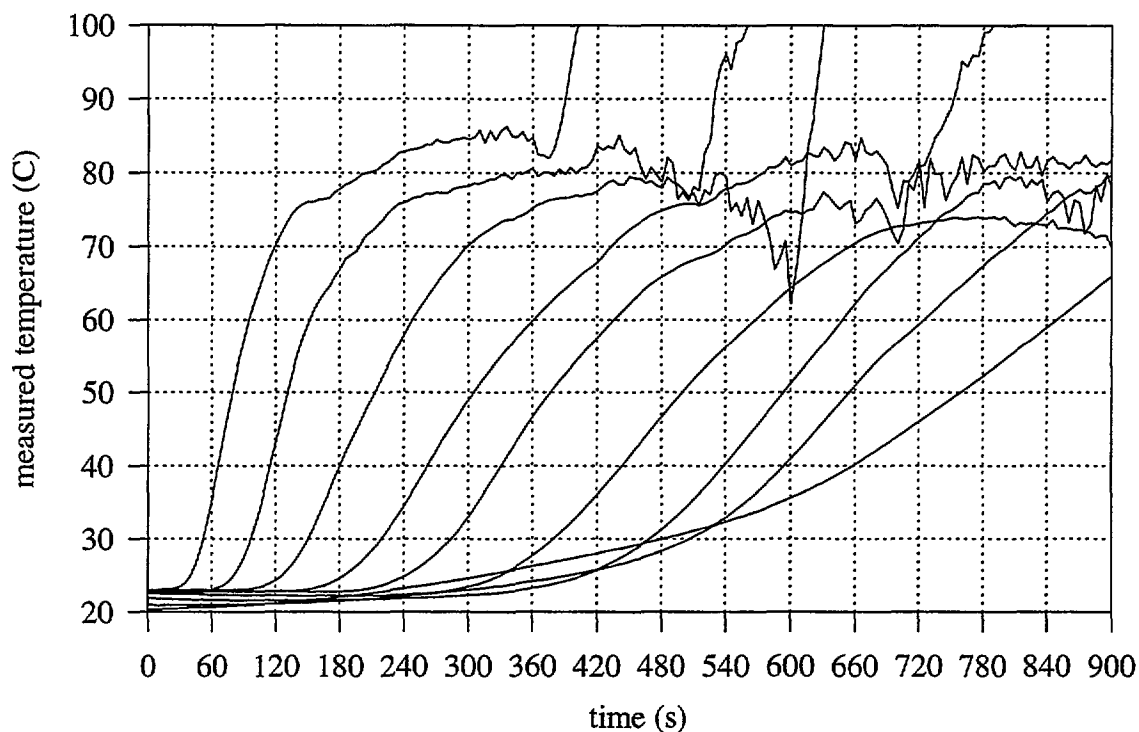


FIGURE 44A. Thermocouple Measurements From Foam Test K

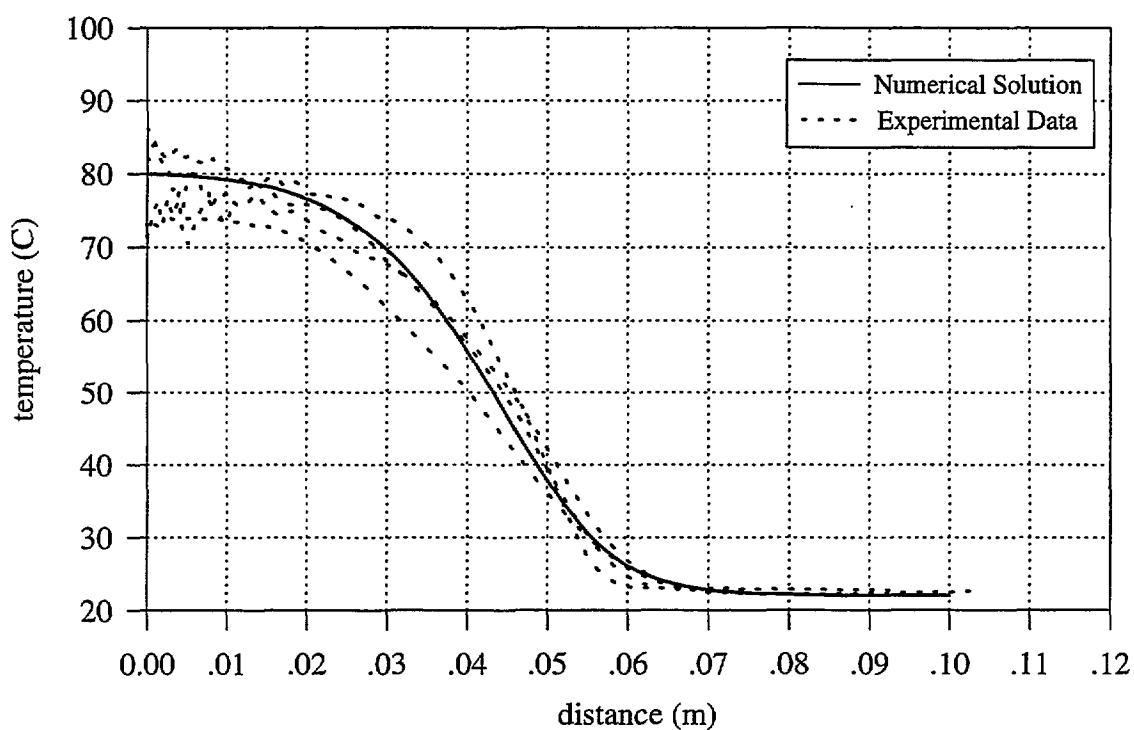


FIGURE 44B. Experimental and Numerical Temperature Profiles, Case K

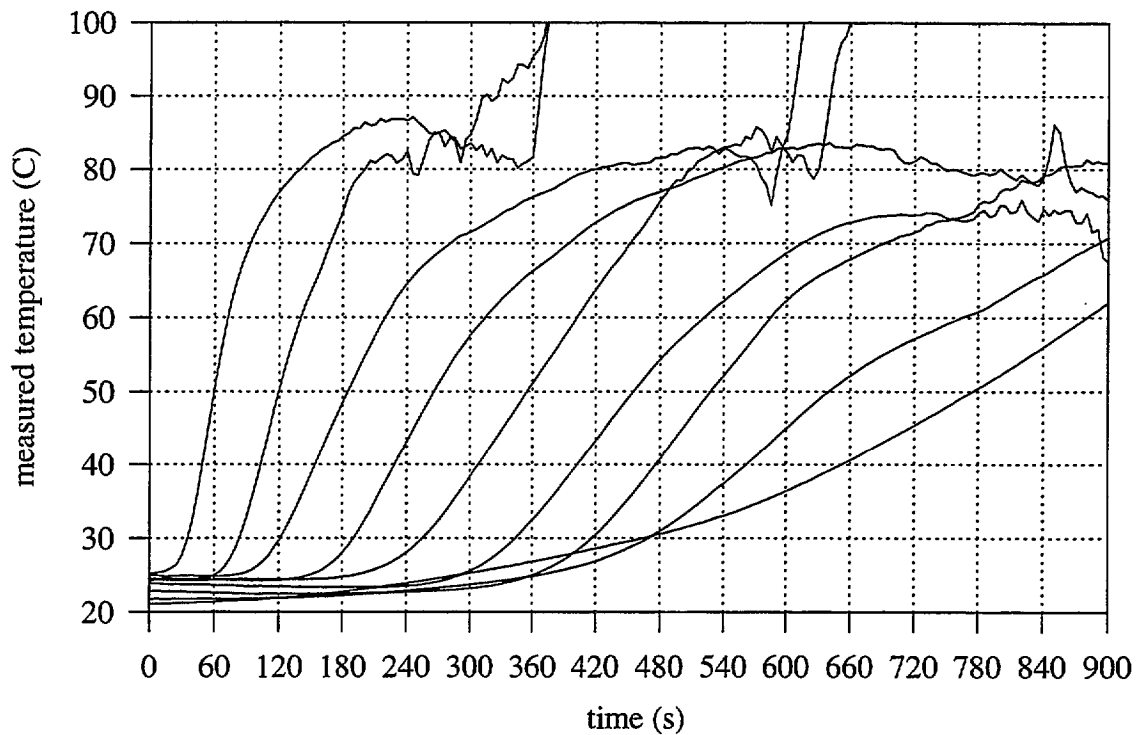


FIGURE 45A. Thermocouple Measurements From Foam Test L

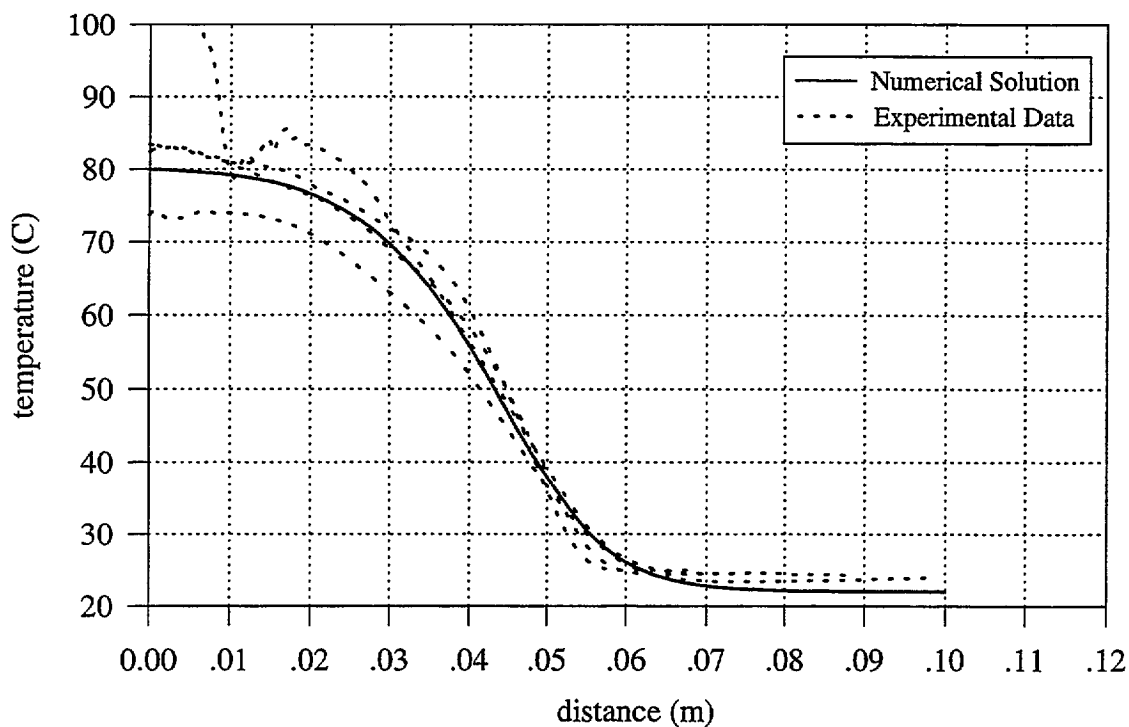


FIGURE 45B. Experimental and Numerical Temperature Profiles, Case L

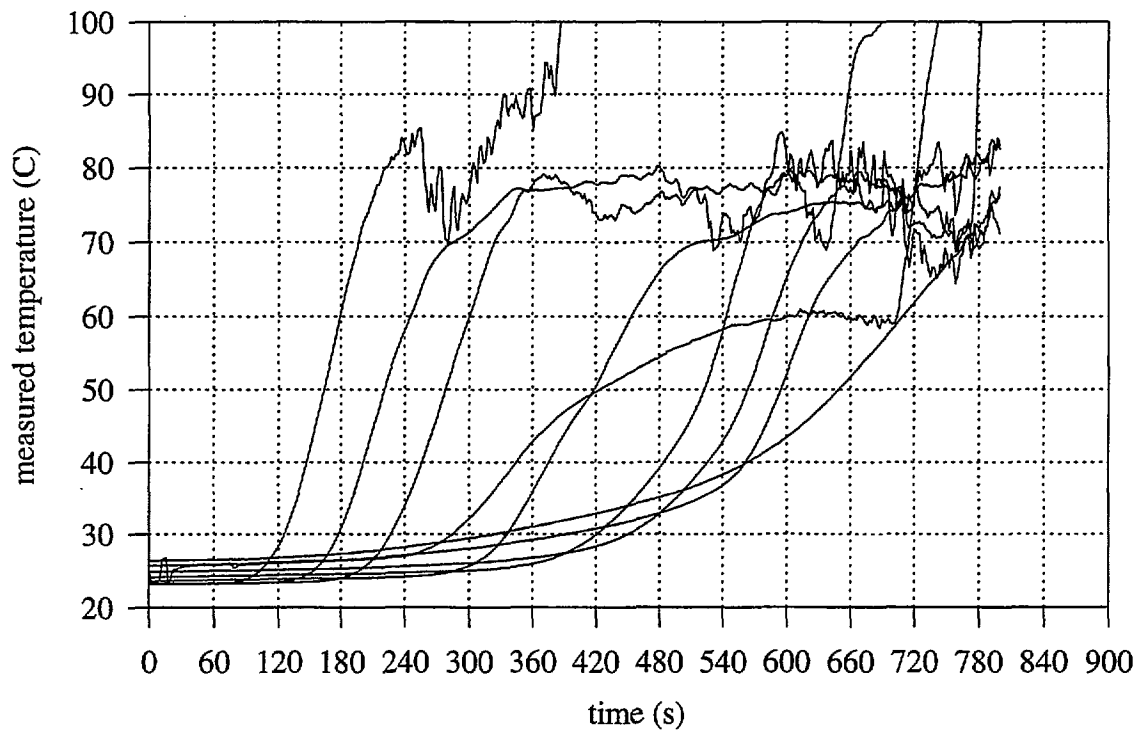


FIGURE 46A. Thermocouple Measurements From Foam Test M

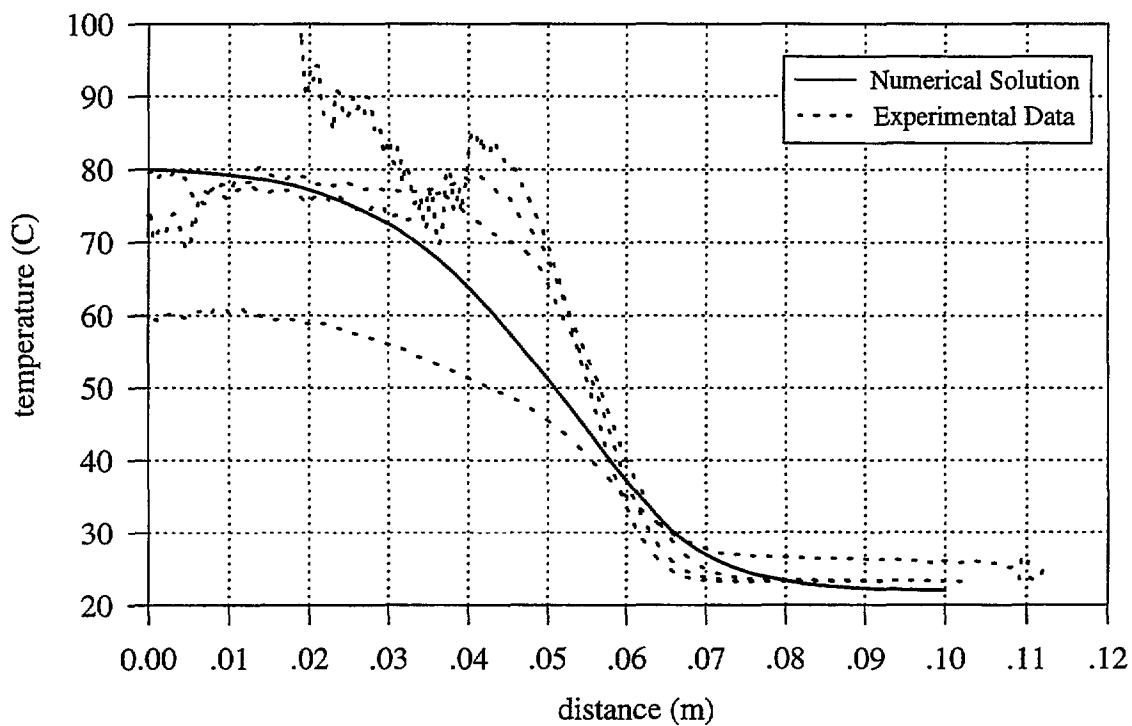


FIGURE 46B. Experimental and Numerical Temperature Profiles, Case M

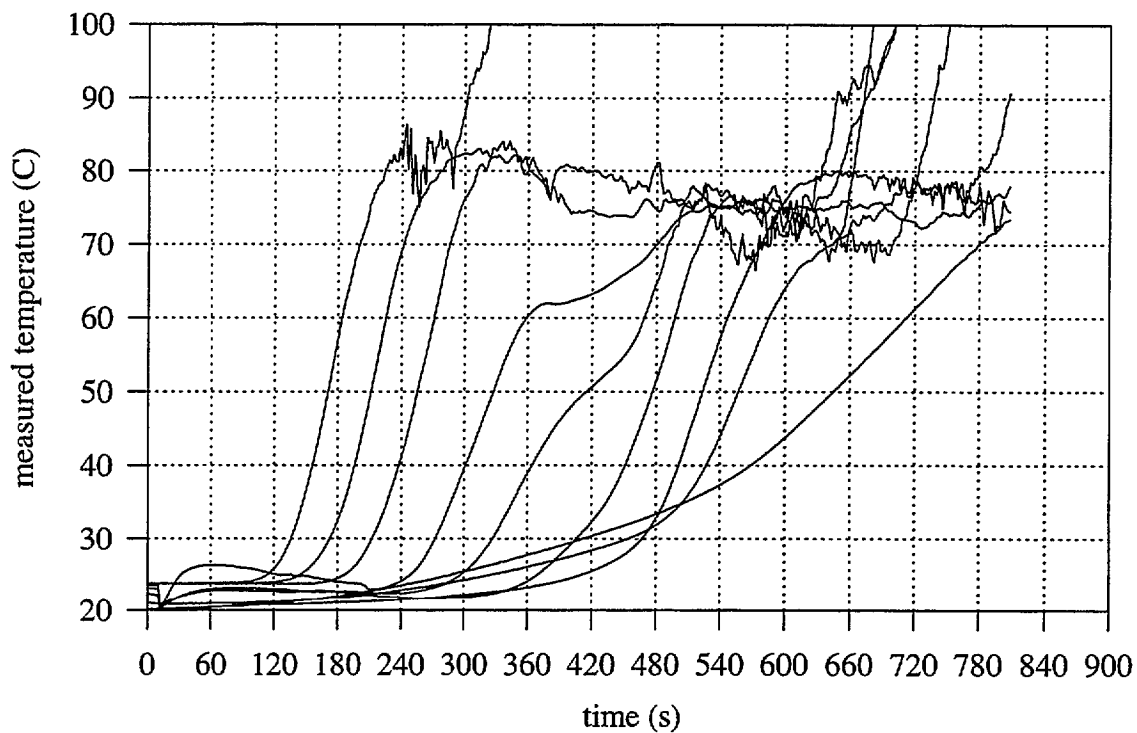


FIGURE 47A. Thermocouple Measurements From Foam Test N

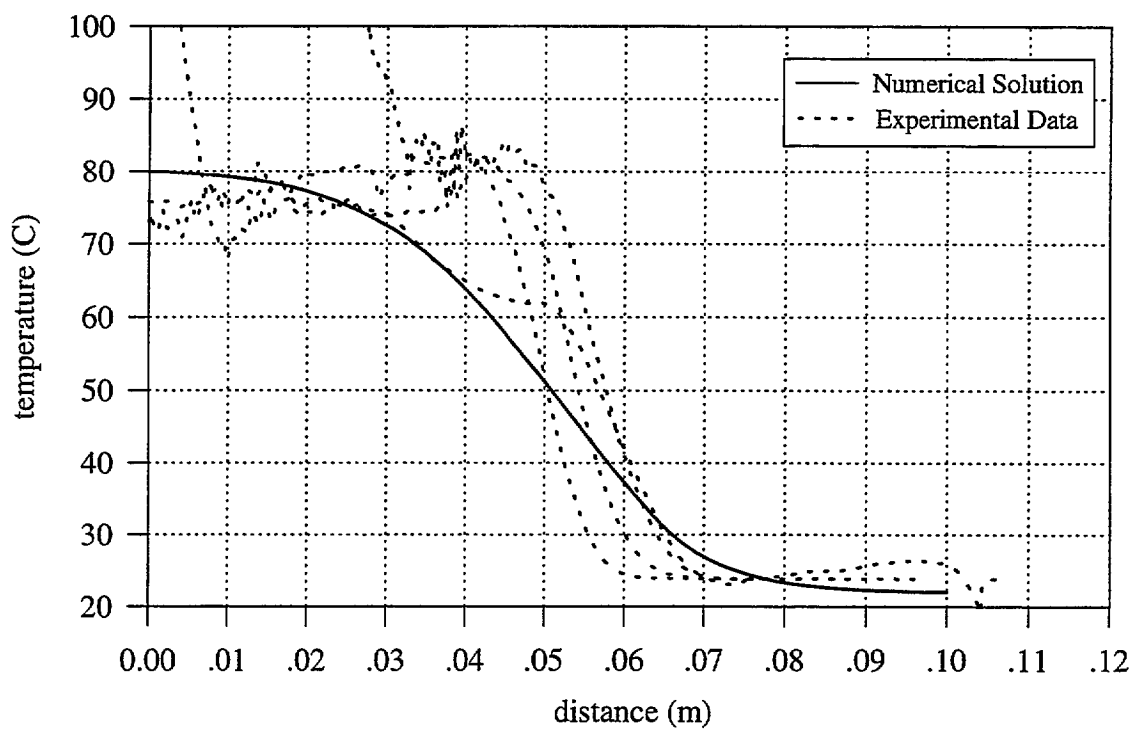


FIGURE 47B. Experimental and Numerical Temperature Profiles, Case N

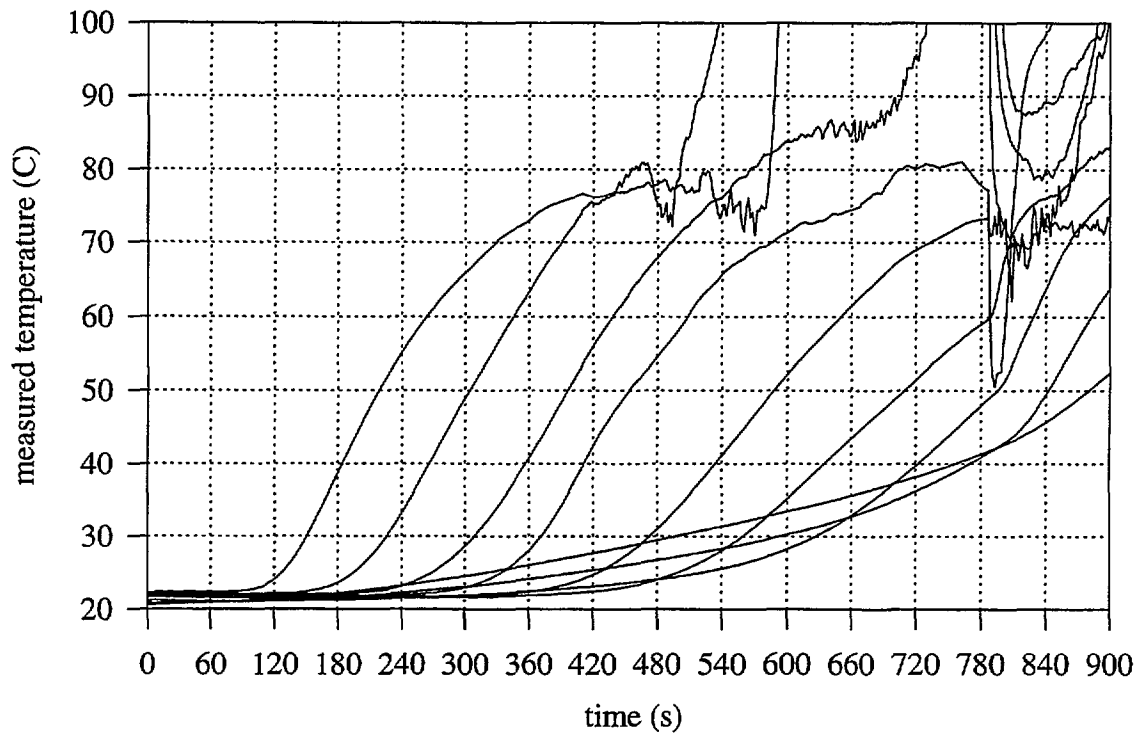


FIGURE 48A. Thermocouple Measurements From Foam Test O

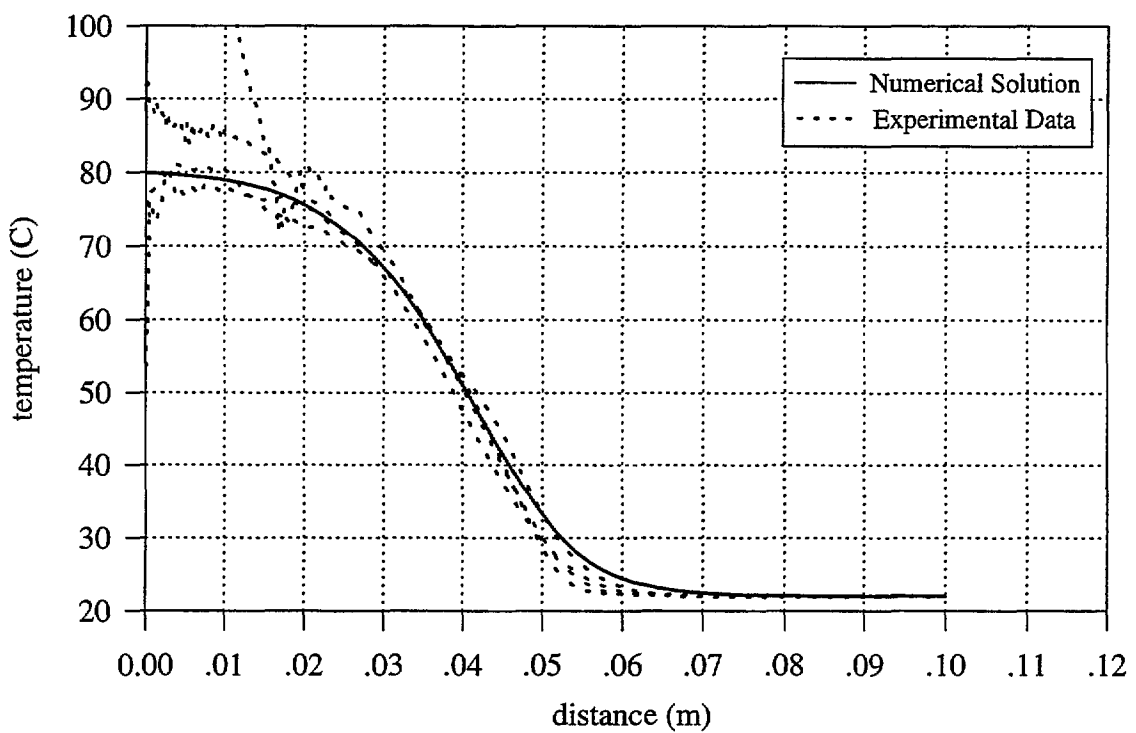


FIGURE 48B. Experimental and Numerical Temperature Profiles, Case O

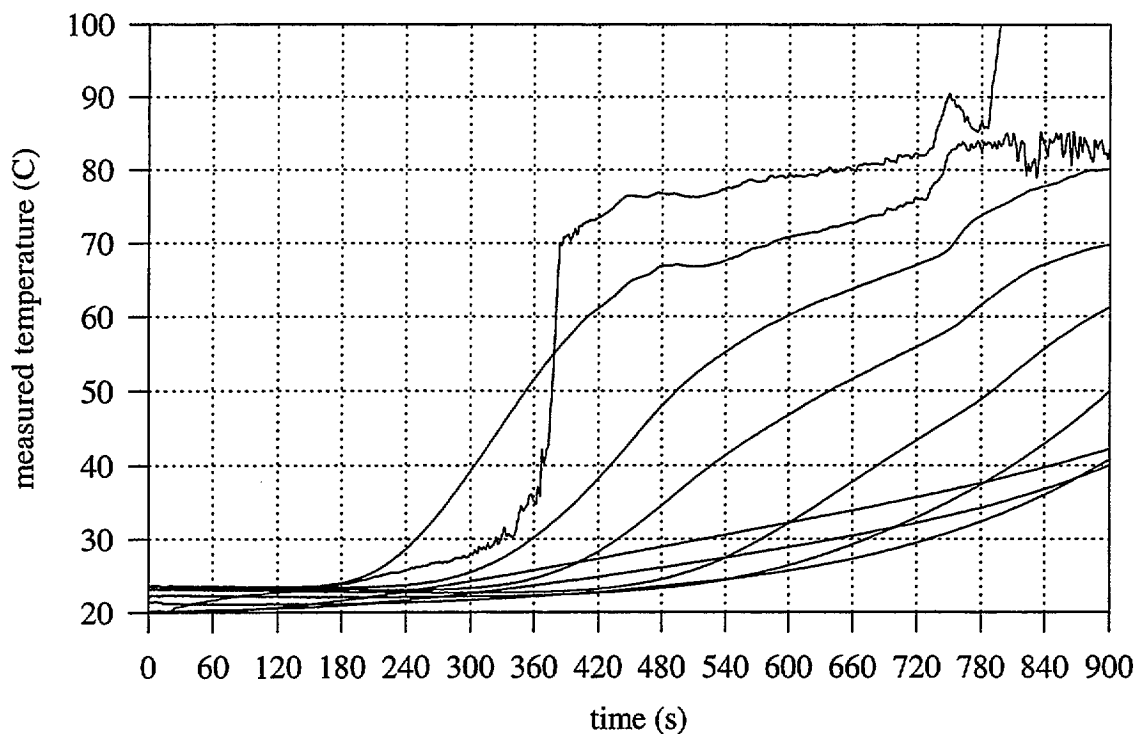


FIGURE 49A. Thermocouple Measurements From Foam Test P

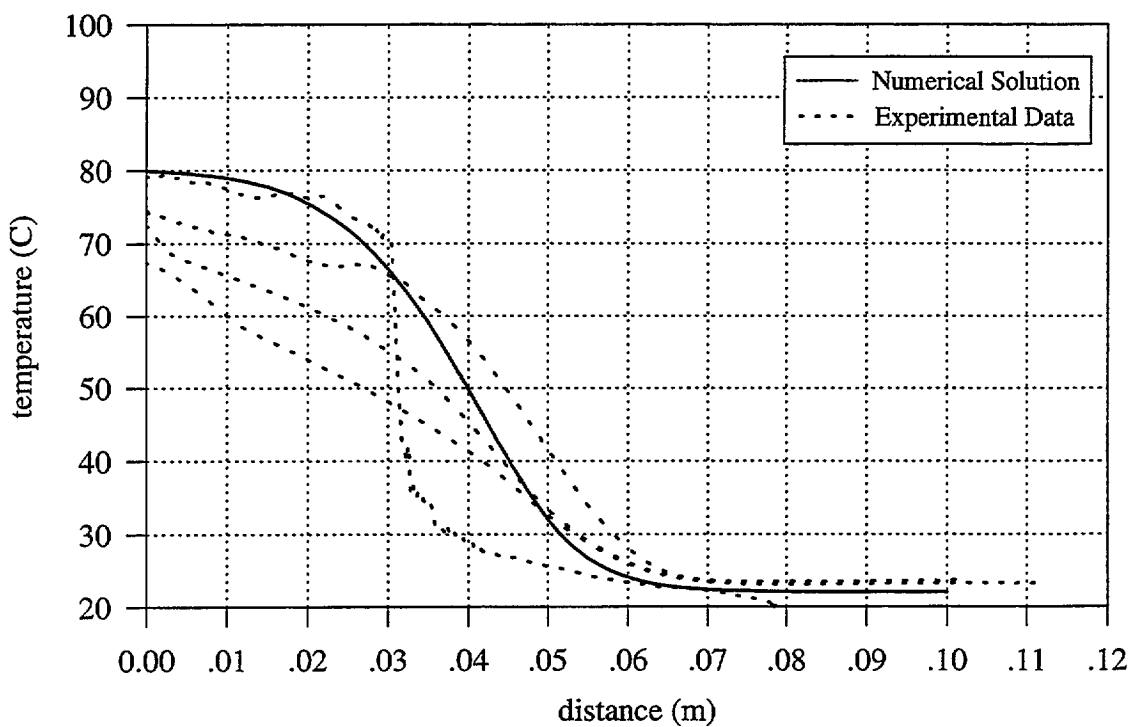


FIGURE 49B. Experimental and Numerical Temperature Profiles, Case P

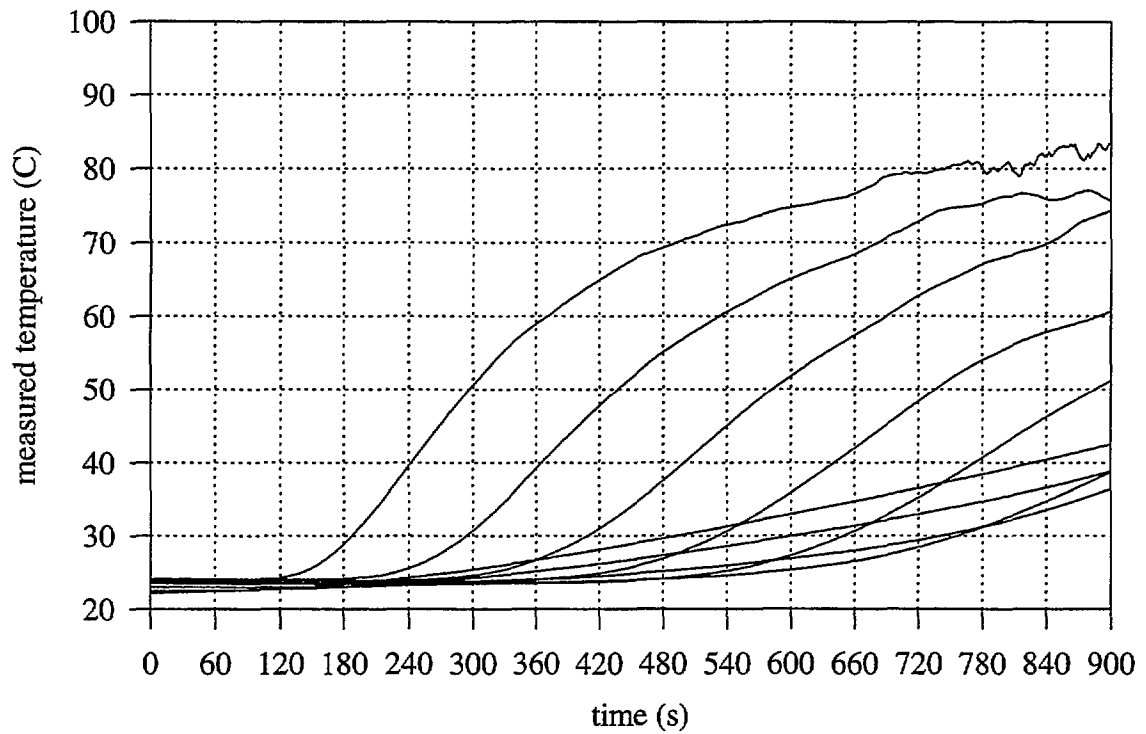


FIGURE 50A. Thermocouple Measurements From Foam Test Q

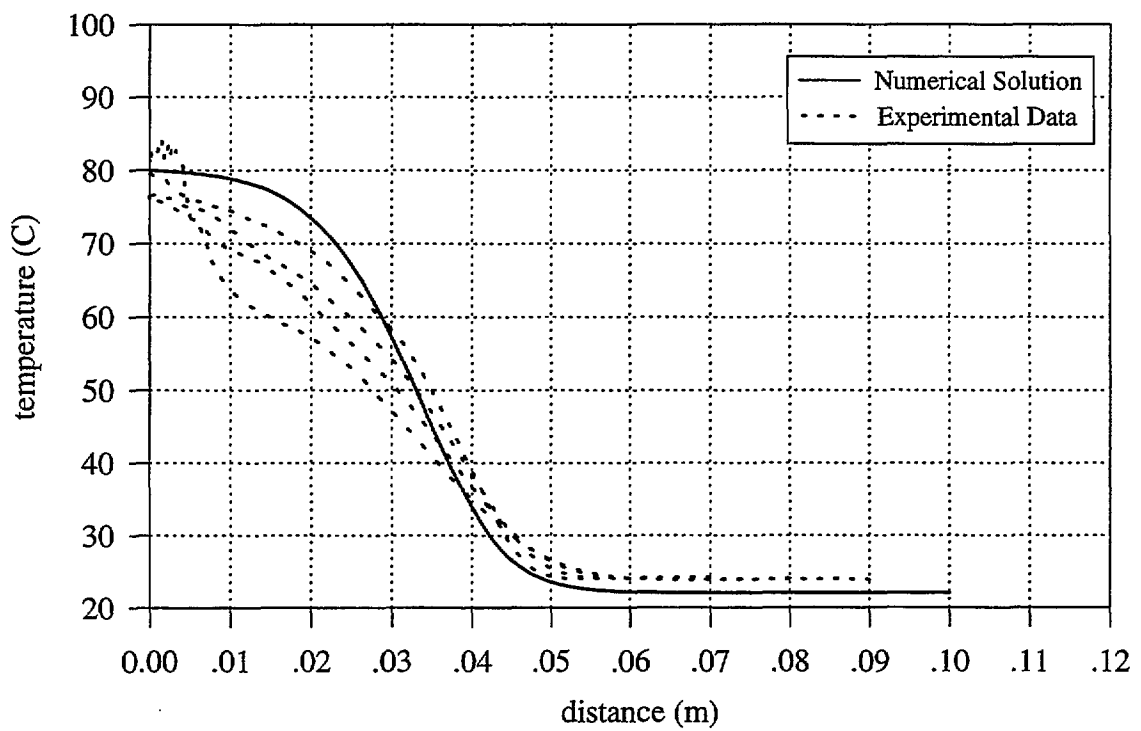


FIGURE 50B. Experimental and Numerical Temperature Profiles, Case Q

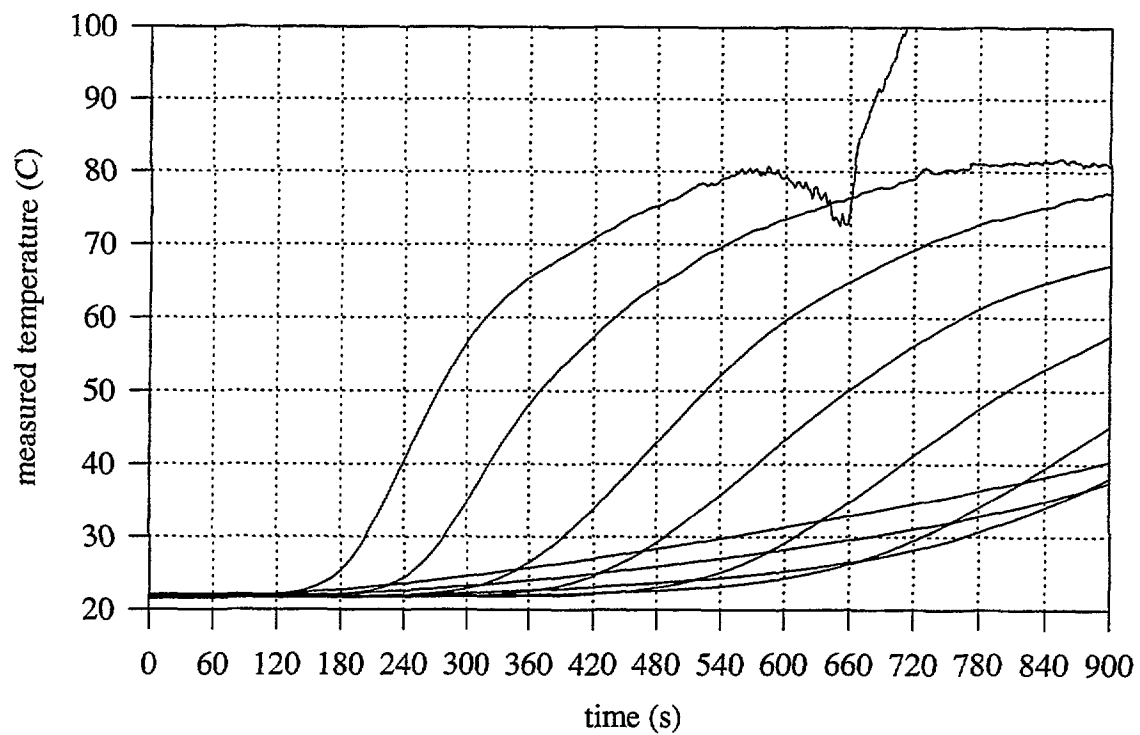


FIGURE 51A. Thermocouple Measurements From Foam Test R

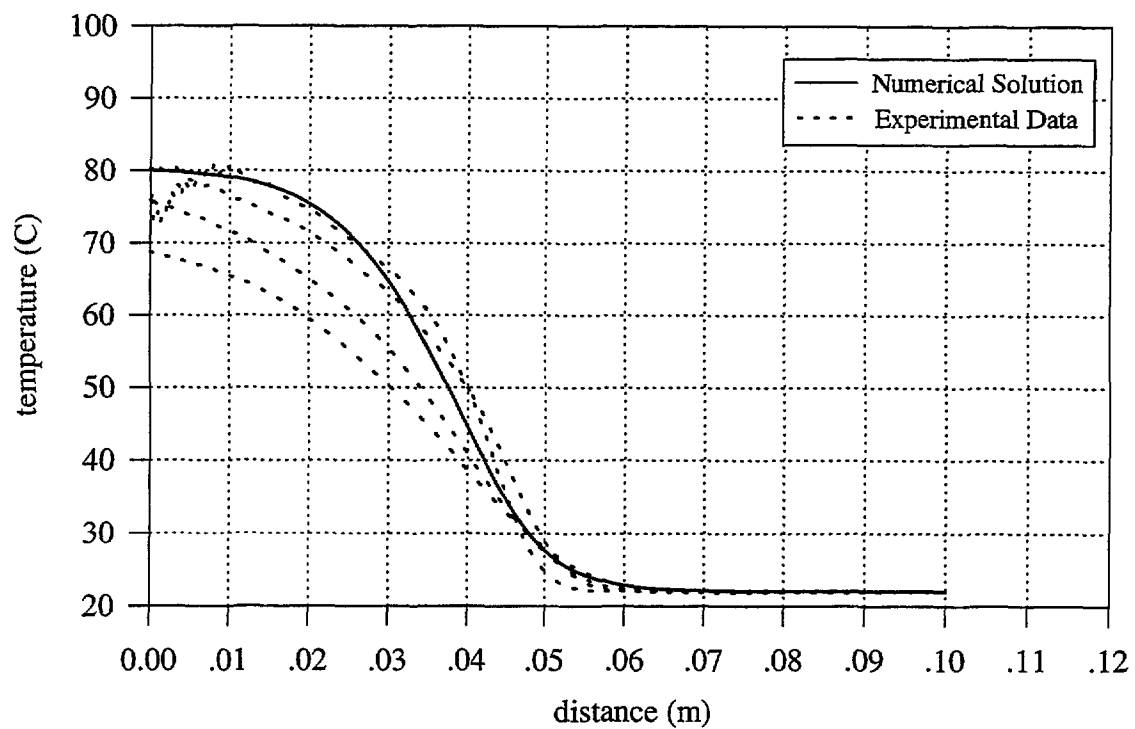


FIGURE 51B. Experimental and Numerical Temperature Profiles, Case R

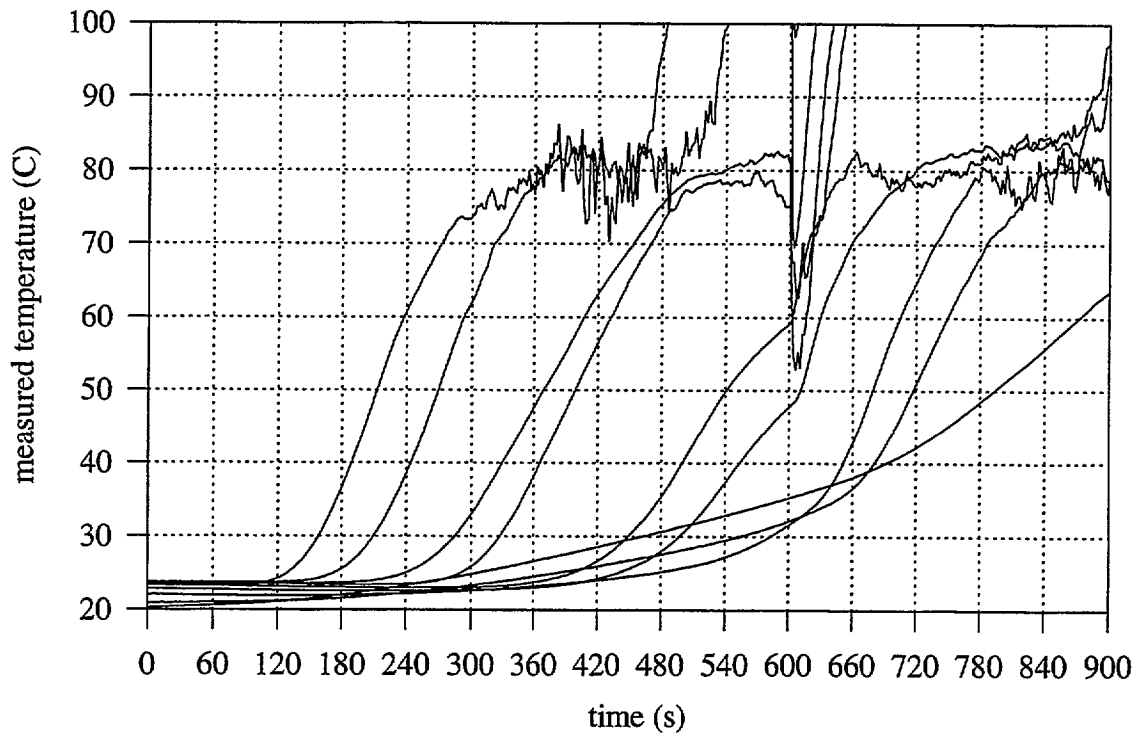


FIGURE 52A. Thermocouple Measurements From Foam Test S

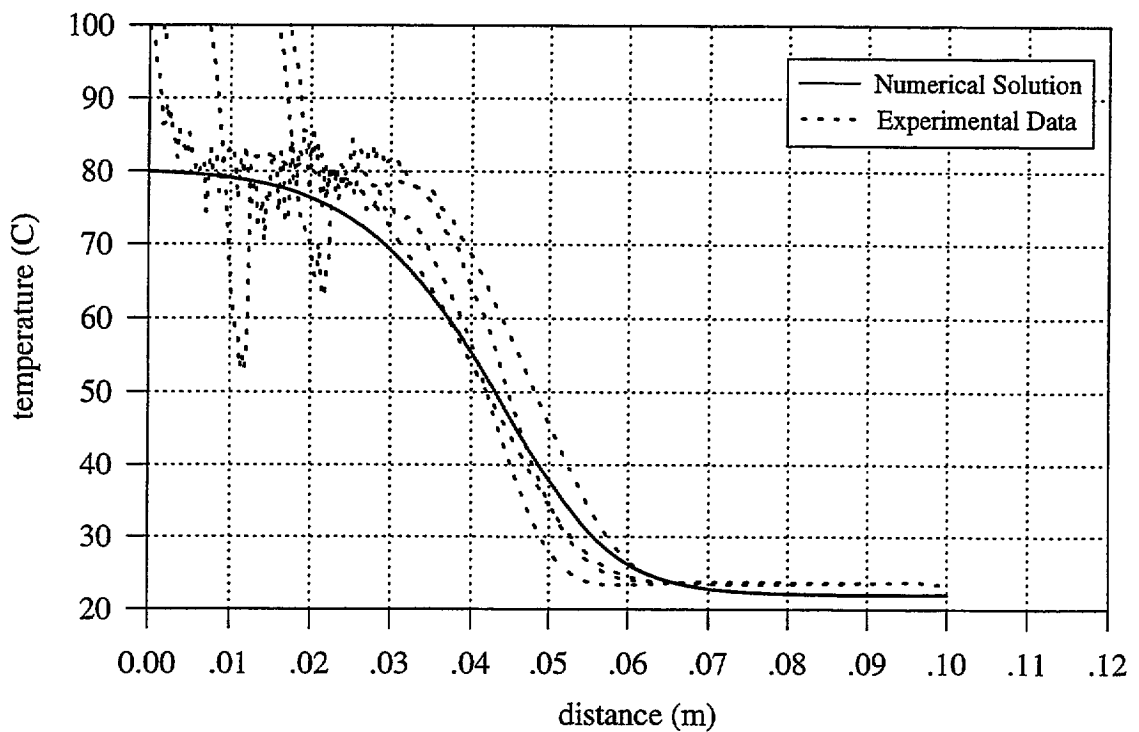


FIGURE 52B. Experimental and Numerical Temperature Profiles, Case S

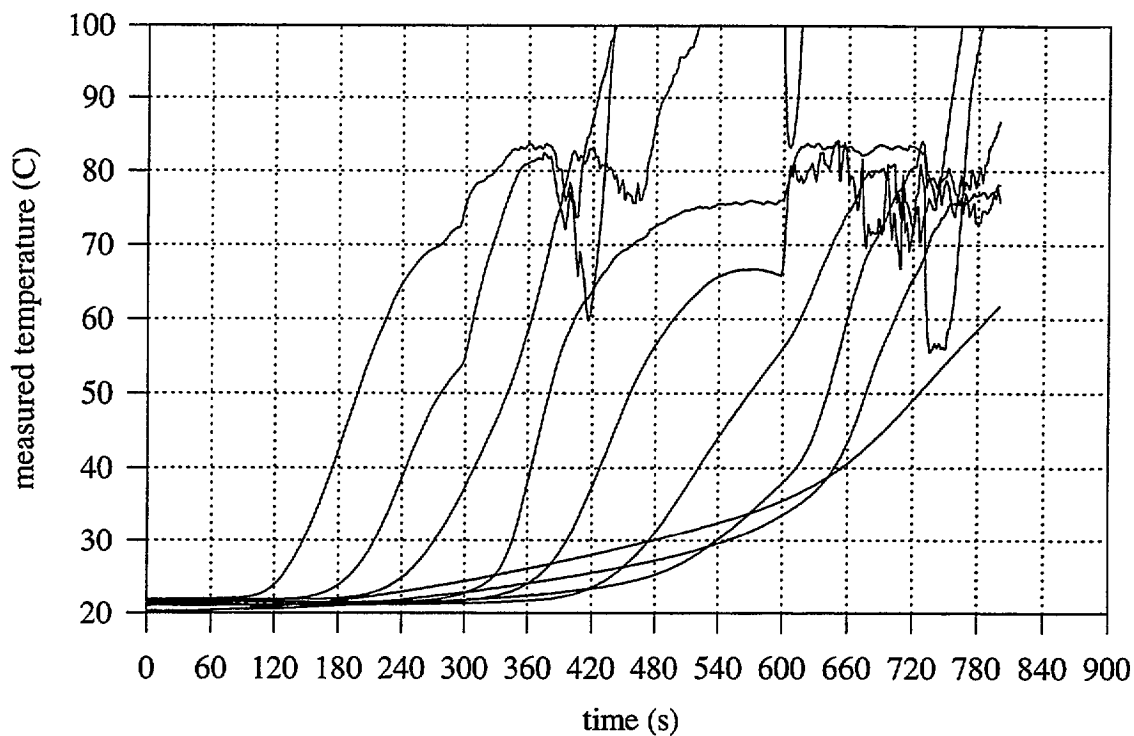


FIGURE 53A. Thermocouple Measurements From Foam Test T

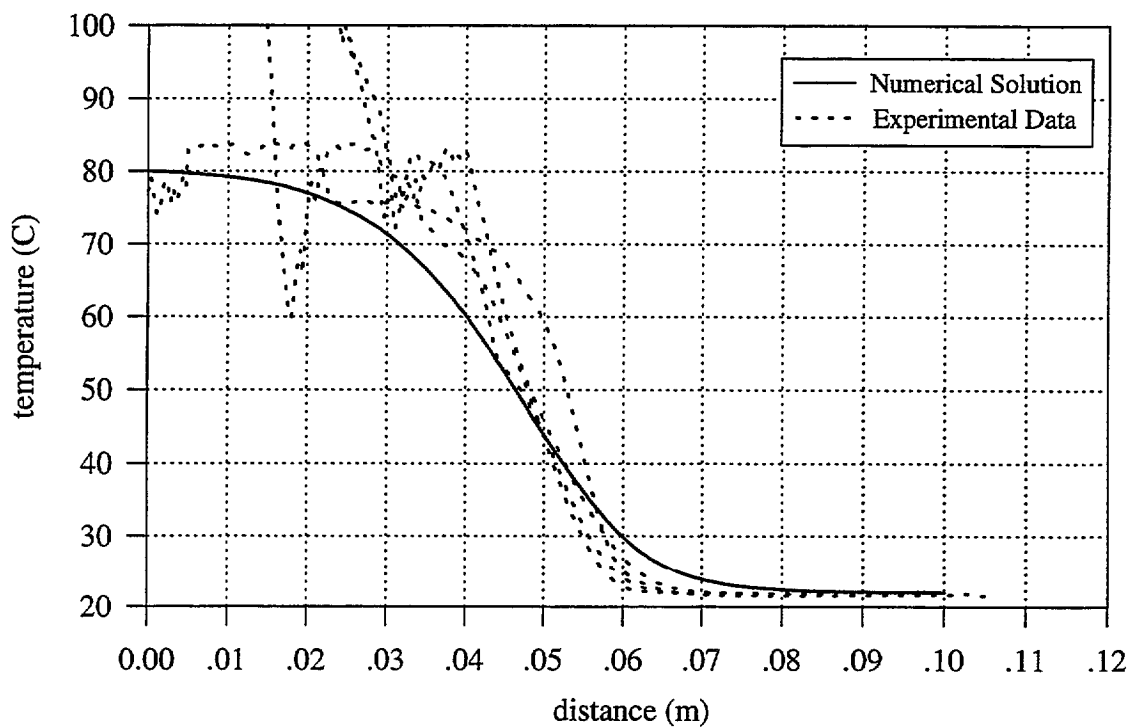


FIGURE 53B. Experimental and Numerical Temperature Profiles, Case T

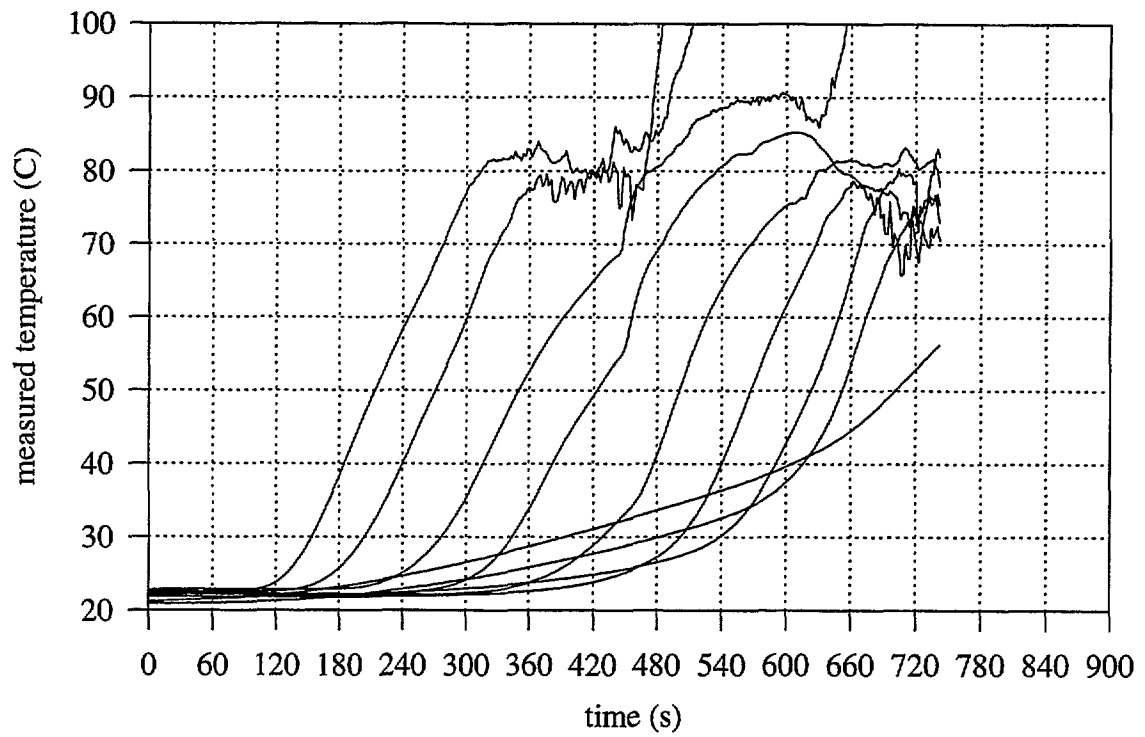


FIGURE 54A. Thermocouple Measurements From Foam Test U

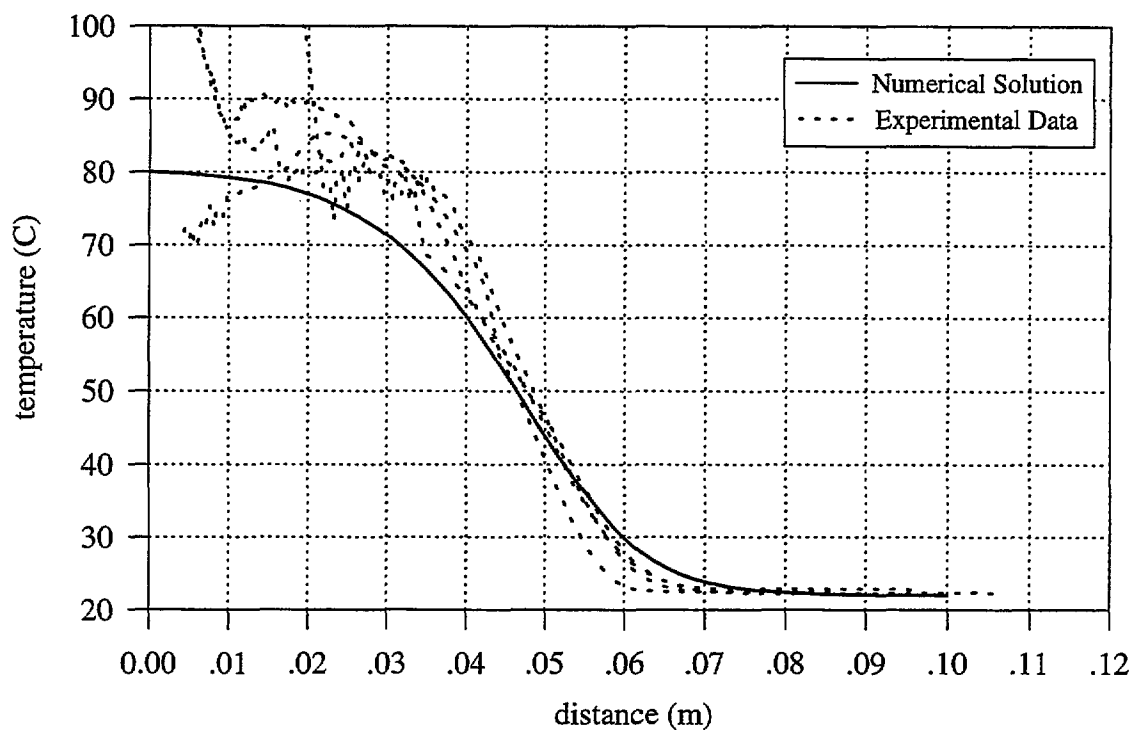


FIGURE 54B. Experimental and Numerical Temperature Profiles, Case U

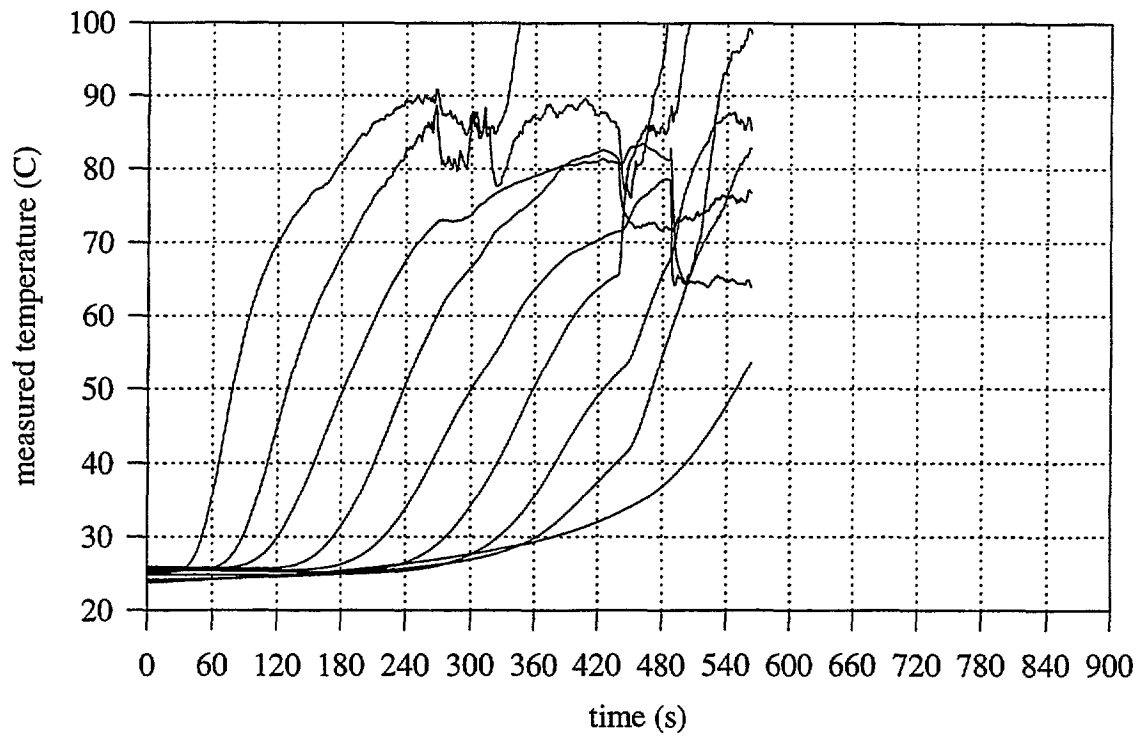


FIGURE 55A. Thermocouple Measurements From Foam Test V

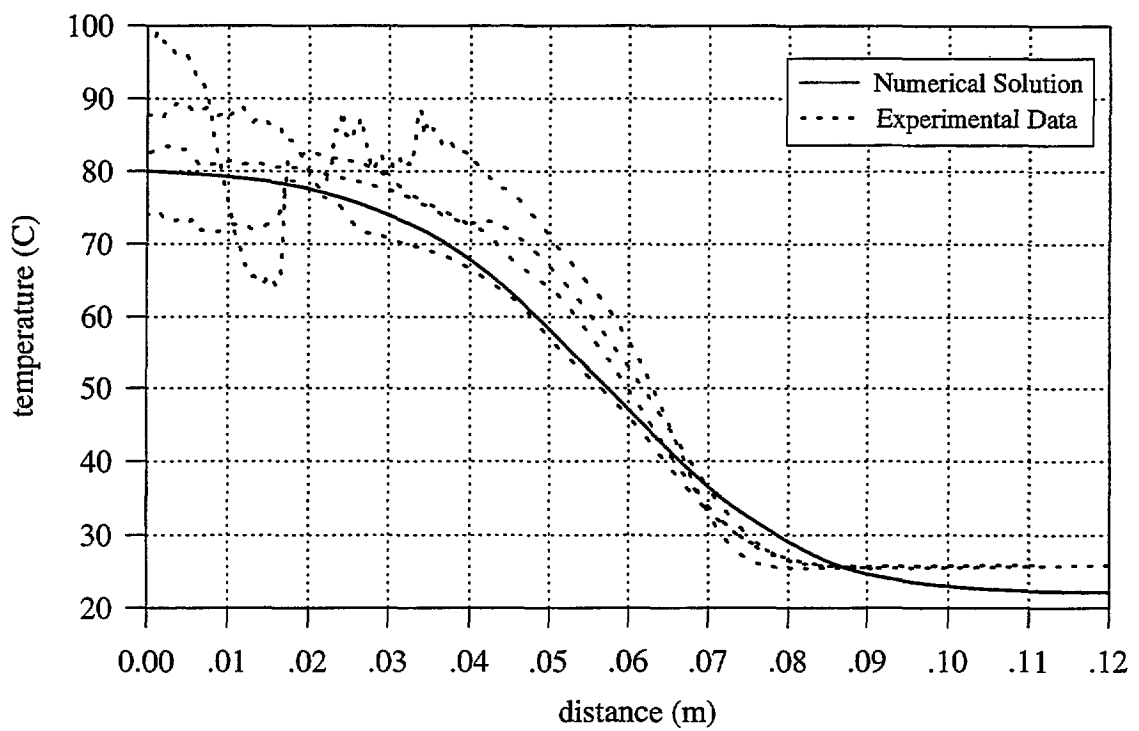


FIGURE 55B. Experimental and Numerical Temperature Profiles, Case V

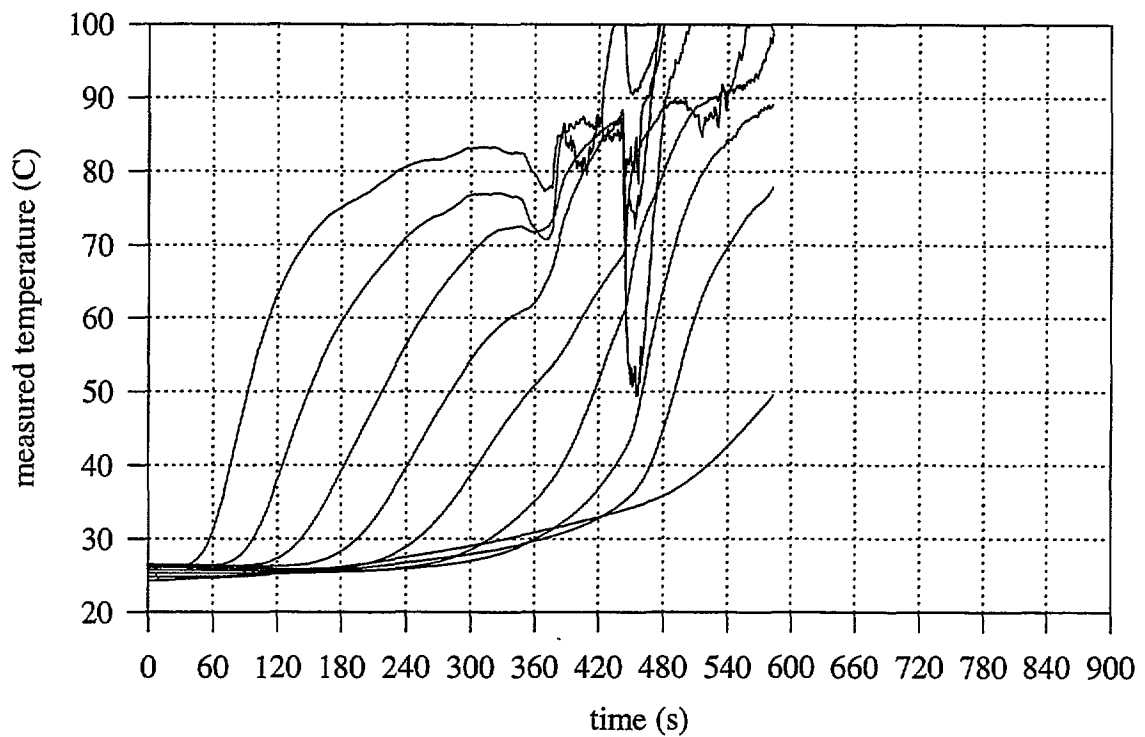


FIGURE 56A. Thermocouple Measurements From Foam Test W

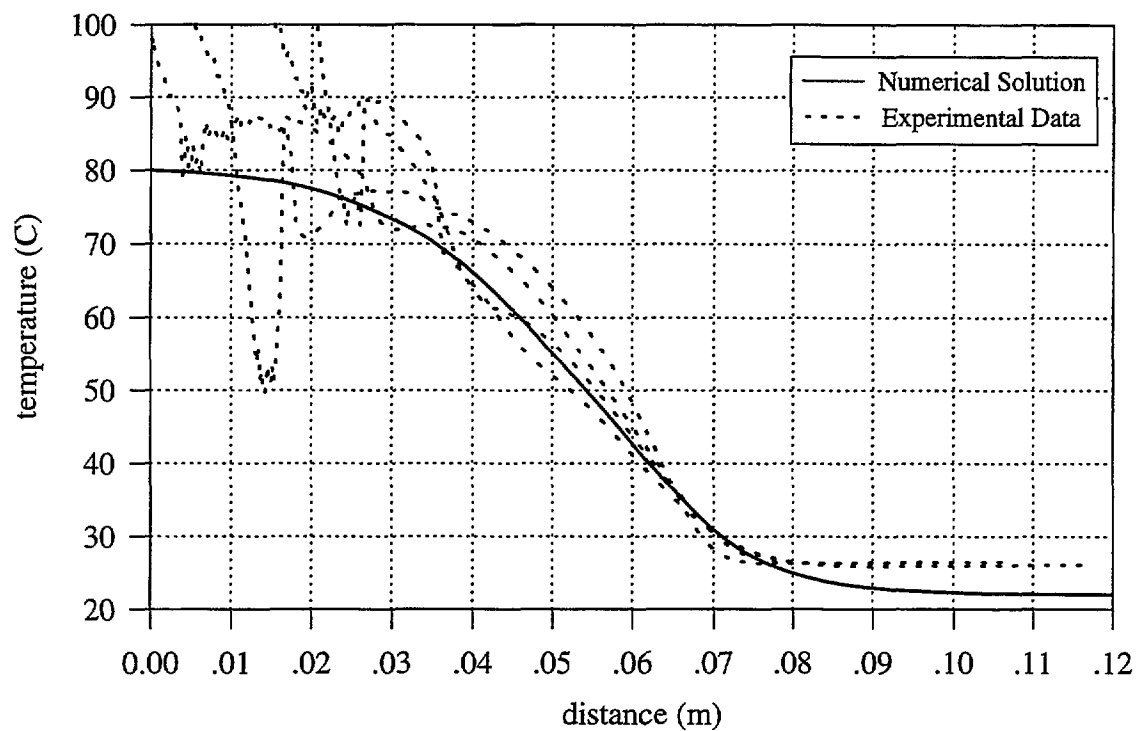


FIGURE 56B. Experimental and Numerical Temperature Profiles, Case W

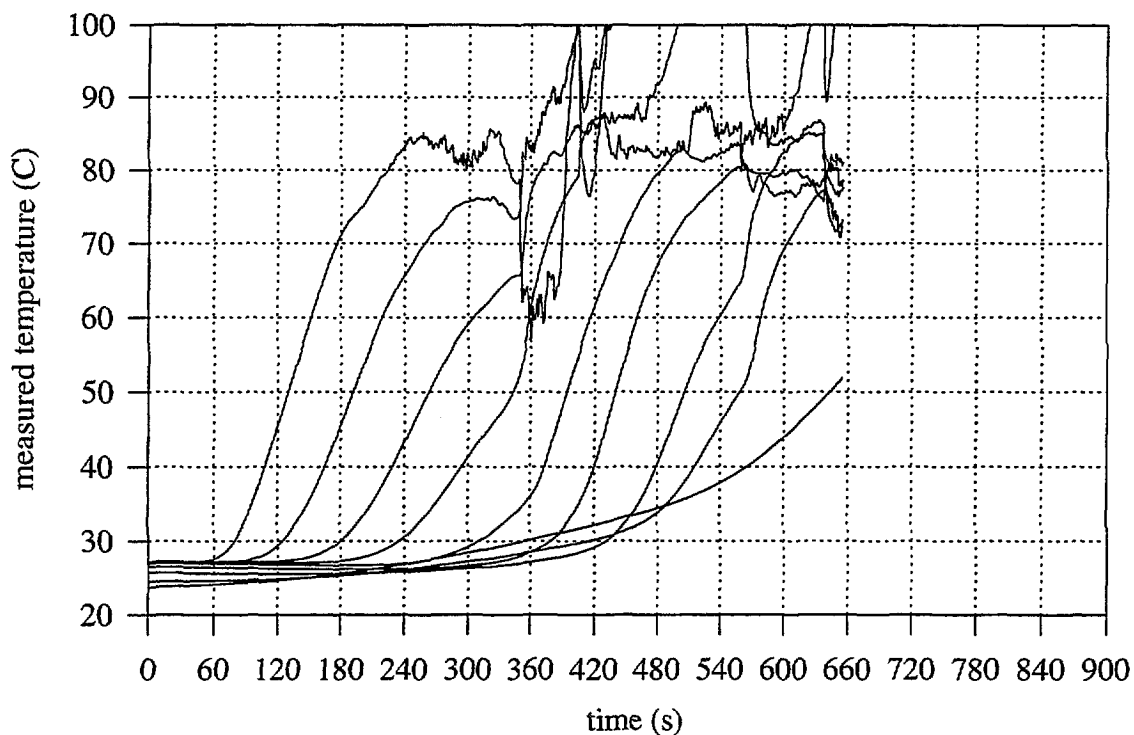


FIGURE 57A. Thermocouple Measurements From Foam Test X

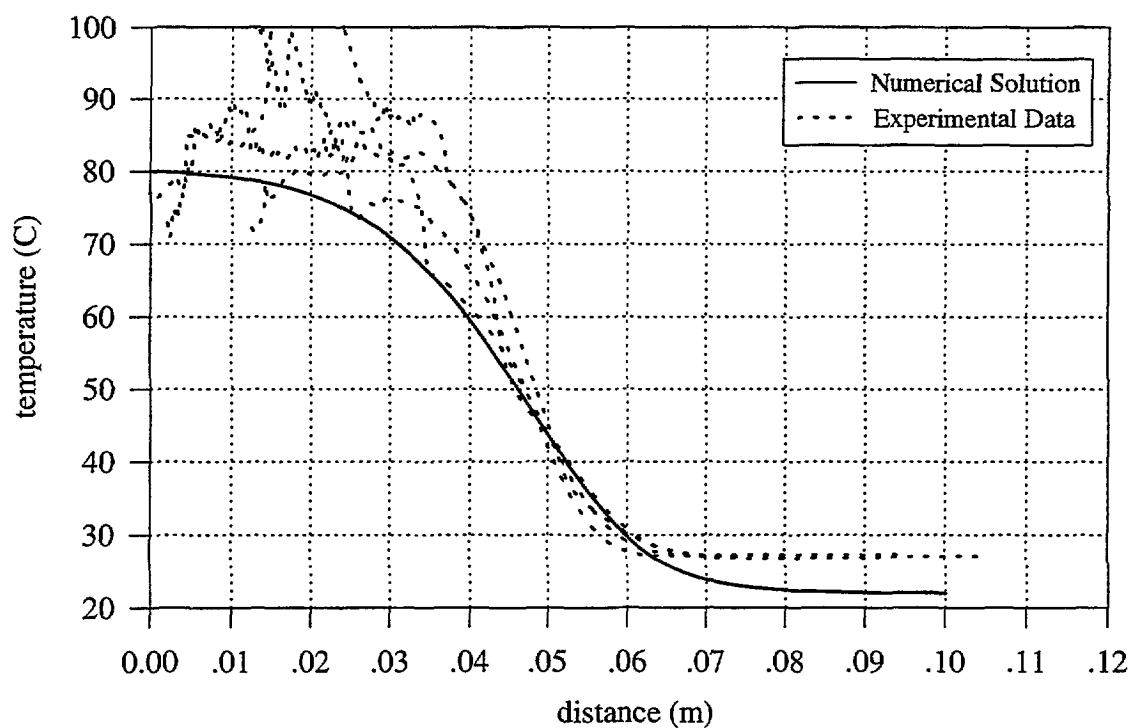


FIGURE 57B. Experimental and Numerical Temperature Profiles, Case X

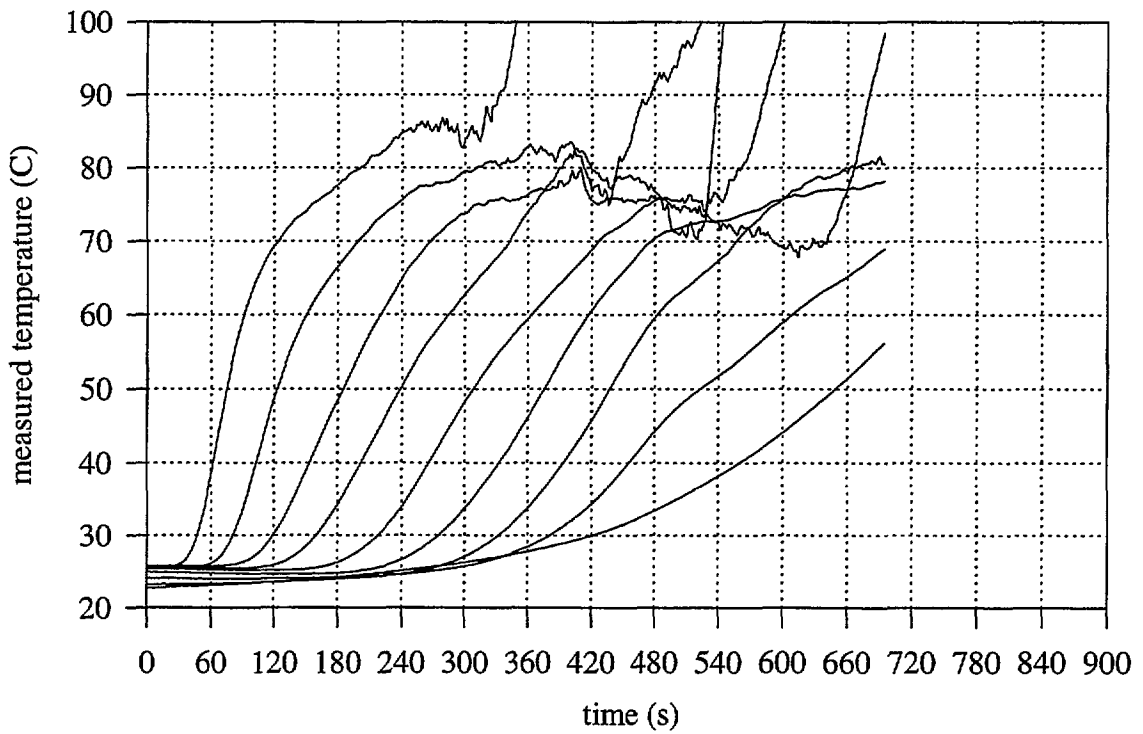


FIGURE 58A. Thermocouple Measurements From Foam Test Y

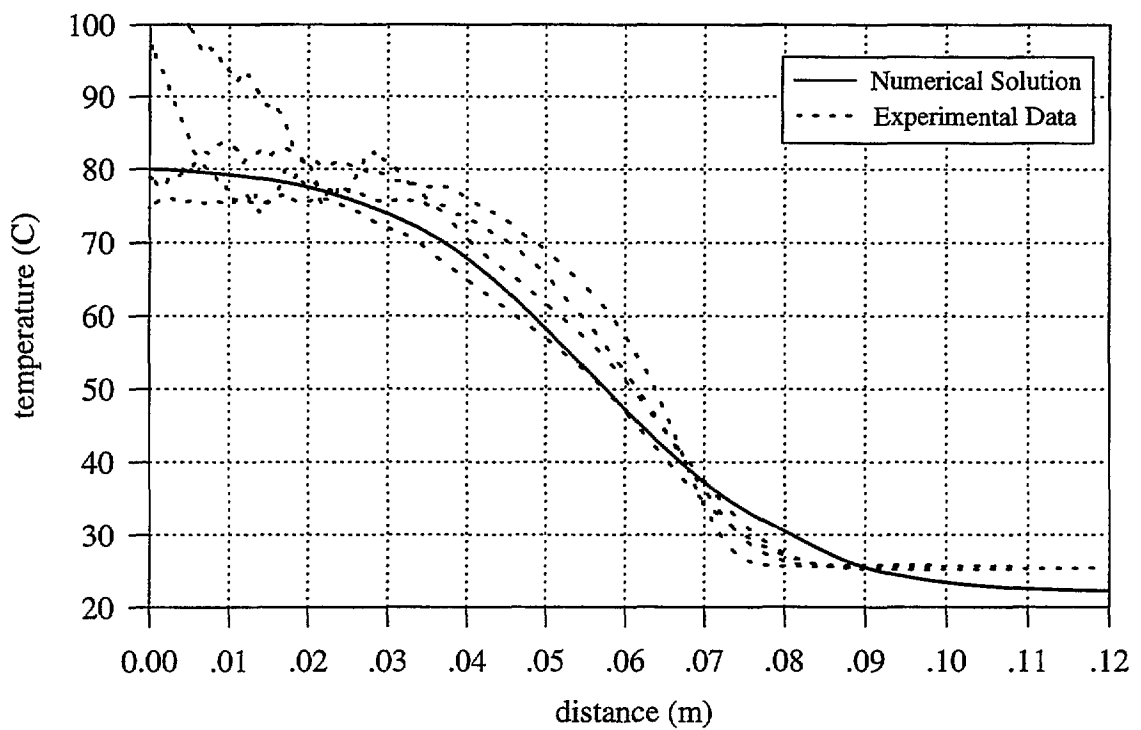


FIGURE 58B. Experimental and Numerical Temperature Profiles, Case Y

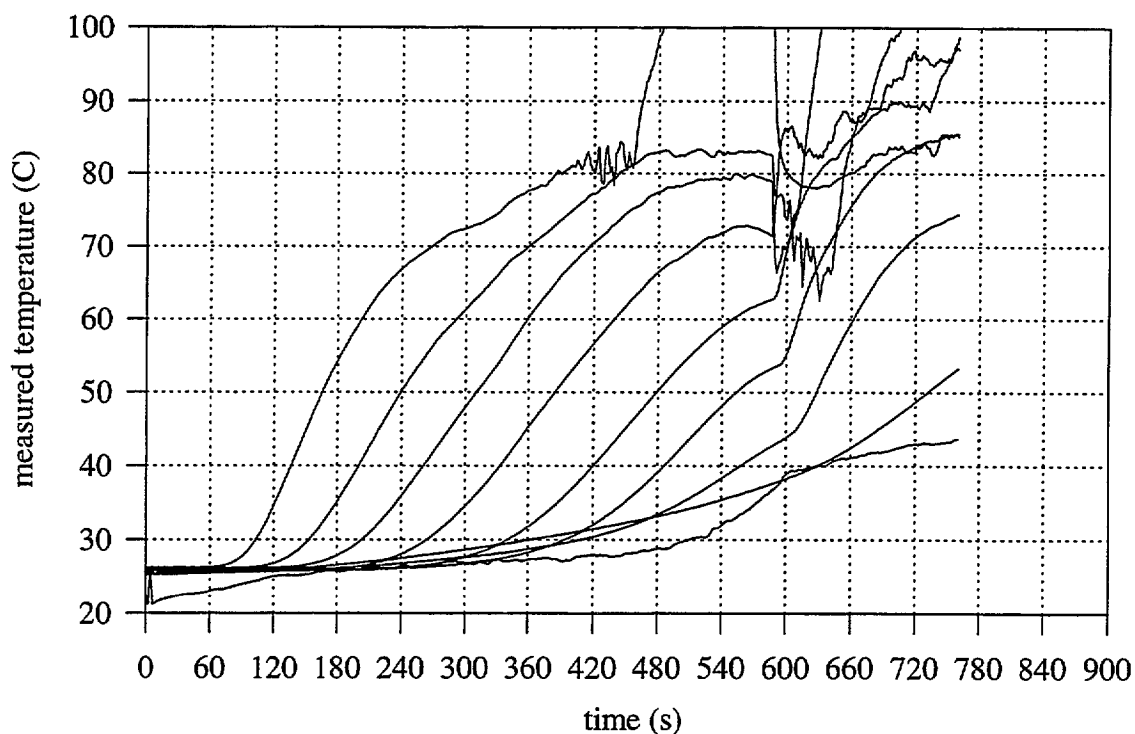


FIGURE 59A. Thermocouple Measurements From Foam Test Z

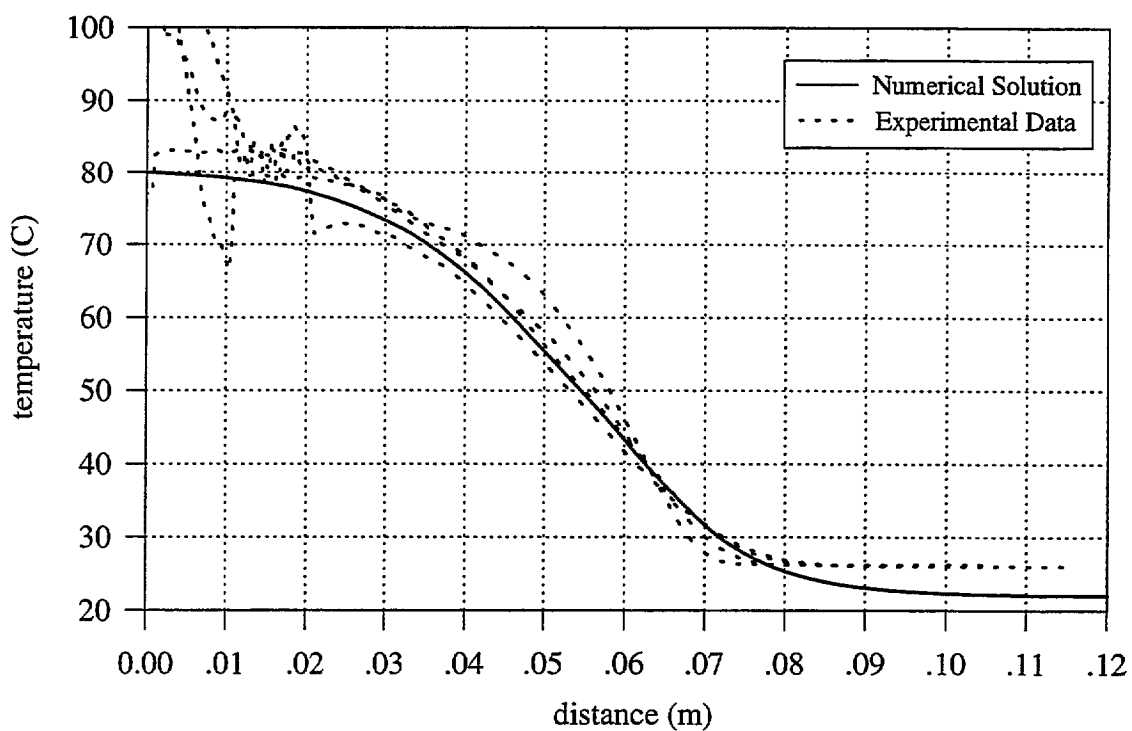


FIGURE 59B. Experimental and Numerical Temperature Profiles, Case Z

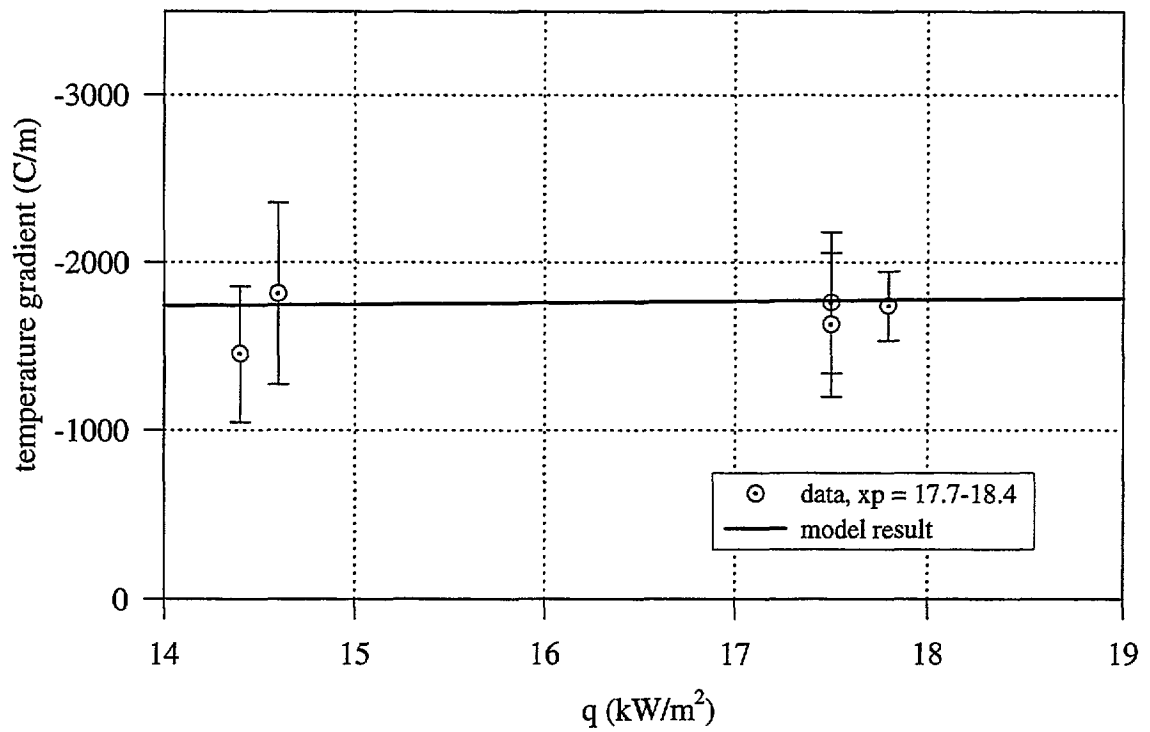


FIGURE 60. Temperature Gradient versus Heat Flux

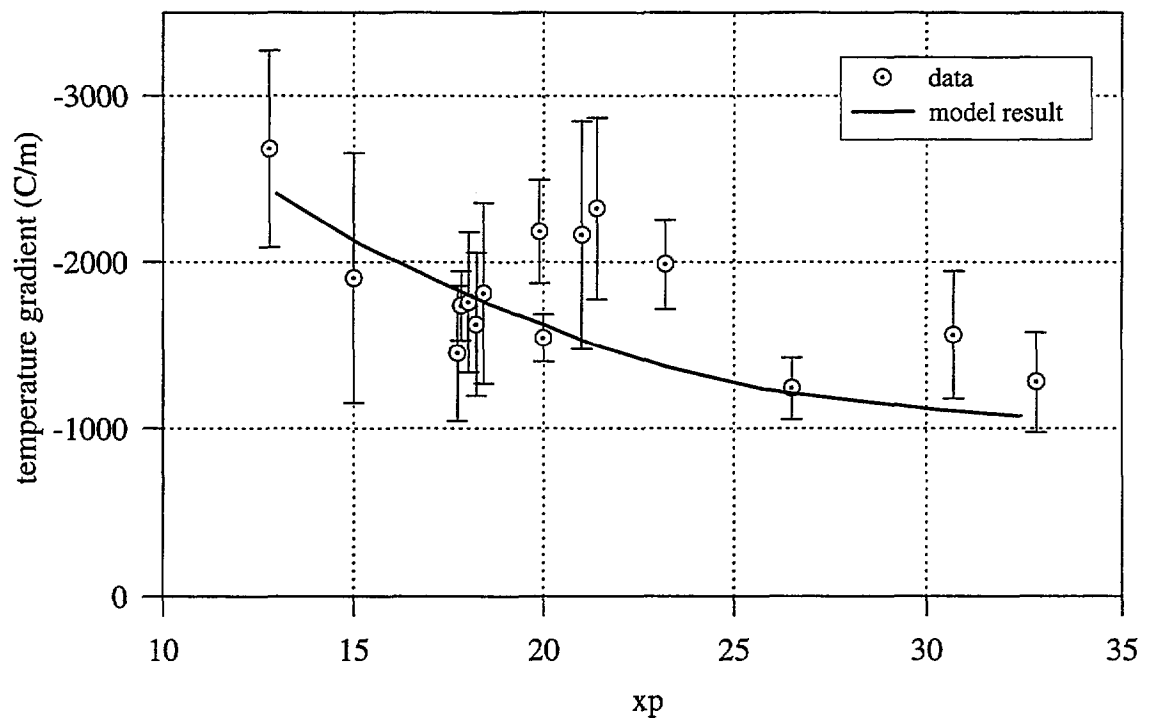


FIGURE 61. Temperature Gradient versus Expansion Ratio

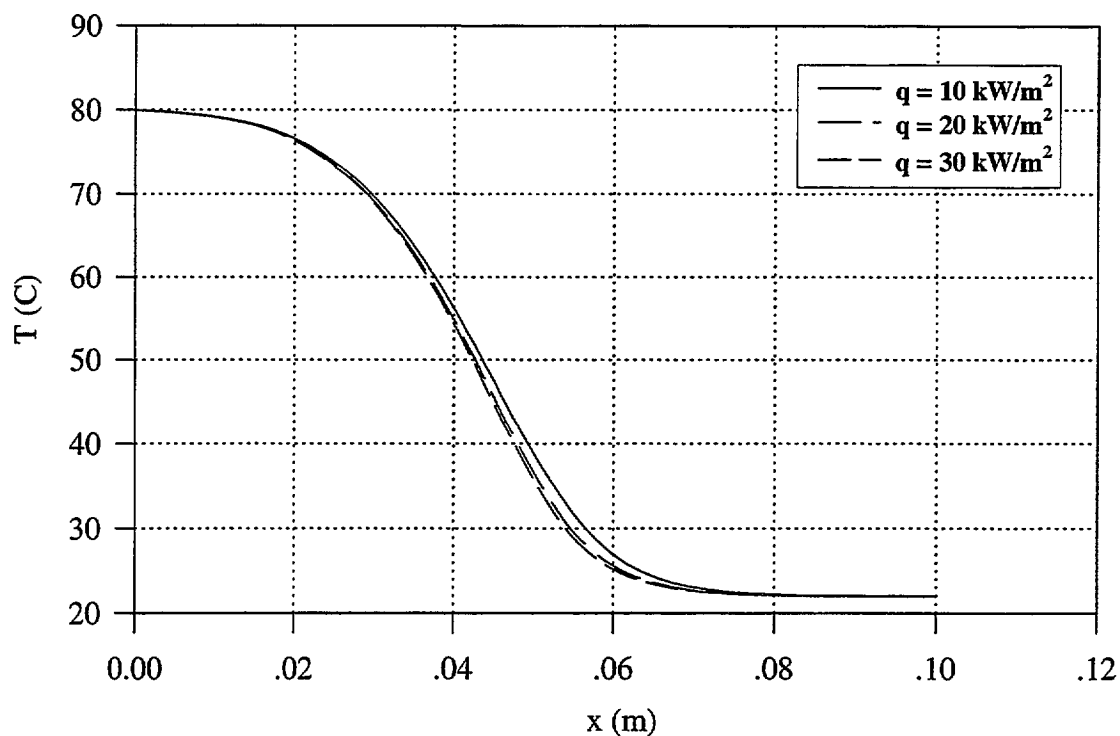


FIGURE 62. Temperature Profiles for Three Heat Fluxes, $x_p = 18.2$

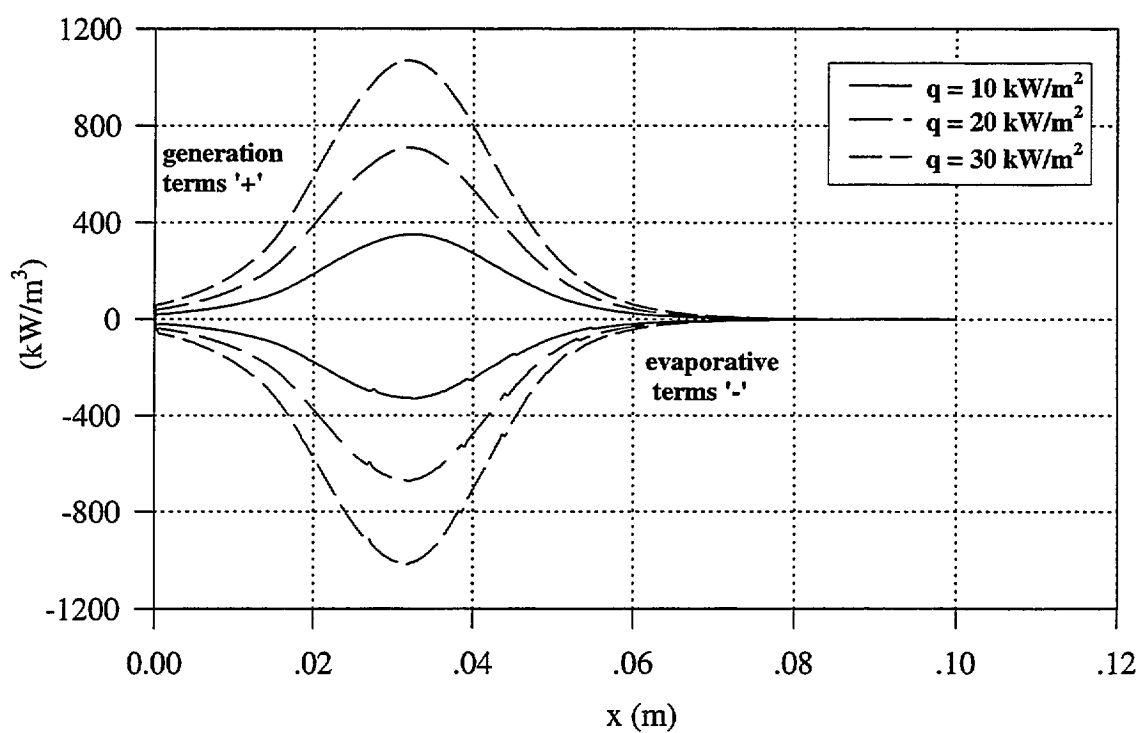


FIGURE 63. Generation and Evaporative Terms for Three Heat Fluxes

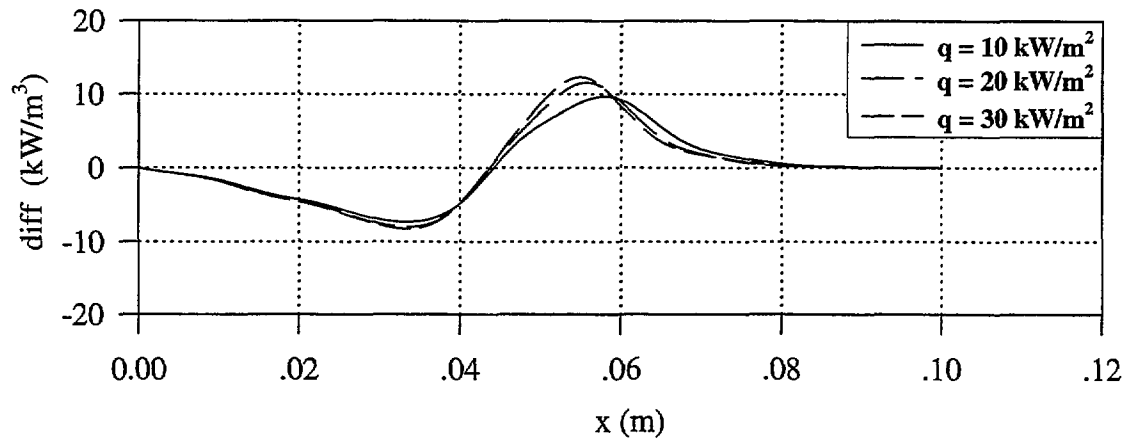


FIGURE 64. Diffusion Term for Three Heat Fluxes, $x_p = 18.2$

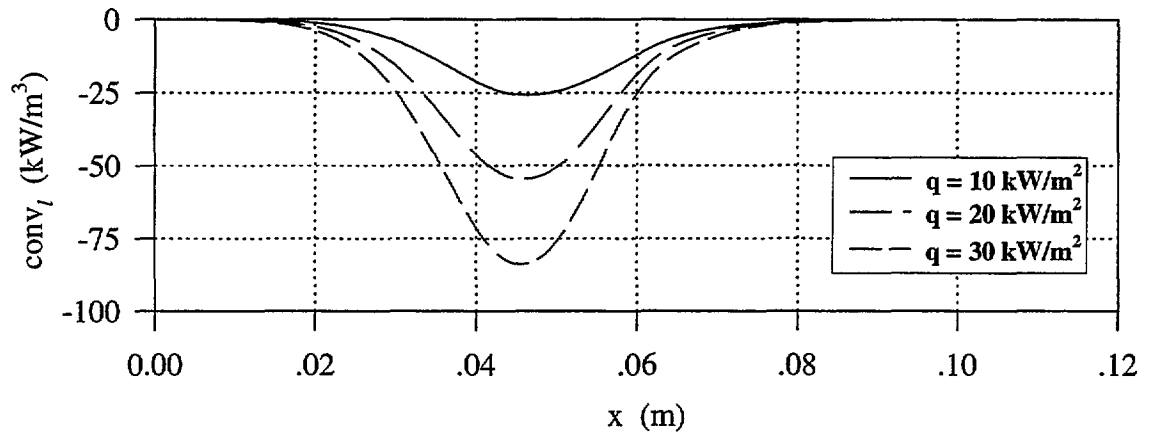


FIGURE 65. Liquid Convection Term for Three Heat Fluxes, $x_p = 18.2$

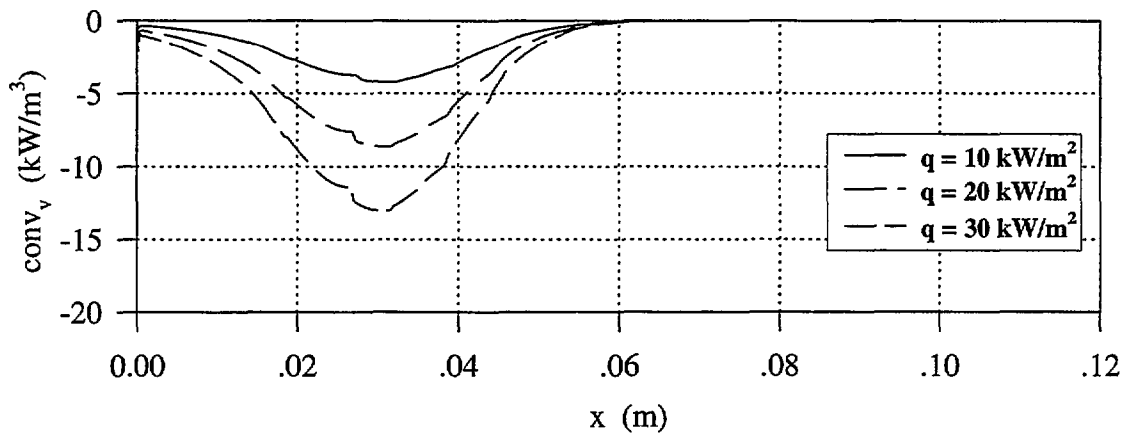


FIGURE 66. Vapor Convection Term for Three Heat Fluxes, $x_p=18.2$

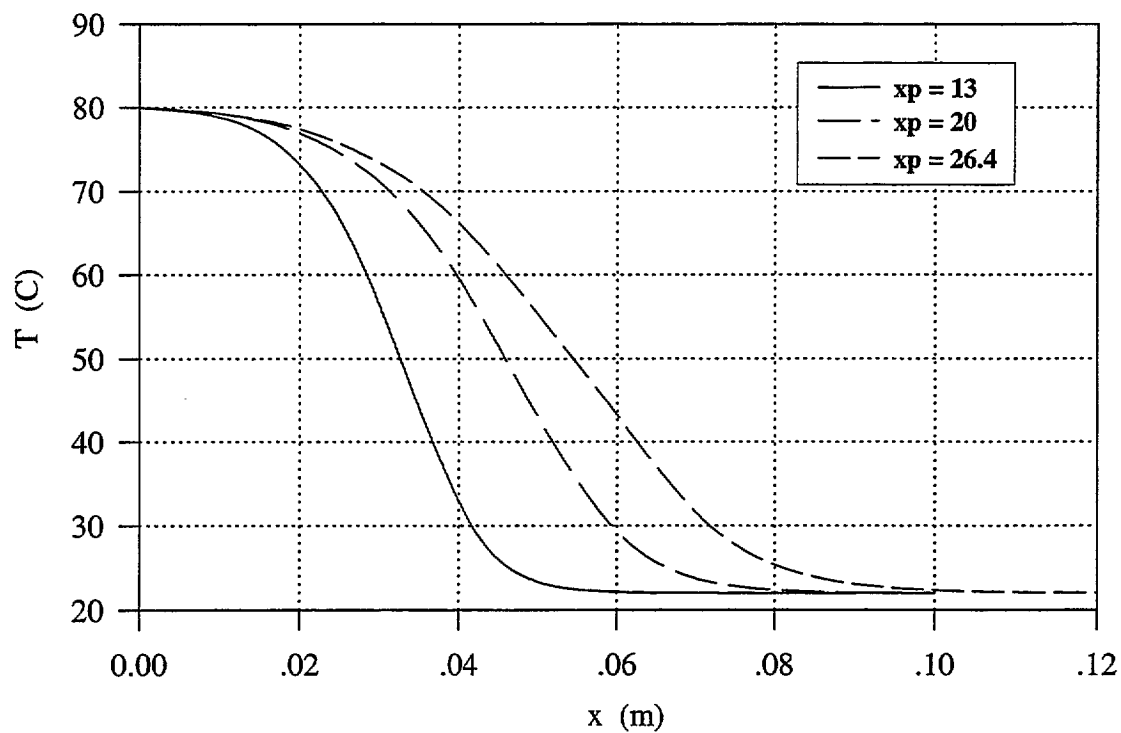


FIGURE 67. Temperature Profiles for Three Expansion Ratios

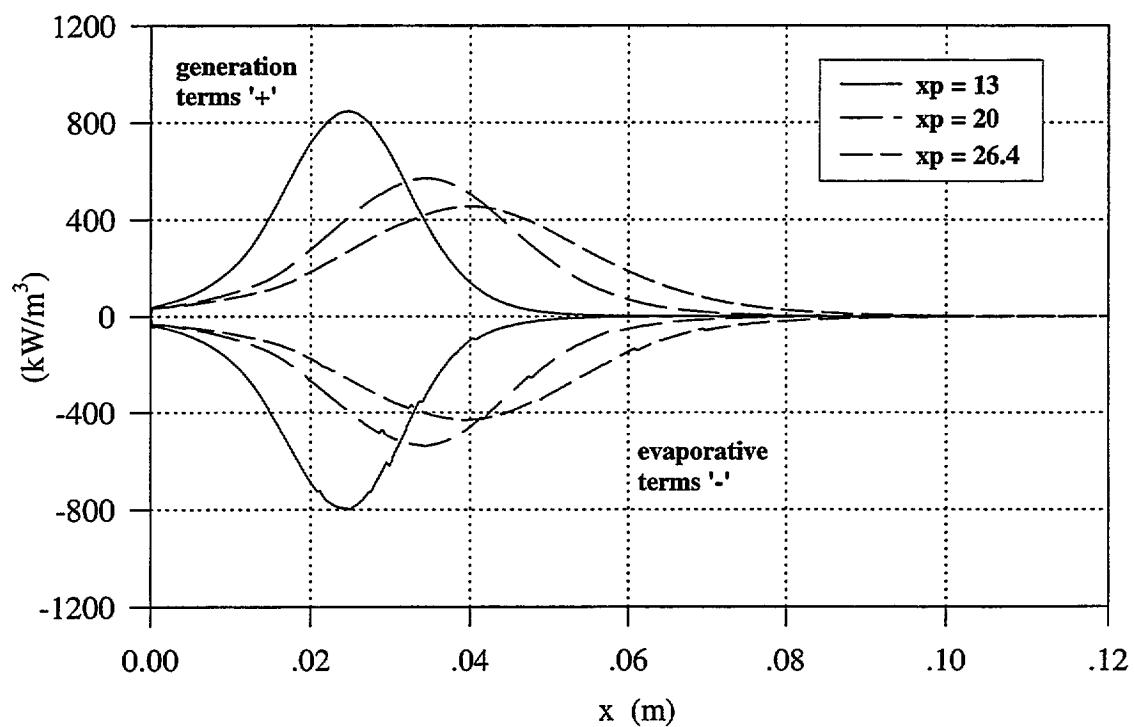


FIGURE 68. Generation and Evaporative Terms for Three Expansion Ratios

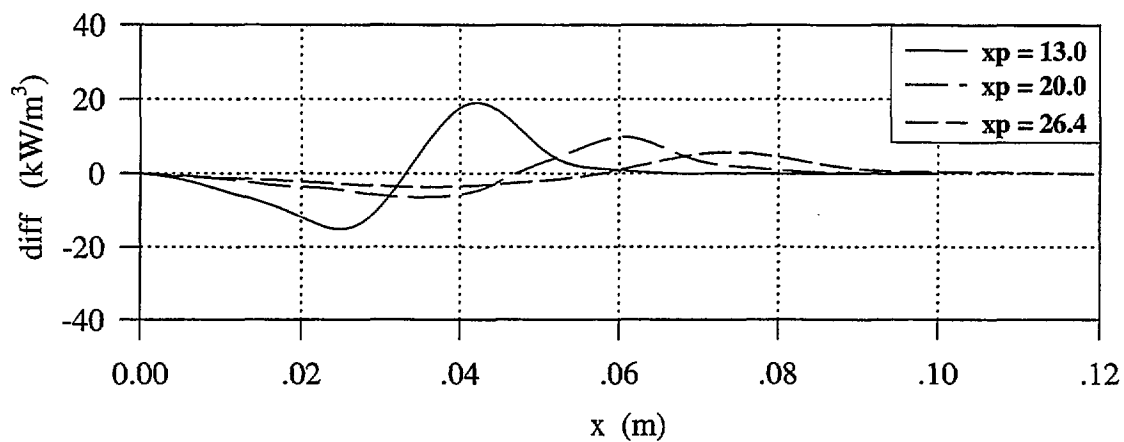


FIGURE 69. Diffusion Term for Three Expansion Ratios

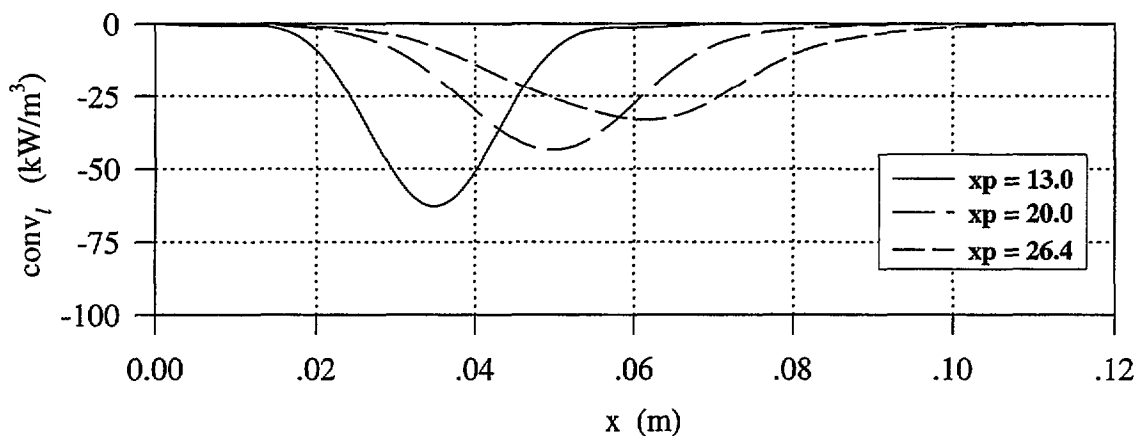


FIGURE 70. Liquid Convection Term for Three Expansion Ratios

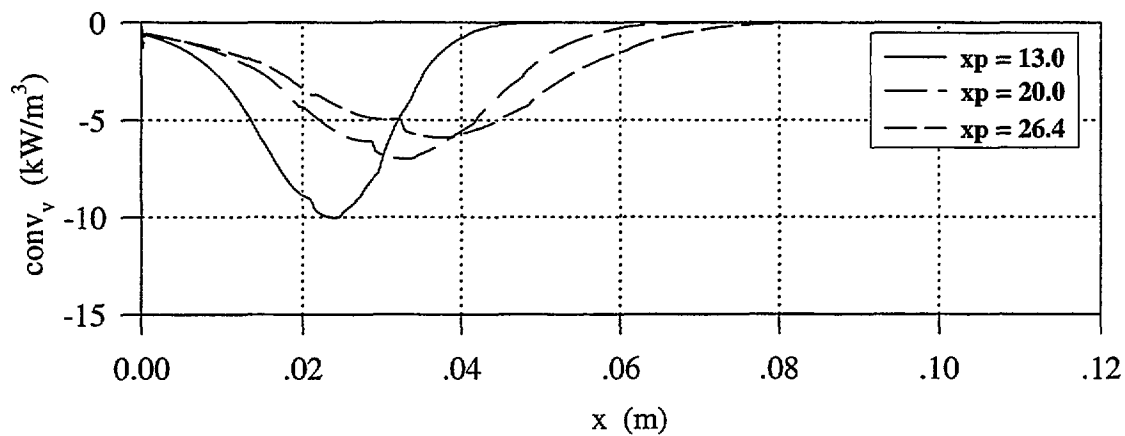


FIGURE 71. Vapor Convection Term for Three Expansion Ratios

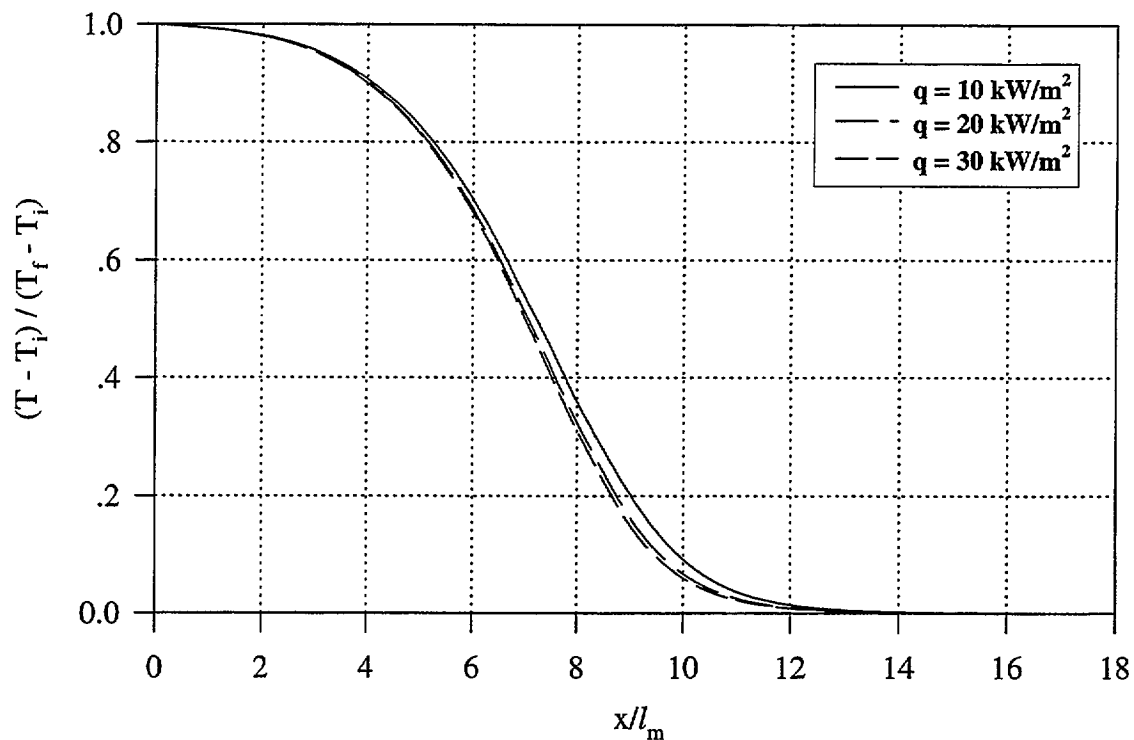


FIGURE 72. Dimensionless Temperature Profiles for Three Heat Fluxes

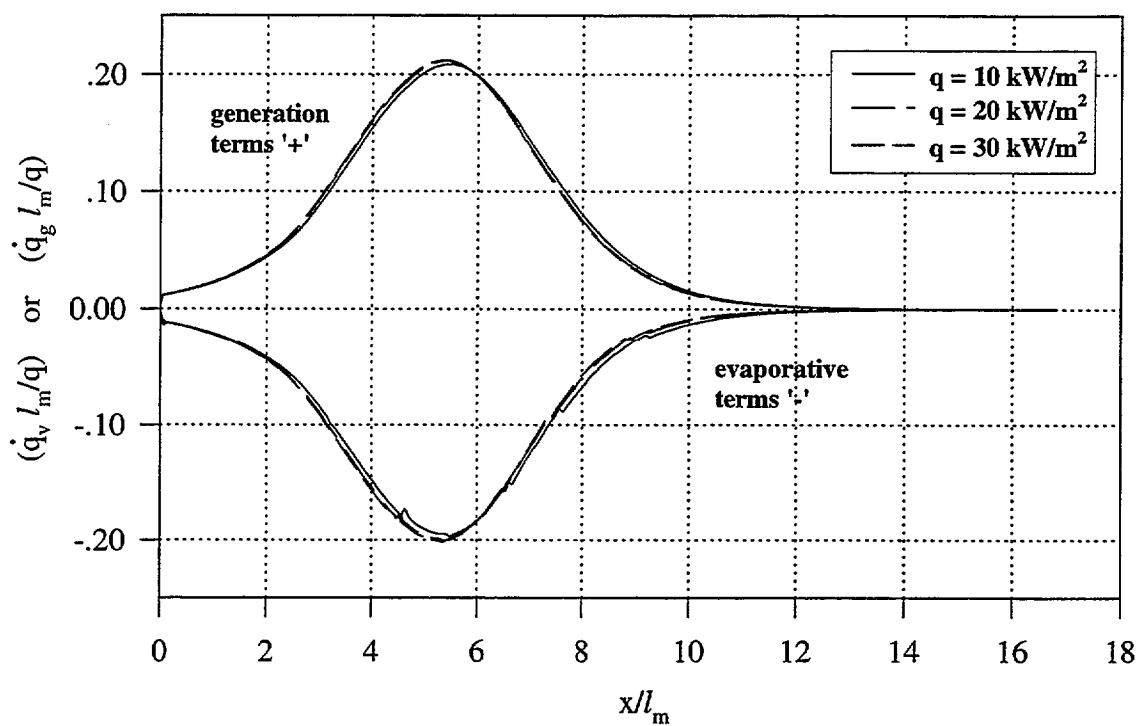


FIGURE 73. Dimensionless Generation and Evaporative Term Profiles

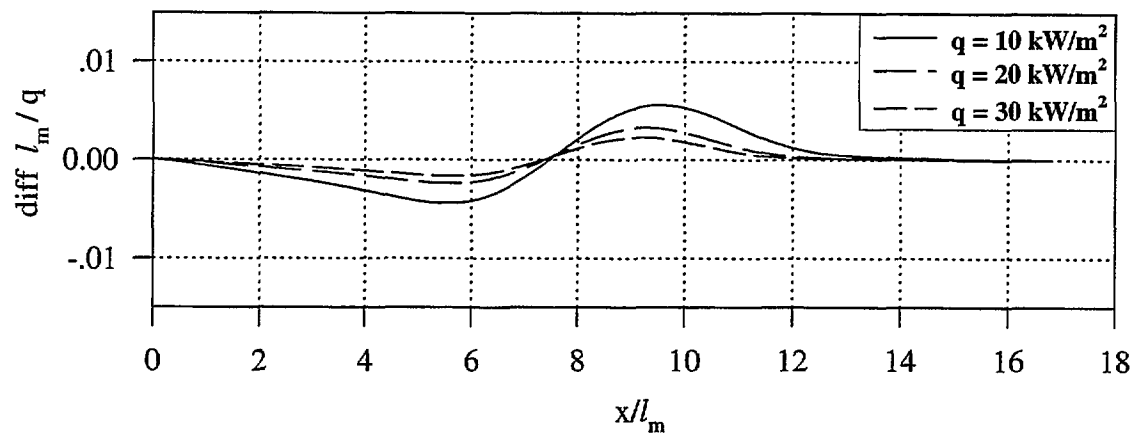


FIGURE 74. Dimensionless Diffusion Term for Three Heat Fluxes

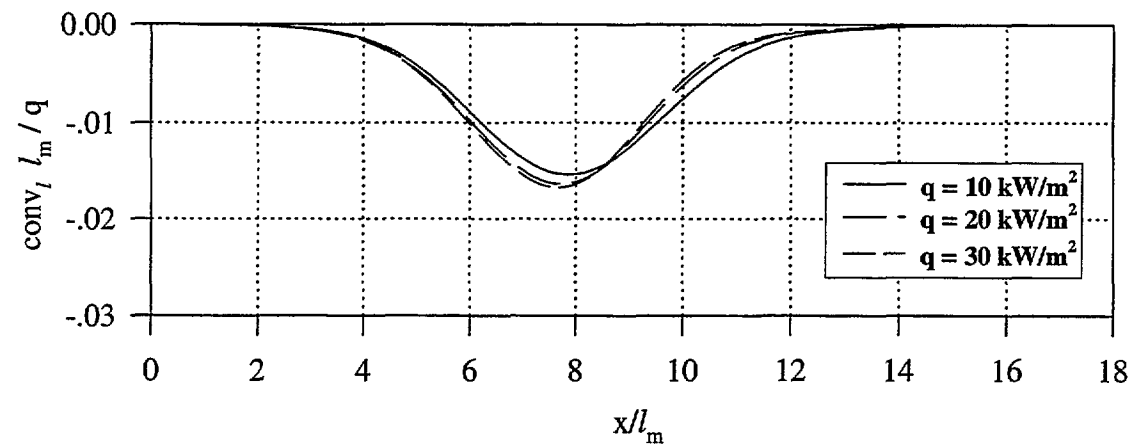


FIGURE 75. Dimensionless Liquid Convection Term for Three Heat Fluxes

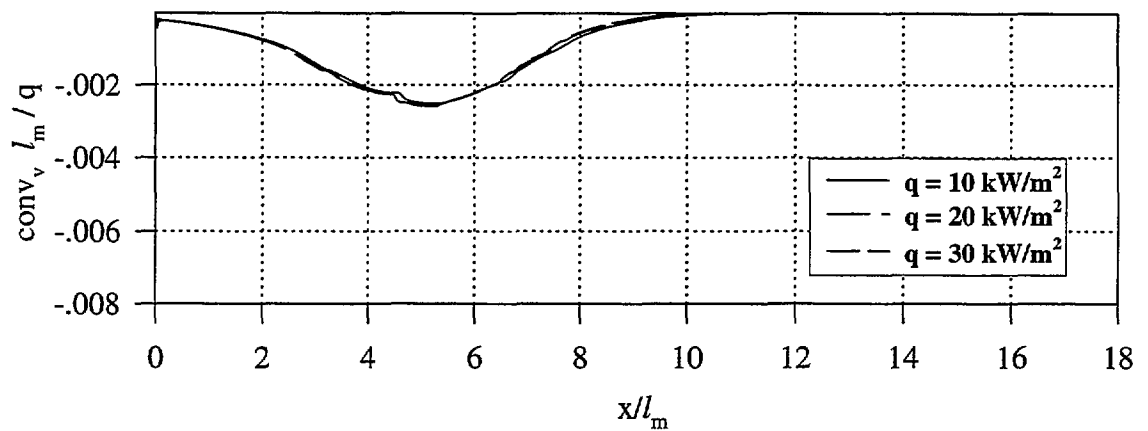


FIGURE 76. Dimensionless Vapor Convection Term for Three Heat Fluxes

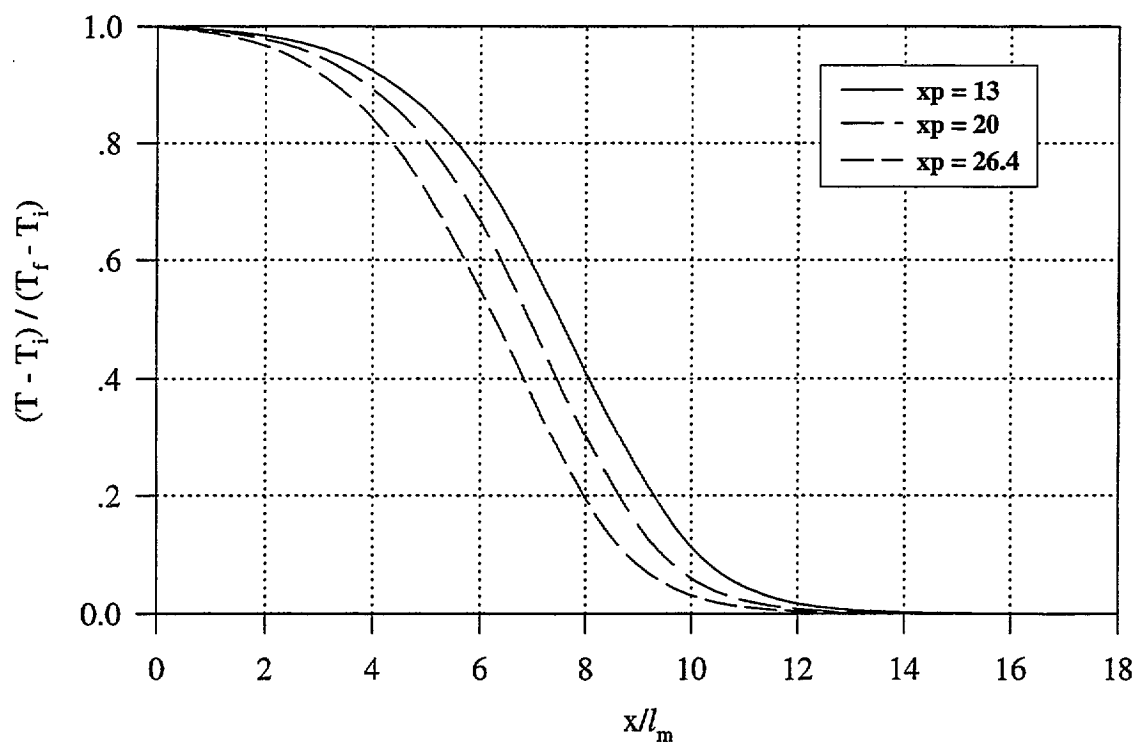


FIGURE 77. Dimensionless Temperature Profiles for Three Expansion Ratios

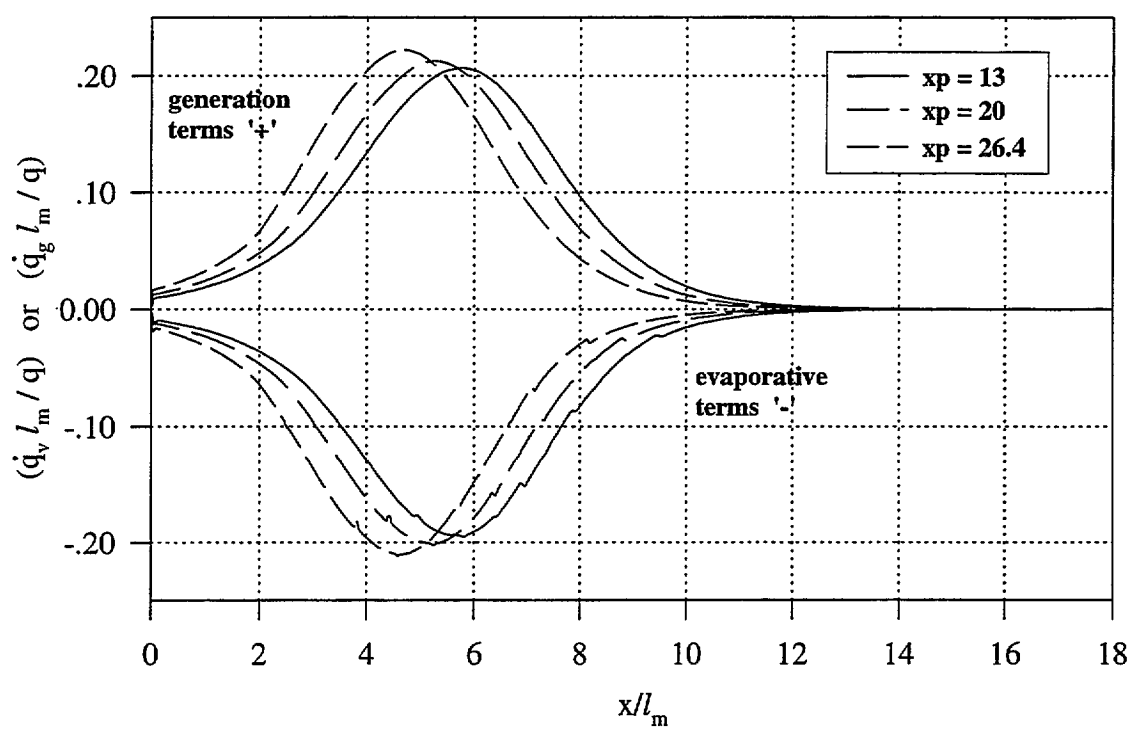


FIGURE 78. Dimensionless Generation and Evaporative Term Profiles

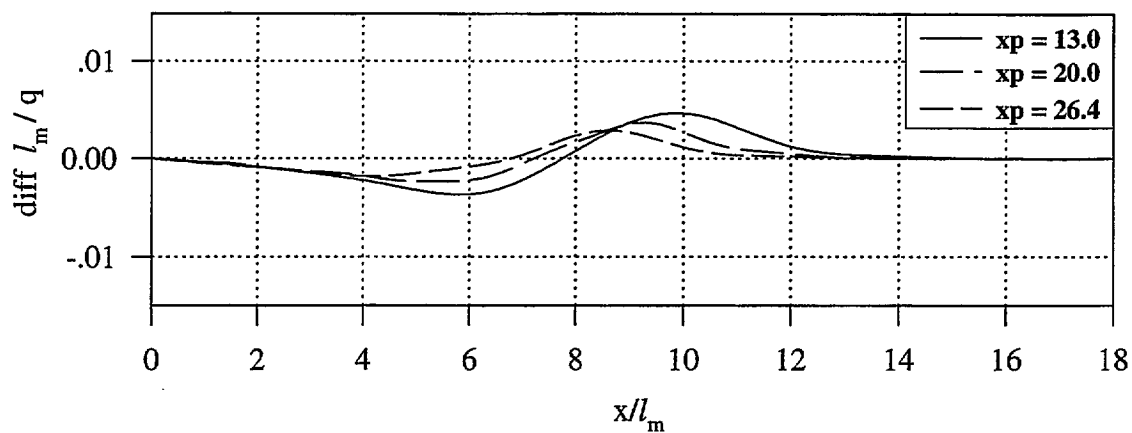


FIGURE 79. Dimensionless Diffusion Term for Three Expansion Ratios

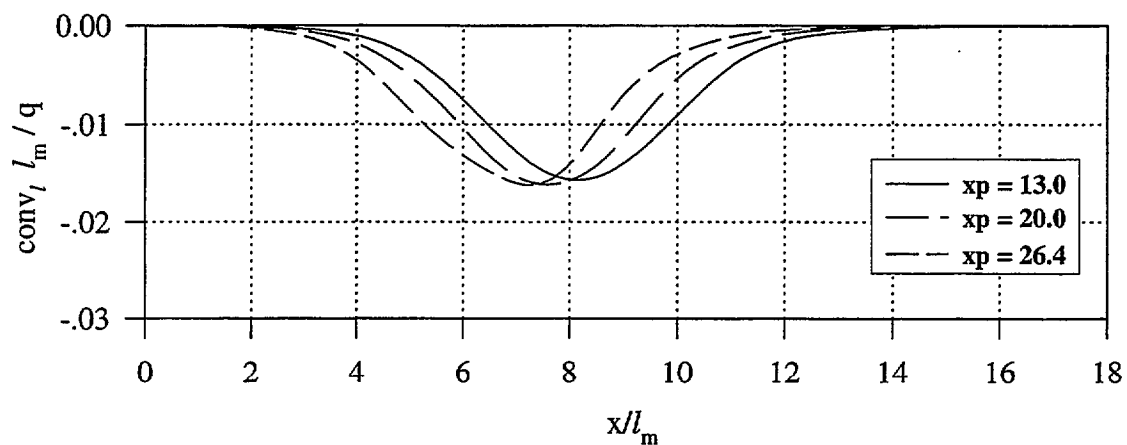


FIGURE 80. Dimensionless Liquid Convection Term for Three Expansion Ratios

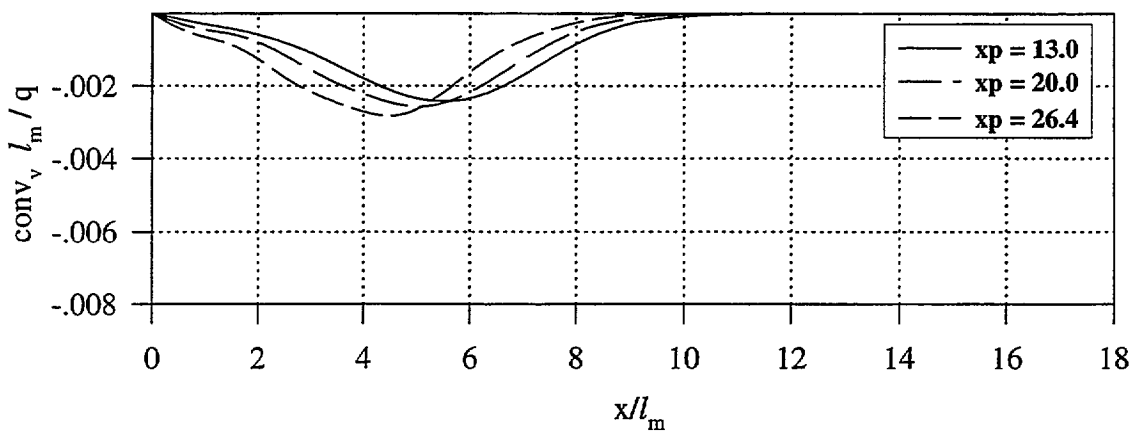


FIGURE 81. Dimensionless Vapor Convection Term for Three Expansion Ratios

REFERENCES

1. Bikerman, J. J. et al, *Foams: Theory and Industrial Applications*, Reinhold Publishing Corporation, New York, 1953.
2. NFPA Publication SPP-44, Fire-fighting foams and other foam systems.
3. National Foam, Field Catalog, *Introduction to Foam*, 1987
4. Wilson, A.J., *Foams: Physics, Chemistry and Structure*, Springer Verlag, New York, 1989.
5. National Fire Protection Association, Standard, NFPA Standard 11, Standard for Low-Expansion Foam, 1994.
6. Underwriters Laboratory, Standard for Safety, UL 162, Seventh Edition, *Foam Equipment and Liquid Concentrates*, March 30, 1994.
7. Naval Sea Systems Command, Military Specification, MIL-F-24385F, *Fire Extinguishing Agent, Aqueous Film-Forming Foam (AFFF) Liquid Concentrate, for Fresh and Sea Water*, January 1992.

8. Colletti, D. J., "Class A Foam: An Emerging Technology, Compressed-Air Foam Mechanics," *Fire Engineering*, Vol 147, No 3, March 1994, pp61-66.
9. Colletti, D. J., "Quantifying the Effects of Class A Foam in Structure Firefighting: The Salem Tests," *Fire Engineering*, Vol 146, No 2, February 1993, pp 41-44.
10. Rochna, R. R., "Foam on the Range," *Fire Chief*, Vol 38, No 6, June 1994, pp 34-38.
11. Briggs, A. A. and Webb, J. S., "Gasoline Fires and Foam", *Fire Technology*, Vol 24, No 1, February, 1988, pp 48-58.
12. Wesson, H. R., Welker, J. R. and Brown, L. E., "Control LNG-spill fires", *Hydrocarbon Processing*, Vol 51, No 12, December 1972, pp 61-64.
13. Stechishen, E., *The Effectiveness of Forest Fire-Fighting Foams*, PNFI Technical Reports, 1991, Chalk River, Ontario, Canada.
14. Madrzykowski, D., *Study of the Ignition Inhibiting Properties of Compressed Air Foam*, NISTIR 88-3880, October 1988, U.S. Department of Commerce, NIST, Gaithersburg, MD.

15. Persson, H., "Fire Extinguishing Foams Resistance Against Heat Radiation,"
Proceedings of the 1st International Conference on Fire Suppression Research,
Stockholm, Sweden, May 5-8, 1992, pp 359-376.
16. Boyd, C. F., telephone conversation with S. Biddle, Durra Foam
Representative, Chubb National Foam, Inc., Exton, PA, concerning
applicability of foam products for fire-protection roles, August 1994.
17. Gardon, R., "An instrument for Direct Measurement of Intense Thermal
Radiation," *Rev. of Scientific Instruments*, Vol 24, No. 5, 1953, pp. 360-370.
18. Omega, Catalog, Vol 29, The Temperature Handbook, 1995.
19. Park, R. M., *Manual on the Use of Thermocouples in Temperature
Measurements*, Fourth Edition, ASTM, Philadelphia, PA, 1993.
20. Carslaw, H. S. and Jaeger, J. C., *Conduction of Heat in Solids*, Second Edition,
Oxford at the Clarendon Press, 1959, pp 282-294.
21. Rohsenow, W. M., Choi, H., *Heat Mass, and Momentum Transfer*, Prentice
Hall, Englewood Cliffs, 1961, pp 122-124.

22. White, F. M., *Viscous Fluid Flow*, Second Edition, McGraw-Hill, Inc., USA, 1991, pp 82-83.
23. Morrison, F. A. Jr., "Transient Multiphase Multicomponent Flow in Porous Media," *Int. J. Heat and Mass Transfer*, V 16, 1973, pp.2331-2342.
24. Sahota, M. S. and Pagni, P. J., "Heat and Mass Transfer in Porous Media Subject to Fires," *Int J Heat and Mass Transfer*, V 22, 1979, pp.1069-1081.
25. Siegel, R. and Howell, J. R., *Thermal Radiation Heat Transfer*, Second Edition, Hemisphere Publishing Corporation, USA, 1981.
26. Tong, T. W., Liu, W. L. and Subramanian, E., *The Effect of Multiple Scattering in Measuring the Radiation Properties of Absorbing and Scattering Media*, AIAA-83-1454, June, 1983, Montreal, Canada.
27. Avallone, E. A. and Baumeister, T. III., *Marks' Standard Handbook for Mechanical Engineers*, Ninth Edition, McGraw-Hill Book Company, 1987.
28. Boyd, C. F., telephone conversation with J. R. Howell, Baker-Hughes Centennial Professor, The University of Texas at Austin, concerning dependence of scattering coefficient on wavelength, September 20, 1995.

29. Van Wylen, G. J. and Sonntag, R. E., *Fundamentals of Classical Thermodynamics*, 3rd Edition, John Wiley and Sons, USA, 1985.
30. Skochdopole, R. E., "The Thermal Conductivity of Foamed Plastics," *Chemical Engineering Progress*, Vol 57, No. 10, October, 1961, p57.
31. Schuetz, M. A., Glicksman, L. R., *A Basic Study of Heat Transfer Through Foam Insulation*, Proceedings of the SPI 6th International Technical/Marketing Conference.
32. Glicksman, L. R., Torpey, M. R., *A Study of Radiant Heat Transfer Through Foam Insulation*, ORNL/Sub/86-09099/3, October 1988, Massachusetts Institute of Technology.
33. ASTM Standards, C177-63, *Standard Method of Test for Thermal Conductivity of materials by Means of the Guarded Hot Plate*, 1967.
34. Kennedy, W. L., *An IBM Computer Program for Determining the Thermal Diffusivity of Finite Length Samples*, USAEC IS-137, 1-59, 1960.

NIST-114
(REV. 6-93)
ADMAN 4.09

U.S. DEPARTMENT OF COMMERCE
NATIONAL INSTITUTE OF STANDARDS AND TECHNOLOGY

MANUSCRIPT REVIEW AND APPROVAL

(ERB USE ONLY)

ERB CONTROL NUMBER

DIVISION

PUBLICATION REPORT NUMBER

CATEGORY CODE

NIST-GCR-96-702

PUBLICATION DATE

NUMBER PRINTED PAGES

October 1996

INSTRUCTIONS: ATTACH ORIGINAL OF THIS FORM TO ONE (1) COPY OF MANUSCRIPT AND SEND TO THE SECRETARY, APPROPRIATE EDITORIAL REVIEW BOARD

TITLE AND SUBTITLE (CITE IN FULL)

Fire Protection Foam Behavior in a Radiative Environment

CONTRACT OR GRANT NUMBER

60NANB5D0136

TYPE OF REPORT AND/OR PERIOD COVERED

Final Report September 1996

AUTHOR(S) (LAST NAME, FIRST INITIAL, SECOND INITIAL)

Boyd, C. F., di Marzo, M.
Mechanical Engineering Department
University of Maryland, College Park, MD 20742

PERFORMING ORGANIZATION (CHECK (X) ONE BOX)

☐
☐
☐

NIST/GAITHERSBURG

NIST/BOULDER

JILA/BOULDER

LABORATORY AND DIVISION NAMES (FIRST NIST AUTHOR ONLY)

SPONSORING ORGANIZATION NAME AND COMPLETE ADDRESS (STREET, CITY, STATE, ZIP)

U.S. Department of Commerce
National Institute of Standards and Technology, Gaithersburg, MD 20899

PROPOSED FOR NIST PUBLICATION

☐
☐
☐
☐
☐

JOURNAL OF RESEARCH (NIST JRES)

J. PHYS. & CHEM. REF. DATA (JPCRD)

HANDBOOK (NIST HB)

SPECIAL PUBLICATION (NIST SP)

TECHNICAL NOTE (NIST TN)

☐
☐
☐
☐
☐

MONOGRAPH (NIST MN)

NATL. STD. REF. DATA SERIES (NIST NSRDS)

FEDERAL INF. PROCESS. STDS. (NIST FIPS)

LIST OF PUBLICATIONS (NIST LP)

NIST INTERAGENCY/INTERNAL REPORT (NISTIR)

☐
☐
☐
☒

LETTER CIRCULAR

BUILDING SCIENCE SERIES

PRODUCT STANDARDS

OTHER NIST-GCR

PROPOSED FOR NON-NIST PUBLICATION (CITE FULLY)

☐

U.S.

☐

FOREIGN

PUBLISHING MEDIUM

☐
☐
☐

PAPER

DISKETTE (SPECIFY)

OTHER (SPECIFY)

☐

CD-ROM

SUPPLEMENTARY NOTES

ABSTRACT (A 2000-CHARACTER OR LESS FACTUAL SUMMARY OF MOST SIGNIFICANT INFORMATION. IF DOCUMENT INCLUDES A SIGNIFICANT BIBLIOGRAPHY OR LITERATURE SURVEY, CITE IT HERE. SPELL OUT ACRONYMS ON FIRST REFERENCE.) (CONTINUE ON SEPARATE PAGE, IF NECESSARY.)

A model is developed which predicts the behavior of a fire-protection foam subjected to heat radiation. Foam expansion ratio and radiative heat flux are input to the model. A mass and energy balance yield the foam destruction rate and the temperature distribution within the foam.

The energy equation is solved in a coordinate system moving with the foam front. Separate air, vapor, and liquid convection terms are computed. Radiation absorption is accounted for with a volumetric generation term. The absorption model is based upon experimental measurements. A volumetric evaporative term accounts for the latent heat of liquid vaporized within the foam. Liquid vaporization rates are determined from the liquid continuity equation. Saturated conditions and thermodynamic equilibrium are assumed throughout. Thermal diffusion is computed using an experimentally determined thermal conductivity.

KEY WORDS (MAXIMUM OF 9; 28 CHARACTERS AND SPACES EACH; SEPARATE WITH SEMICOLONS; ALPHABETIC ORDER; CAPITALIZE ONLY PROPER NAMES)

computer models; fire protection; fire research; foam expansion; heat flux; heat radiation; insulation; temperature profiles

AVAILABILITY

☒
☐
☒

UNLIMITED

☐

FOR OFFICIAL DISTRIBUTION - DO NOT RELEASE TO NTIS

ORDER FROM SUPERINTENDENT OF DOCUMENTS, U.S. GPO, WASHINGTON, DC 20402

ORDER FROM NTIS, SPRINGFIELD, VA 22161

NOTE TO AUTHOR(S): IF YOU DO NOT WISH THIS
MANUSCRIPT ANNOUNCED BEFORE PUBLICATION,
PLEASE CHECK HERE. ☐

WORDPERFECT

